The Role of Reactive Oxygen Species during Early Embryogenesis of *Xenopus laevis*

A thesis submitted to The University of Manchester for the degree of

DOCTOR OF PHILOSOPHY in the Faculty of Life Sciences

2015

YUE HAN

Table of content

Index of Figures

Index of Tables

Abstract

Institution: The University of Manchester **Name**: Yue Han

Degree Title: PhD Developmental Biology **Date**: 2015

Thesis Title: The role of reactive oxygen species during early embryogenesis of *Xenopus laevis*

Embryonic development involves a variety of cellular processes, including cell growth, cell proliferation, cell differentiation, cell migration and cell death. The precise regulation of these events is essential for morphogenesis and development. Reactive oxygen species (ROS) have been reported as important second messengers to modulate a variety of proteins and signalling pathways, thereby regulating several cellular processes. Previous studies have shown that fertilisation induces an oxidative burst in sea urchins. However, a role for this fertilisation induced ROS during embryonic development in this system has not been shown. Amphibian embryos, such as those from *Xenopus laevis (X. laevis),* provide an ideal system to study the role of ROS during embryonic development. We previously established a HyPerYFP line in *X. laevis*, which permits the visualisation of ROS levels in living oocytes, fertilised eggs and early embryos. Using this line, I showed that fertilisation triggers a dramatic increase in intracellular ROS levels, and this increase in ROS levels is sustained throughout early embryogenesis. Lowering ROS levels using antioxidants (e.g. NAC) impairs mesoderm formation and results in severe developmental defects, which are associated with a down-regulation of several signalling pathways, including PI3K/Akt, TGF-β/Nodal and Wnt/β-catenin signalling. I also showed that the dysregulation of these signalling pathways could be partially rescued by addition of the oxidant H_2O_2 or the ROS inducer menadione, suggesting that the fertilisation induced ROS helps activate several signalling pathways required for mesoderm formation. Further investigations through loss and gain of function analyses revealed that fertilisation induced calcium wave, which is dependent on IP_3, activates ROS production from mitochondria, via the mitochondrial complexes II, III and IV. In addition, treatment of early embryos with mitochondrial inhibitors results in defects in cell division during early embryogenesis. Together, my findings suggest that a sustained high level of ROS is essential for cell cycle progression and the activation of early signalling events, therefore ensuring proper early embryonic development in *X. laevis*.

Declaration

No portion of the work referred to in the thesis has been submitted in support of an application for another degree or qualification of this or any other university or other institute of learning.

Copyright Statement

Acknowledgements

Firstly I would like to express my deepest and sincere gratitude to my supervisor Professor Enrique Amaya for his patient guidance and support throughout my PhD. I would also like to thank my adviser Dr. Kimberly Mace and my tutor Dr. Caroline Milner for their kindly suggestions and advice on my thesis writing and editing. I would also like to thank Dr. Karel Dorey and his lab members for the help and advice on my project. Special thanks to Dr. Yutaka Matsubayashi for his patient guidance and advice on statistical analysis and the suggestions he has given in the joint lab meeting.

Secondly I would like to thank all past and present members of Amaya lab, for their help, guidance and advice during my PhD. Particular thanks to Dr. Siwei Zhang and Dr. Jingjing Li for their generous help with protocols and frequent discussions on project. Additionally, I would like to thank Dr. Shoko Ishibashi for making constructs and bring great advice to my project and thesis. I would also like to thank Dr. Yaoyao Chen, Dr. Nick R. Love and Dr. Ximena Soto for support and advice on my project. Special thanks to Robert Lea and Rachel Lea for their help in lab work and school life.

Additionally I am also deeply grateful to my precious friends for their companies and encouragement, which made my PhD life much easier, fun and colourful.

My deepest gratitude will give to my parents for their endless love and support throughout my life. I am also indebted to my husband for his taking care, support and understanding in last ten years, for making me delicious food and taking me home from lab no matter how late it is; for always standing by my side without doubt, for companying me all the time and filling every day of my life with laugher.

Finally, I would like to thank Healing Foundation Centre for funding my PhD program over the past four years.

Abbreviations

Amplex Red	N-acetyl-3,7-dihydroxyphenoxazine
AKT	Protein Kinase B (PKB)
APO	Apocynin
ASK1	Apoptosis signal regulated kinase 1
ATP	Adenosine triphosphate
APC	Adenomatosis polyposis coli
BME	β-mercaptoethanol
BMK1	Big MAP kinase 1
BMP	Bone morphogenic protein
BSA	Bovine serum albumin
Complex I	NADH dehydrogenase
Complex II	Succinate dehydrogenase
Complex III	Ubiquinol-cytochrome *c* reductase
Complex IV	Cytochrome *c* oxidase
Complex V	ATP synthase
DCFH-DA	Dichlorodihydrofluorescein diacetate
DHE	Dihydroethidium
Dvl	Dishevelled
DMSO	Dimethyl sulfoxide
DPI	Diphenylene iodonium
EDTA	Ethylenediamine tetracetic acid
EGF	Epidermal growth factor
EGTA	Ethylene glycol tetracetic acid
EtOH	Ethanol
ER	Endoplastic reticulum
ETC	Electron transport chain / respiratory chain
FAD	flavin adenine dinucleotide

Fe-S	Iron-sulfur centre
FGF	Fibroblast growth factor
FMN	Flavin mononucleotide
FQR	Flavoprotein-ubiquinone oxidoreductase
Fz	Frizzled
GFP	Greeen fluorescent protein
GPDH	Glycerol 3-phosphate dehydrogenase
GSH	Glutathione
GSK3β	Glycogen synthase kinase 3 beta
GVBD	Germinal vesicle break down
HCG	Human choriongonadotropin
HRP	Horse raddish peroxidase
HS	Heparan sulfate
H_2O_2	Hydrogen peroxide
IP_3	Inositol 1,4,5-trisphosphate
IP_3R	Inositol 1,4,5-trisphosphate receptor
JNK	C-Jun N-terminal kinases
LEF	Lymphoid enhancer factor
MAMFA	MOPS, EGTA, Magnesium sulphate, Formaldehyde
MAPK	Mitogen-activated protein kinase
MBT	Mid-blastula transition
MMR	Mark's Modified Ringers
MRC	Mitochondrial respiratory chain / electron transport chain
MS222	Tricaine methanesulfonate
NaAc	Sodium Acetate
NAC	N-acetyl cysteine
NADPH	Nicotinamide adenine dinucleotide phosphate
NOX	NADPH oxidase
NRX	Nucleoredoxin

OGDH	2-oxoglutarate dehydrogenase
PCP	Planar cell polarity
PCR	Polymerase chain reaction
PDGF	Platele-derived growth factor
PDH	Pyruvate dehydrogenase
PDK	Phosphoinositide-dependent protein kinase
PKC	Protein kinase C
PLB	Passive lysis buffer
PLC	Phospholipase C
PI3K/Akt	Phosphatidylinositol-3-Kinase and Protein Kinase B
PIP_2	Phosphatidylinositol 4,5 bisphosphate
PIP_3	Phosphatidylinositol 3,4,5 triphosphate
Prx	Peroxiredoxin
PTEN	Phosphatase and tensin homolgy
PTP	Protein tyrosine phosphatase
Q	Ubiquinone / coenzyme Q
QH_2	Ubiquinol / reduced ubiquinone / reduced coenzyme Q
Redox	Oxidation and reduction
REMI	Restriction enzyme mediated intergration
RET	Reverse electron transport
ROS	Reactive oxygen species
RTK	Receptor tyrosine kinases
Ry	Ryanodine
RyR	Ryanodine receptor
SDS-PAGE	Sodium dodecyl sulphate polyacrylamide gel electrophophoresis
SOD	Superoxide dismutase
TBST	Tris-Buffered Saline with Tween-20
TCA cycle	Tricarboxylic acid cycle / Kreb's cycle / citric acide cycle
TCF	T-cell factor
TGF-β	Transforming growth factor beta

Trx	Thioredoxin
VEGF	Vascular endothelial growth factor
WT	Wide type
X. laevis	*Xenopus laevis*
YFP	Yellow fluorescent protein
ΔP	Proton motive force
ΔΨm	Mitochondrial transmembrane potential

Chapter 1: General Introduction

1.1. Reactive oxygen species (ROS)

Reactive oxygen species (ROS) is a collective term used to describe a number of free oxygen radicals and reactive molecules derived from molecular oxygen, including superoxide anion (O_2^-), hydroxyl radical ($HO^·$), hydrogen peroxide (H_2O_2) and singlet oxygen (O_2) [1]. It has long been known that ROS can cause damage to cells by deleteriously modifying biological molecules, such as lipids, proteins and nuclear acids, therefore the reports of ROS are usually linked with aging and a number of distinct human diseases, such as cardiovascular disease, neurological disorders, cancers and chronic inflammation [2-5]. For a long time, ROS were only recognised as a kind of toxic by-products from aerobic metabolism. However, as research progressed over the last two decades, another voice of ROS emerged, claiming that they can function as second messengers to fine-tune the complicated network of signal transduction, thus triggering or modulating various cellular activities, such as cell proliferation, cell differentiation and cell death [6]. Any alterations of intracellular ROS levels may induce a cellular signal and determine the behaviour of cells. So far, numerous studies in distinct disease systems provided appreciable evidence of ROS regulation on signalling pathways and cellular activities; nonetheless, *in vivo* proof of ROS modulation is still limited and could benefit from further study. In this chapter, I will briefly delve into the general background of ROS including ROS generation, ROS elimination, ROS detection and how ROS act in concert with signalling pathways to modulate cellular activities.

1.1.1. ROS production

Generally, endogenous ROS are produced by partial reduction of molecular oxygen through gaining one electron to generate superoxide, a precursor of other oxidants. Superoxide can rapidly be converted to H_2O_2, a relatively stable non-radical ROS, which can follow a further oxidation to form diverse hydroxyl radicals. This chain of ROS production is mainly relied on the amount of superoxide and H_2O_2, which can be produced by multiple mechanisms in different organelles depending on cell types or tissues (Figure 1-1) [6, 7]. Here, I briefly summarise the mechanisms of ROS production and the major contributors of intracellular ROS within cells.

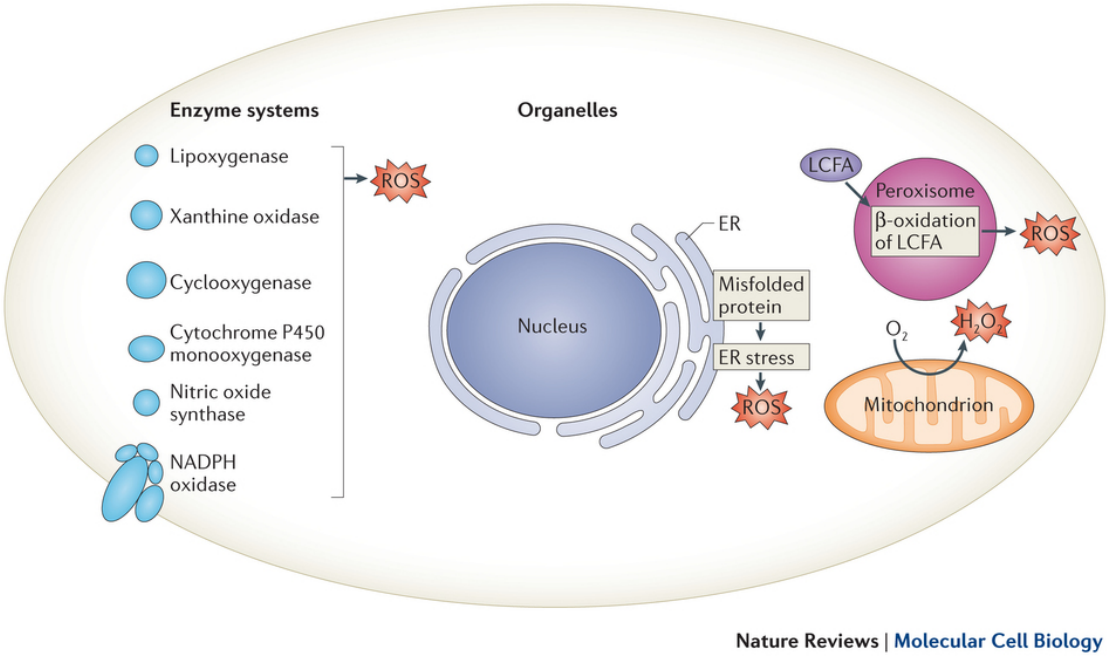

Figure 1-1: All possible sites of ROS generation in cells.

Figure 1-1 depicts the major endogenous sources of ROS in cells, including mitochondria, membrane-bound NADPH oxidases, peroxisome, endoplasmic reticulum (ER), cytochrome P450, lipoxygenase, xanthine oxidase, cyclooxygenase and nitric oxide synthase. This figure is taken from a review paper of Kira M. Holmstrom and Toren Finkel **[7]**.

1.1.1.1. ROS arising from the mitochondrial respiratory chain (MRC)

Mitochondria have a four-layer structure, comprising matrix, inner mitochondrial membrane, inter membrane space and outer mitochondrial membrane. There are five big protein complexes embedded within the inner mitochondrial membrane, named complex I (NADH dehydrogenase), complex II (succinate dehydrogenase), complex III (ubiquinol-cytochrome *c* reductase), complex IV (cytochrome *c* oxidase) and complex V (ATP synthase). As the main energy factory, mitochondria generate adenosine triphosphate (ATP) during oxidative phosphorylation, accompanying the flow of electrons down the respiratory chain. In this process, electrons are passed through proteins via a chain reaction of oxidation-reduction events, culminating at complex IV with the reduction of molecular oxygen to water [8]. Since this electron transport chain (ETC) is not fully efficient in generating ATP, some leakage of intermediate steps could induce the reduction of single electron from molecular oxygen, resulting in the generation of superoxide anions. As a main precursor of ROS, superoxide can then be catalysed by superoxide dismutase (SOD) to form H_2O_2 or undergo a series of

reactions to produce other forms of ROS [8-10]. In most cell types, mitochondria are considered to be the major contributor of intracellular ROS. Studies using isolated mitochondria suggest eight distinct sites to generate superoxide, including respiratory complexes and individual enzymes (Figure 1-2), among which mitochondrial respiratory chain is thought to be the primary contributor to mitochondrial ROS [7, 10, 11].

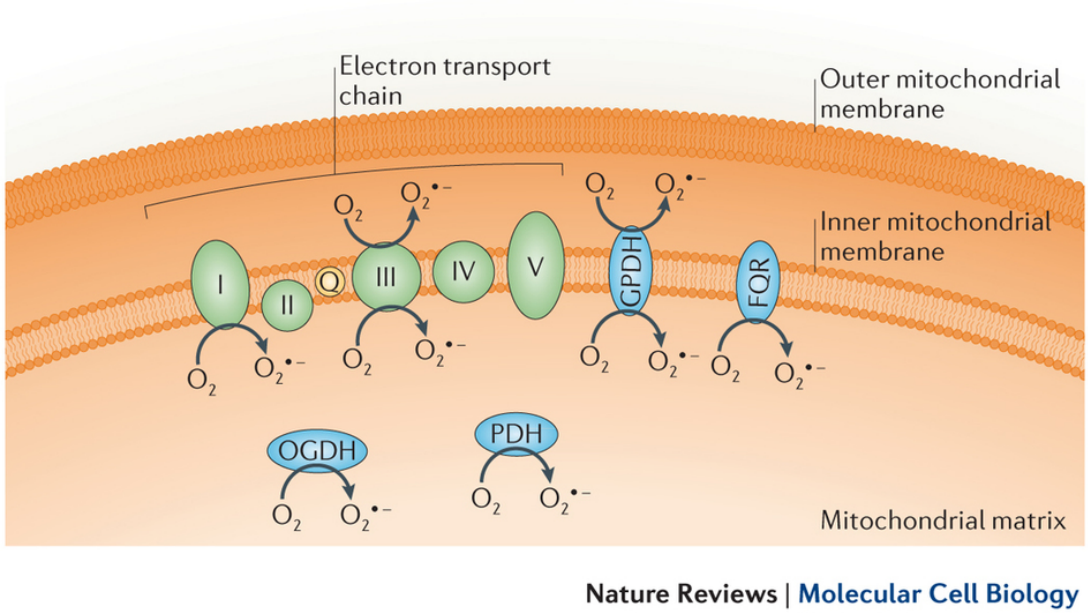

Figure 1-2: Sites of ROS production within mitochondria.

Figure shows the multiple sites of ROS (superoxide) generation within mitochondria. Mitochondrial complex I to V are localised within the inner mitochondrial membrane, among which complex I and III are regarded as two major contributors of superoxide production. Other enzymes producing ROS within mitochondrial including 2-oxoglutarate dehydrogenase (OGDH), pyruvate dehydrogenase (PDH), glycerol 3-phosphate dehydrogenase (GPDH) and electron transfer flavoprotein-ubiquinone oxidoreductase (FQR). Q states for coenzyme Q10. This figure is from a review paper written by Kira M. Holmstrom and Toren Finkel **[7]**.

a. Mitochondrial complex I and ROS production

Based on *in vitro* studies of isolated mitochondrial proteins, the main sites of mitochondrial ROS production are considered to be mitochondrial complex I and complex III [7-9]. Mitochondrial complex I is a highly complicated membrane-bound enzyme, with 46 different subunits and 9 redox cofactors, including a flavin mononucleotide (FMN) and 8 iron-sulfur (Fe-S) clusters, which catalyse the oxidation of NADH with reduction of Q to QH_2 [12]. It may leak electrons and generate ROS at its NADH binding site or the Q binding site [13]. Evidence showed that isolated complex I can generate superoxide at a low rate in the presence of NADH, interestingly, the complex I inhibitor rotenone can increase this rate several fold. The explanation of this phenomenon is that rotenone binds to Q site and blocks electron transfer from Fe-S to Q, causing electrons to back up to reduce the upstream centre FMN, therefore producing ROS with reduction of molecular oxygen [9]. This site of where complex I generate superoxide is called site IF. Another site capable of producing large amounts of ROS within mitochondrial complex I is the Q binding site (site IQ), where superoxide is produced during reverse electron transport (RET). With the supply of electrons from succinate or glycerol 3-phosphate or fatty acid oxidation, Q can be reduced to QH_2 and generate a proton motive force (ΔP), which drives electrons back into complex I and reduce NAD^+ to NADH. In this situation, rotenone (complex I Q site inhibitor) significantly decreased ROS production, confirming that ROS production is due to the electrons entering into complex I through the Q binding site [9, 11]. However, the *in vivo* mechanism of ROS production in mitochondrial complex I is still obscure.

b. Mitochondrial complex III and ROS production

Except complex I, the other enzyme that has long been regarded as another main source of ROS within mitochondria is complex III. Complex III contains three common structures, cytochrome *b*, cytochrome c_1, and Rieske Fe-S centre, and functions by catalysing the oxidation of QH_2 and transferring the electrons to cytochrome *c* [14]. It was reported that complex III could produce superoxide largely in the presence of antimycin A, which blocks electron transfer at centre *i* and results in a small accumulation of semiquinone at centre *o* (IIIQo), thus generating superoxide with the reduction of molecular oxygen. Although these *in vitro* studies show that complex III can be induced to generate ROS with antimycin A, the physiological status is still far from known.

c. Mitochondrial complex II and ROS production

Besides mitochondrial complex I and III, complex II has also gained scientific attention in relation to ROS generation. It comprises four subunits, including a flavoprotein subunit, an Fe-S protein subunit, and two transmembrane cytochrome *b* heme subunits [15]. In the respiratory chain, complex II works independently from complex I with oxidation of succinate to fumarate in the TCA cycle and passing electrons to Q. In detail, when succinate is oxidised, two electrons are transferred to flavin and passed through the Fe-S clusters to reduce Q to QH_2 [15]. In this process, superoxide can be generated. Some researchers showed that the superoxide generation from succinate oxidation within complex II could be diminished after treatment with rotenone (complex I inhibitor), suggesting this superoxide generation is principally from RET by complex I [16]. Nevertheless, other evidence showed that complex II could produce ROS in both forward reaction with electron provided by succinate, and reverse reaction with electron provided by reduced Q pool [17]. The authors showed that when inhibiting complex I and III, a robust ROS (H_2O_2) production was still observed from complex II in isolated rat skeletal mitochondria. Besides, low concentration of succinate largely promotes the ROS generation from complex II, which borders or exceeds the reported maximum rates of ROS generation obtained from complex I and III. In addition, they also showed this ROS production could be greatly abolished by malonate, a competitive inhibitor of complex II (flavin site inhibitor) but only partially decreased by atpenin A5 (Q binding site inhibitor of complex II), suggesting the ROS production mainly from the flavin site at complex II. Moreover, they also showed complex II produces ROS in the reverse reaction with electrons from reduced Q pool [17]. Together, these results suggest the contribution of complex II to mitochondrial ROS production.

d. Mitochondrial complex IV and ROS production

Mitochondrial complex IV or cytochrome c oxidase accepts electrons from cytochrome c and transfers them to molecular oxygen to form water. Cyanide or sodium azide can block the downstream ETC by inhibiting electron transport in complex IV. Investigation with these inhibitors in isolated mitochondria showed that complex IV contributes little to ROS production [18].

Other sites generating ROS within mitochondria include GPDH, PDH, OPDH and FQR, however, their mechanisms of generating ROS are poorly characterised and need further study [11].

e. Mitochondrial membrane potential and ROS production

In addition to the direct sites of ROS production within mitochondria, an increasing body of evidence show a strong correlation between mitochondrial membrane potential and ROS generation [19]. These data demonstrate an enhanced ROS generation by mitochondria with high membrane potential. A study of ROS production in Drosophila melanogaster showed that ROS generation by mitochondrial complex I from RET was dramatically diminished by FCCP (mitochondrial uncoupler) with only a small decrease of mitochondrial membrane potential, demonstrating a strong correlation between mitochondrial membrane potential and ROS generation [18]. In contrast, other studies also showed an increase in ROS production associated with a high mitochondrial membrane potential, confirming the role of mitochondrial membrane potential on mitochondrial ROS generation [20, 21].

From above introduction, we know that mitochondrial complex I, II, III, IV can generate ROS in different situations. However, it also should be noted that, limited by the techniques for measuring mitochondrial ROS *in vivo*, so far the studies of mitochondrial ROS generation are largely based on isolated mitochondria or isolated mitochondrial complexes, which cannot be used as evidence to estimate the status of mitochondrial ROS generation *in vivo.* Therefore, the *in vivo* ROS production by mitochondrial respiratory chain (MRC) is still unclear.

1.1.1.2. ROS from NADPH oxidases (Noxes)

Apart from the MRC, another major source of ROS in cells is NADPH oxidases (Noxes). Noxes are found expressed in many tissues and cell types. They were identified as a cluster of trans-membrane proteins, which transport an electron from NADPH to molecular oxygen and form superoxide [22]. Different from mitochondria and other sources that generate ROS as by-products, NADPH oxidases are featured to generate ROS as their main function [23]. The seven members of Nox family named as Nox1, Nox2, Nox3, Nox4, Nox5, Duox1 and Duox2 (dual oxidases), share several conserved structural domains, including an NADPH-binding site, an FAD-binding site, six conserved transmembrane domains and four highly conserved heme-binding histidines (Figure 1-3) [22, 24]. Nox1 to Nox4 have a similar size and structure. Nox5 builds on the structure of Nox1-4 by adding an EF-hand calcium-binding domain at the N terminus. Duox1 and Duox2, in addition to the Nox1-4 homologous domain and calcium-binding region, have an extra transmembrane domain followed by a

peroxidase like homology [22-24] (Figure 1-3). These Nox enzymes are considered to be single electron transporters, that pass one electron from NADPH to FAD, then to the two hemes, and finally to molecular oxygen, generating superoxide, a precursor of other ROS [22].

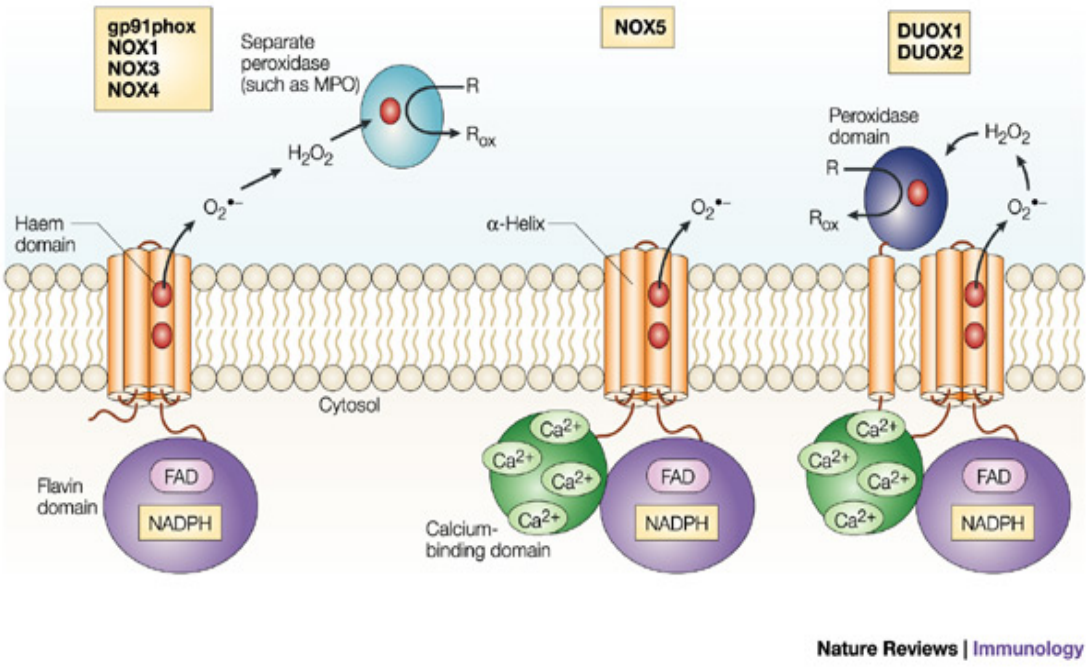

Figure 1-3: Transmembrane domain structure of Nox family enzymes.

Figure shows the main structure of Nox family enzymes, which are all membrane-bound proteins and contain a six transmembrane α-helix domain, an independent cytoplasmic FAD and NADPH binding domain and two haems. Among them, Nox5, Duox1 and Duox2 possess an additional calcium-binding site, while Duox1 and Duox2 also have an extra transmembrane α-helix domain followed by a peroxidase like homology, which are thought to catalyse ROS produced from other Noxes and generate additional ROS forms outside the membrane. In this figure, Nox1, Nox2 (gp91phox), Nox3 and Nox4 are shown as one on the left side, Nox5 is shown in the middle, Duox1 and Duox2 are shown on the right.This figure is from a review paper, published by J. David Lambeth **[24]**.

a. Activation of Nox1 to Nox4

Although Nox family proteins share conserved structural properties, they differ in their mechanism of activation. Briefly, Nox1 to Nox4 are activated by protein-protein interactions, while Nox5, Duox1 and Duox2 are calcium activated (Figure 1-4). The activation of Nox1 to Nox4 requires additional proteins, such as the membrane-bound protein $p22^{phox}$, cytosolic proteins $p47^{phox}$, $p67^{phox}$, small GTPase Rac and $p40^{phox}$. Among all of these proteins, $p22^{phox}$ also called Cyba, functions especially as a common component, required for the activation of Nox1 to Nox4 [22, 24, 25]. It is considered that $p22^{phox}$ helps stabilise Nox proteins for Nox1 to Nox4 and interact with cytosolic factors for only Nox1, Nox2 and Nox3, but not Nox4. Because Nox4 does not need cytosolic components for its activity, it is only $p22^{phox}$ dependent [26].

b. Activation of Nox5, Duox1 and Duox2

Nox5 with its isoforms of NOX5-α, -β, -γ, and -δ are distinguished from Nox1 to Nox4 by the presence of EF-hand, calcium-binding domain at the N terminus, which acts as an independent folding unit and leads to conformational changes in response to elevated intracellular calcium levels. Nox5 does not require $p22^{phox}$ or other cytosolic factors for its activity; it is only regulated by the increase of cytoplasmic calcium [27, 28]. In addition, Nox5-ε, which is a short version of Nox5, lacking of EF-hand domain, has been reported to be able to bind to Nox5-β and functioning as a dominant negative of Nox5 [29, 30].

Duox1 and Duox2 build on the structure of Nox5 with an additional transmembrane domain at the N terminus. Heterologously misexpression experiments have shown that Duox enzymes can generate ROS in HEK293 cells in a calcium dependent manner [31].

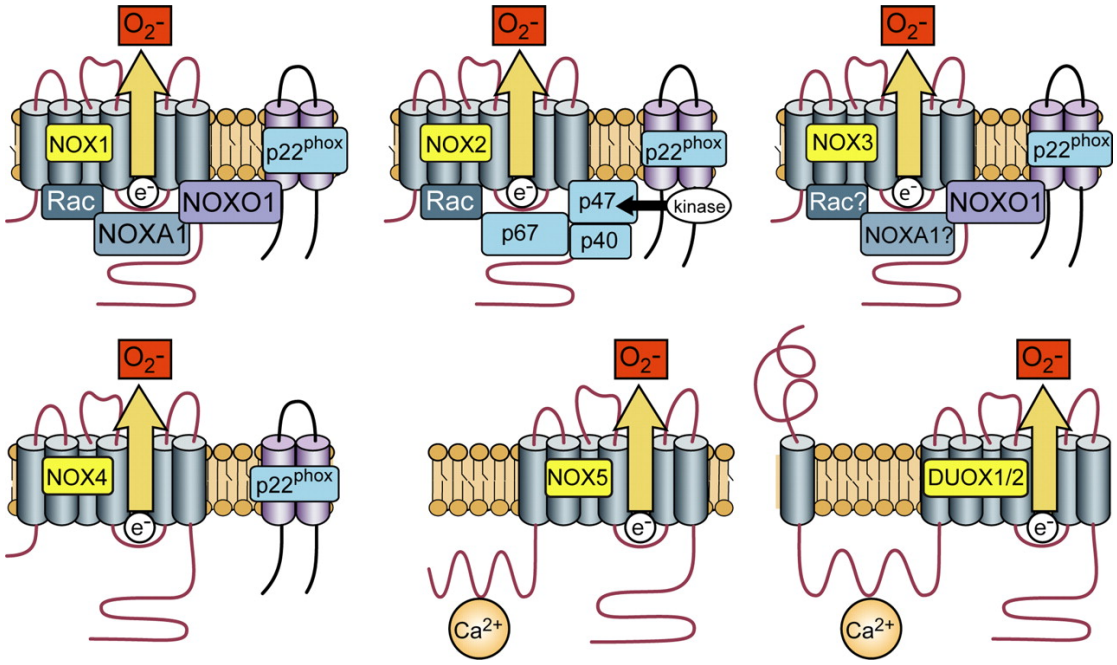

Figure 1-4: Activation mode of NADPH oxidases.

Figure 1-4 shows the activation mechanism of Nox enzymes. Briefly, Nox1 to Nox4 require a common subunit $p22^{phox}$ (showed in light purple colour) to be activated, while Nox5 and Duoxes are directly activated by calcium without requiring other subunits. This figure is taken from a review paper published by Karen Bedard and Karl-Heinz Krause **[22]**.

c. Nox family inhibitors

Diphenylene iodonium (DPI) is the most common inhibitor of Nox enzymes [32]. It inhibits various flavoenzymes and is generally considered to be a fairly nonspecific inhibitor of several electron transporters. Though it inhibits all of the Nox enzymes, at high concentrations it also inhibits other enzymes, such as mitochondria complex I [33], cytochrome P450 monoxygenases [34], xanthine oxidase [35] and nitric oxide synthase [36]. Another commonly used inhibitor of Nox family is apocynin (APO). It functions by forming an inhibitory compound prior to blocking the translocation of cytoplasmic subunits or via inhibiting the assembly of Nox complexes [37]. Though APO has been used as an inhibitor of Nox4 [38] and Nox5 [39], some studies have also shown that APO can act as an antioxidant in endothelial cells and vascular smooth muscle cells, which has raised the question as to its specificity as a Nox enzyme inhibitor [40].

1.1.1.3. ROS from other sources

In addition to mitochondria and Nox family enzymes (the best characterised intracellular sources of ROS), there are a variety of other enzymes that could catalyse the endogenous ROS production, such as xanthine oxidase, cytochrome P450 enzymes, lipoxygenases, nitric oxide synthase and cyclooxygenases. Besides, some organelles, like peroxisome and ER are also reported to produce ROS [7]. However, the contribution of ROS from these sources needs clarification and further research.

1.1.2. ROS elimination

ROS play significant roles in several biological processes but their levels must be kept under strict control as they can also cause severe damage to cells if they are allowed to be produced uncontrollably or reach excessively high concentrations. When the cells fail to balance the rate of ROS generation and scavenging, ROS will accumulate and cause oxidative stress. Oxidative stress can bring damage to one or more biomolecules including proteins, DNA, RNA and lipids. In addition, data show that some human diseases have a relationship with high ROS levels, such as Alzheimer disease [41], Parkinson disease [42, 43], cancer and aging process [44]. Therefore, cells need efficient defence systems to control the intracellular ROS levels in response to cell homeostasis [45]. These antioxidant defence systems that decrease the amount of active ROS in cells can be subdivided into two systems. One involves enzymatic systems, including the family of superoxide dismutase (SOD), catalase, glutathione peroxidase (GPx), peroxiredoxin (Prx) and thioredoxin (Trx) enzymes; the other is non-enzymatic system including glutathione (GSH), Vitamin C, Vitamin E, β-carotene and uric acid [46-49].

1.1.2.1. Enzymatic antioxidant systems

The antioxidant enzymes have different targets and possess distinct functions in different organelles, cells and tissues. For instance, superoxide dismutase family (SOD, Mn-SOD, Cu/Zn-SOD) exists in both cytoplasm and mitochondrial matrix, functioning particularly on converting superoxide to H_2O_2. It displays a more concentrated presence in mitochondrial matrix in the form of Mn-SOD and is believed to be the most important isoenzyme among the SOD family. Catalase and peroxidases (include Gpx) are also primary antioxidant enzymes, which can directly target H_2O_2 and catalyse the decomposition of H_2O_2 to water and molecular oxygen. Catalase is found

in peroxisomes in most eukaryotic cells, whereas peroxidases exist in the cytoplasm, in which Gpx functions in recycling the GSH antioxidant system. Additionally, Trx, a small molecule antioxidant enzyme has been found to exist ubiquitously in many organisms. It functions to facilitate the reduction of proteins and donates electrons to peroxidases and ribonucleotide reductase. Besides, it can be reduced by thioredoxin reductase in a NADPH-dependent reaction, maintaining itself in a reduced state in cells [50]. In brief, the function of these antioxidant enzymes varies from cell types, tissues and organisms.

1.1.2.2. Non-enzymatic antioxidant systems

In addition to the protein-based enzymatic scavengers, cells also have plenty of non-enzymatic molecules, such as GSH, vitamin E, vitamin C, β-carotene and uric acid. Among all of them, glutathione (GSH) is thought to be the most important one [51]. GSH is a small tripeptide with a single cysteine residue and formed by glutamate, cysteine and glycine. It exists in cytosol, nuclei and mitochondria, and has been considered to be the major soluble antioxidant in these cell compartments [52]. GSH can directly react with free radicals in non-enzymatic reactions or functions as electron donor in the reduction of peroxides catalysed by Gpx. It can be recycled through reduction of its oxidised form GSSG by glutathione reductase [53]. In addition to GSH, other non-enzymatic antioxidants also play important roles in protecting cells from oxidative stress. For example, vitamin E functions in protecting against lipid peroxidation, and vitamin C acts in aqueous environment to keep body from oxidative stress [54]. These non-enzymatic antioxidants work together with the enzymatic antioxidants to balance the intracellular redox state and allowing the cells to function properly.

1.1.3. ROS detection

Directly measuring ROS might seem to be the preferred method, but because of the diversity of ROS and their extreme instability, it is complicated and difficult to detect or measure ROS during development. Therefore, early studies of ROS assessment have largely been made by indirectly measuring the products from interactions of ROS with other cellular components [55]. Intracellular redox system includes a complex interaction of reduced and oxidized forms of a variety of molecules, such as NAD(P)+/NAD(P)H, FAD+/FADH, ubiquinones, peroxides and thiols-disulphides glutathione (GSH/GSSG). By measuring relative concentrations of redox molecules

(e.g. NAD(P)+/NAD(P)H, GSH/GSSG), the intracellular ROS levels can be measured indirectly [56]. However, these methods are indirect, nonspecific and may lead to overestimation in intact cells or tissues. As technology developed, many fluorescent probes that target specific component of ROS or total ROS have emerged and have been applied in different cells and tissues. These include some fluorescent dyes, such as dihydroethidium (DHE) and its mitochondrial targeted form (mitoSOX), and dichlorodihydrofluorescein diacetate (DCFH-DA). However, these approaches have limitations. For example, though DHE and mitoSOX are designed to detect superoxide in cells and mitochondria by oxidising superoxide to form a specific fluorescent product 2-hydroxyethidium, they may also form other fluorescent ethidium by nonspecific redox reactions, which can overlap with 2-hydroxyethidium, making superoxide difficult to be distinguished or quantified accurately [57]. For DCFH-DA, although it is popularly used for intracellular H_2O_2 measurement, it cannot be reliable. For one aspect, it does not directly react with H_2O_2; for another aspect it can help generating superoxide and H_2O_2 when being oxidised to DCF [57]. Therefore, more specific and sensitive probes are needed. Amplex Red is one of the reliable probes, which can react with H_2O_2 in the presence of HRP and form highly fluorescent resorufin on an equimolar basis [57]. For this reason, Amplex Red has been extensively applied for ROS assessment in isolated cells, vessels and mitochondria.

Although a variety of methods can be employed for ROS detection, more sensitive methods are still needed for accurately and directly detecting of ROS *in vivo*. Fluorescent protein-based redox probes helped solve this problem to some extent. These ROS sensors can be applied for live imaging of intracellular ROS levels in the cytoplasm or within organelles, contributing to the observation of the dynamic state of intracellular ROS. So far, a number of fluorescent probes sensitive to ROS levels have been developed, as reviewed by Hernandez-Garcia [58]. In particular, a yellow fluorescent protein (YFP) based ratiometric probe, named HyPerYFP was successfully applied for the observation of ROS levels in real time. This genetically encoded ratiometric probe, containing a bacterial H_2O_2 sensitive OxyR domain and fused with a circularly permuted YFP, is highly specific to H_2O_2 over other ROS [59]. HyPerYFP has a single emission, peaking at 520 nm, and two separate excitations, peaking at 420 nm and 500 nm. It can have a reversible conformational change in response to the ROS levels within cells and can be detected by microscopy imaging. Either strengthened or weakened signal of H_2O_2 can be easily detected through HyPerYFP ratiometric analysis [60]. However, a weakness of this ROS sensor is that it is also pH sensitive, therefore parallel experiments on measuring pH status need to done when performing HyPerYFP based ROS detection [59]. Another ROS sensor similar as HyPerYFP is

roGFP. It is built up by inserting cysteine residues into appropriate positions of the green fluorescent protein (GFP), which lead to reversible formation of disulfide bonds according to the intracellular redox state. Either formation or breakdown of these cysteine bridges will change the structure of fluorescent protein, and then the redox potential can be monitored by the altering fluorescence. Same as HyperYFP, roGFP has two fluorescence excitation maxima at about 400 and 490 nm, which can respond to changes in local redox states by displaying rapid and reversible ratiometric alteration in fluorescence [58] .

The detection of mitochondrial generated ROS build on distinct ROS sensors by adding a triphenylphosphonium (TPP) cation component, which helps accumulation of these ROS reporters within mitochondria. Commonly used mitochondrial targeted ROS probes include mitoSOX [57], mitoHyPer [61] and mitoB. As described previously, mitoSOX has its limitation on ROS detection, but it can be used as a good probe when quantifying ROS with mass spectrometry. MitoB is a ratiometric mass spectrometry probe. It is converted to mitoP when being oxidised and upon measuring the amount of mitoP versus mitoB, we can quantify the concentration of H_2O_2 generated within mitochondria [62]. MitoHyPer is created by adding a TPP moiety on HyPerYFP, and has been used for *in vivo* mitochondrial ROS detection.

1.1.3.1. Application of HyPerYFP in Xenopus

As introduced above, HyPerYFP can be used in live cells as an approach to visualise intracellular ROS levels. Nick Love and colleagues generated a transgenic line in *X. laevis*, which could ubiquitously express HyPerYFP from CMV promoter, making the observation of the dynamic of ROS in Xenopus possible [63]. The F0 transgenic X. laevis were generated using REMI [64] with SwaI and a CMV:HyPerYFP plasmid, and F0 successfully passed the gene to F1 generation. The figure below showed F1 generation tadpoles expressing HyPerYFP and had an increased HyPer ratio in response to H_2O_2 treatment.

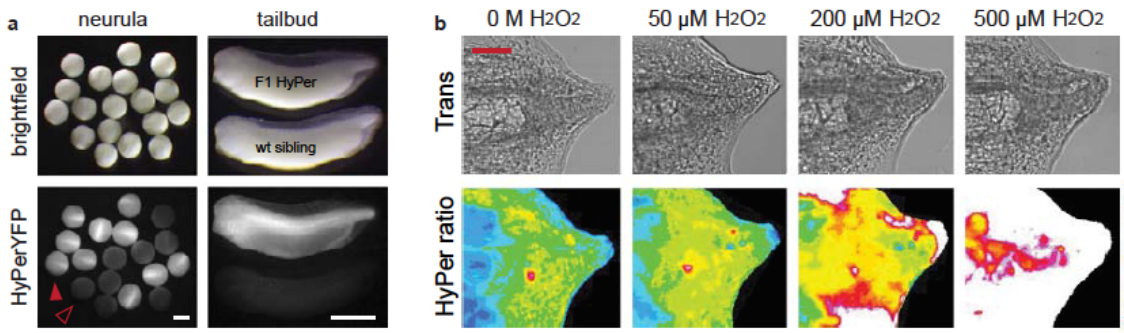

Figure 1-5. Application of HyPerYFP in *X. laevis* tadpoles.

Panels show HyPerYFP expressing F1 generation embryos. (a) Panels show brightfield and fluorescent images of F1 HyPerYFP transgenic siblings versus nontransgenic siblings at the neurula and tailbud stages. Closed red arrow points to the transgenic HyPerYFP expressing embryos and open red arrow points to the non-transgenic siblings. Scale bar is 1000 micron. (b) Panels show a regenerating tail and its HyPerYFP imaging in transgenic tadpoles at 48 hours after amputation after exposure to increasing H_2O_2 concentrations. Scale bar is 200 micron. This figure is a reproduction of data published by Love et al. **[63]**.

1.1.4. Role of ROS in biological processes

It has been reported that ROS participate in various cellular processes in response to extracellular and intracellular signals. As introduced, ROS can be produced by numerous enzymes and can be removed quickly by antioxidant systems for redox state balance. Any alterations of intracellular ROS levels will induce a cellular signal, which can either damage cells or be used as intracellular messengers to regulate the activities of several proteins, including several transcription factors. In general, ROS play key roles in initiating and responding to various biological and cellular processes across the animal kingdom.

1.1.4.1. ROS and proliferation

ROS exhibit a dual effect in cell proliferation, in which low levels are required for cell growth, while high levels lead to apoptosis or necrosis. In particular, low levels of H_2O_2 and superoxide, usually submicromolar concentrations, have been reported to promote proliferation of smooth muscle cells, fibroblasts, amnion cells and aortic endothelial cells [6]. In contrast, higher concentrations of ROS have been found to arrest cell growth and even induce cell death when they fail to adapt the oxidative stress [65]. These results suggest intracellular ROS levels greatly affect cell activities and a certain level of ROS is necessary for cell proliferation. However, the mechanism of how ROS regulate cell proliferation is less well understood. David et al. suggest that one possibility is that ROS can participate in growth factors induced proliferation [66-68]. Another possibility is that ROS may oxidise components involved in proliferation relevant signalling cascades, such as MAPK pathways [69, 70].

1.1.4.2. ROS and differentiation

A role for ROS in cell differentiation has been described in a variety of cell lineages [71-73], in which differentiation can be induced by increased ROS levels [74]. For example, Sardina et al. showed that ROS generation is activated immediately during the process of megakaryocyte differentiation in K562 and HEL cell lines and human CD34(+) cells. Besides, inhibition of this ROS by antioxidants or the Noxes inhibitor DPI prevented megakaryocyte differentiation [75]. Another report also described the role for ROS in regulating differentiation in human embryonic stem cells (hESCs) [76]. The authors found that continuous exposure to ROS could diminish pluripotency of hESCs, and induce hESCs to differentiate into bi-potent mesendoderm, which could be further specified to mesoderm or endoderm via ROS induced MAPK or AKT signalling [77]. These results provide evidence for a role of ROS in cell differentiation and cell fate determination, as well as a role in maintaining the pluripotency of embryonic stem cells.

1.1.4.3. ROS and aging

It is known that mitochondria are a major source of ROS, but this production is a double-edged sword, as mitochondria may also face oxidative damage from the excessive ROS they produce. In 1951, Harman first proposed the hypothesis that ROS (superoxide and H_2O_2) might be a cause of aging [78]. In the subsequent decades, it was widely reported that aging process couples with accumulation of oxidised nuclear, mitochondrial DNA (mtDNA), proteins and lipids from yeast to human, suggesting a negative role of ROS as a cause of aging [79, 80]. In addition, research on antioxidant systems also was consistent with a role for ROS in regulating longevity in lower organisms. In particular, overexpression of antioxidant enzymes, like SOD or catalase, can increase the life-span of *C. elegans* [81], whereas elimination of antioxidant enzymes (Cu/Zn-SOD) can result in a 80% decrease of life span in Drosophila [82]. Besides, a number of aging-related pathways and proteins, such as insulin/ insulin-like growth factor-1 (Ins/IGF-1) signalling pathways, have been shown to cross talk with ROS during aging and longevity determination [83]. All of these data implicate that ROS are involved in the aging process and may contribute to longevity determination.

1.1.4.4. ROS and apoptosis

Apoptosis or programmed cell death is an evolutionarily conserved and synchronised form of cell death, which functions in facilitating the deletion of redundant, infected, injured or malformed cells during the normal life span of metazoans [84]. It is essential for maintaining homeostasis in multicellular organisms. In vitro studies showed that many stimuli including exposure to physical and chemical agents or removal of growth factors could induce apoptosis as reviewed by Sharon Clutton [84]. In 1991, Pierce et al. first reported that apoptosis can be induced by H_2O_2 and prevented by catalase in blastocyst [85]. After that, many studies confirmed this and showed that ROS could induce apoptosis in distinct cell types. For example, Kasahara reported that in neutrophils, H_2O_2 contributes greatly in apoptosis induction and this process can be inhibited by catalase [86]. Besides, increased intracellular glutathione levels could prevent Fas receptor-triggered apoptosis in activated human neutrophils [87]. In 2005, *in vivo* evidence of ROS function on apoptosis in mice supported $P66^{shc}$ (genetic determinant of life span in mammals) triggered mitochondrial ROS (H_2O_2) as signalling molecules for apoptosis. By using genetic deletion $P66^{shc}$ of mouse, Marco et al. found that $P66^{shc}$ enables decreasing equivalents of mitochondrial electron transfer chain via oxidation of cytochrome *c* and triggered mitochondrial apoptosis [88]. These results

show that ROS can induce apoptosis and function as key molecules of signalling pathways by targeting or activating cell death regulators [89].

1.1.4.5. ROS and wound healing

The entire process of wound healing is a complex series of events that occurs simultaneously following injury, and continues for months to years. Normal wound healing progresses is defined in three phases, namely the inflammatory phase, proliferation phase and remodelling phase [90, 91]. In mammals, after an injury, the first step is haemostasis, during which, platelets will initiate a clotting cascade and release chemotaxic factors, such as platelet-derived growth factor (PDGF) and transforming growth factor-beta (TGF-β) to recruit more platelets, fibroblasts and inflammatory cells. Initially, leukocytes and monocytes will migrate to wound region and dominate the inflammatory cell population, but later, they are replaced by macrophages [91]. Then, reepithelialisation occurs and keratinocytes migrate across the wound area. Following this, fibroblasts and endothelial cells undergo fibroplasia and angiogenesis, respectively. Finally, tissue maturation or remodelling takes place, which increases the tensile strength of skin and culminates in a mature scar [92].

Numerous experimental and clinical results have suggested that ROS play critical roles during the process of wound healing including oxidative killing of bacteria, reepithelialisation, angiogenesis, and collagen synthesis [92-94]. Recently, a study in zebrafish suggested a potential role for H_2O_2 during wound healing. This paper reported that a rise in H_2O_2 occurs immediately after wounding at the wound margin and this rise helps coordinate the inflammatory response during wound healing. In particular, they demonstrated that this gradient of H_2O_2 is created by dual oxidase (Duox) in epithelial cells, and required for rapid recruitment of leukocytes to the region of wound. This result also supported the idea that wound margin H_2O_2 production is involved in the rapid recruitment of leukocytes, either through direct chemotactic signalling [95] or via indirectly stimulating a downstream chemoattractant. Thus, H_2O_2 may act as a paracrine, in the early phase of wound healing [60].

1.1.4.6. ROS and regeneration

Regeneration is a process involving regrowth and restoration of cells, which usually contains rearrangement of pre-existing tissue, dedifferentiation, cell proliferation and differentiation. Amphibian embryos have an incredible ability to heal wounds and

regenerate new tissues. For example, tadpoles can regrow a new tail following amputation within nine days. Using Xenopus as a model, Nick R. Love and Yaoyao Chen et al. found that ROS are required for tail regeneration. The same as the case in zebrafish, they observed an increase of H_2O_2 at wound edge of amputated tadpoles, and this ROS was sustained throughout the whole process of tail regeneration. Lowering this injury induced ROS levels with antioxidant or Nox inhibitors, such as DPI, disrupted tail regeneration, suggesting a critical role for ROS production in regulating regeneration and tissue remodelling [63].

1.1.4.7. ROS and embryonic development

Embryonic development starts with fertilization and requires a highly coordinate regulation of various growth factors and signaling pathways. Very little is known about the potential roles of ROS during early embryonic development. However a few isolated studies have suggested that ROS might play roles during early development, although the studies have been somewhat contradictory. For example, experimentally induced ROS production impairs embryo development using *in vitro* cultured mammalian embryos [56]. However, other studies have suggested that a pulse of H_2O_2 has a positive role in promoting bovine embryos development [96]. In addition, a burst in ROS production in both *in vivo* and *in vitro* mouse embryos has been documented [96]. These results, although contradictory, point to a potential role for ROS during early embryonic development. Apart from these results in mammalian embryos, *in vivo* studies using sea urchin and the Devil Stinger (a marine fish) zygotes showed that fertilisation in both was associated with a burst in ROS production [97-99]. In the sea urchin, the fertilisation-induced generation of H_2O_2 is dependent on a specific Nox enzyme, called dual oxidase, Udx1. Further analysis in the sea urchin showed that ROS levels are unequally distributed in sister blastomeres during early embryogenesis. Also inhibiting Udx1 activity resulted in a delay of cleavage, suggesting a functional role for Udx1 induced ROS during early embryogenesis [98]. Despite these experiments, little is known about the role for ROS during embryonic development.

1.1.4.8. ROS and Warburg effect

In normal cells, energy (ATP) is primarily generated in mitochondria via oxidative phosphorylation, whereas in most cancer cells, instead of relying on oxidative phosphorylation, they use aerobic glycolysis for energy generation, even in the presence of oxygen. This phenomenon is called Warburg effect [100]. In contrast to

normal cells, cancer cells use high rate of glycolysis followed by lactic acid fermentation in cytosol to fuel themselves. This process only generates 2 ATPs compared to 36 ATPs yields per molecule of glucose in complete oxidation of pyruvate to carbon dioxide inside mitochondria [100]. An interesting phenomenon accompanies the Warburg effect is the increased steady-state ROS condition in cancer cells [101]. It is reported that cancers exhibit an increased but non-toxic ROS. As introduced above, a certain ROS levels would promote cell proliferation across a variety of cell types [6].
It is unknown why cancer cells switch to a low efficient metabolism and exhibit an increased ROS. Whether there is a link between ROS and metabolism needs further study.

1.2. *Xenopus laevis* as a model system

Xenopus laevis (*X. laevis*) is a species of aquatic frog of the genus Xenopus from South Africa, which is an excellent model system to study early vertebrate development, the process of wound healing, tissue repair and regeneration [102, 103]. Because of its features as an amphibian, Xenopus is easy to be maintained in the lab, and can lay large quantities of eggs upon stimulation with hormone injection. Besides, due to the large size of oocytes / embryos (around 1.2 mm in diameter) and external development, they are much easier to be manipulated and observed than mammalian embryos, making them a good model for investigating the cellular and molecular mechanisms of early vertebrate development [104]. In addition, the genome of Xenopus has been sequenced, which provides large amount of information on Xenopus genes [105], facilitating gain and loss of function studies [106]. Moreover, Xenopus exhibits a high level of genetic similarity to humans, making it also a good system for modelling human diseases. Several additional aspects make this system particular suited for the study of the role of ROS during early vertebrate embryogenesis. This includes the availability of a transgenic HyPerYFP line that permits in vivo imaging of ROS levels throughout development, and the ability of incubating embryos with chemical inhibitors, oxidants and antioxidants.

1.2.1. An overview of early embryonic development of *X. laevis*

Embryonic development involves a diverse number of cellular and molecular processes, and a variety of signalling events. It starts when the mature oocyte / egg is fertilised, which initiates a number of cellular processes, including cell division, pattern formation, morphogenesis, cell differentiation and growth, all of which lead to the

development of a multicellular embryo. *X.laevis* embryonic development has been subdivided into cleavage stage, blastula stage, gastrula stage, neurula stage, tailbud stage and tadpole stage [104, 107]. Here we briefly summarise several important processes during early embryogenesis of *X. laevis*, including oocyte maturation, fertilisation, cleavage, blastula formation, gastrulation and mesoderm formation.

1.2.1.1. Oocyte maturation and fertilisation

X. laevis oocytes are visibly polarised cells with a darkly pigmented animal hemisphere and an unpigmented vegetal hemisphere. In 1972, James N. Dumont subdivided oogenesis *X. laevis* into six stages (I – VI), where he clearly described the appearance and main events during oocyte development [108]. This process can take several months until the oocytes are fully grown (St. VI) and arrested in prophase of meiosis I. At this point the oocytes reach their maximal size (1.3 mm in diameter) with a large nucleus (300-400 nm in diameter), which is called the germinal vesicle. The fully grown oocytes, which are called immature oocytes, remain arrested within the ovary for a long period until they receive hormone stimulation, which stimulates their re-entry into meiosis from prophase of meiosis I, until they arrest again at meiosis II. At this point they are called mature oocytes and at this point the mature oocytes progress through the oviduct and are ovulated (laid) from the female. As they progress through the oviduct, they acquire their jelly coat and they are now competent for fertilisation [109, 110]. In Xenopus, oocyte maturation is induced by the steroid hormone progesterone, therefore *in vitro* collected immature oocytes (St. VI) can be induced for maturation with progesterone and successfully matured oocytes can be identified with a white spot at the animal pole, which corresponds to the displacement of cortical pigment granules where the meiotic chromosomes, arrested in metaphase of meiosis II are located. Thus maturation of the oocyte is associated with the breakdown or disassembly of the germinal vesicle, a process referred to as germinal vesicle break down (GVBD) [109, 111].

Fertilisation begins with sperm entry, which activates the eggs and induces their re-entry into the cell cycle from anaphase and the expulsion of the second polar body. This egg-activation process is accompanied with a calcium wave, which is important for fertilisation and egg activation, and is also a prerequisite for subsequent fertilisation events, such as the cortical granule exocytosis that blocks polyspermy [112, 113]. The mechanisms regulating calcium release and downstream events during fertilisation may vary among species. For example, one important signalling pathway that drives

this calcium increase at fertilisation is mediated by IP_3 receptor, which initiates a single calcium wave from ER in eggs of fish, sea urchin, jelly fish and Xenopus. However, in mouse eggs, it is thought that sperm-specific PLCξ is responsible for the induction of a series of calcium oscillations, which is different from the situation in Xenopus [113].

1.2.1.2. Cleavage and blastula formation

Shortly after fertilisation, a transient contraction of highly pigmented animal cap occurs associated with the extrusion of the second polar body, and eggs subsequently begin a number of rapid cell divisions with no growth. The first cell division happens after 90 minutes post fertilisation, during which time male and female pronuclei fused. After the first cell cycle, *X. laevis* embryos carry out the next eleven divisions quickly and synchronously with an interval time of 20-30 minutes and form a ball of around 4000 cells with blastocoel cavity. During this period, no recognisable G1 or G2 phase is observed in the cell cycle and most of the embryonic genome is silent [114]. As a result, the *X. laevis* blastula forms at stage 7-8 after 4-5 hours post fertilisation. Before or during this stage, most of the downstream cascades of signalling pathways, such as Wnt, MAPK and Smad signalling are not activated, and the development is depending upon maternal mRNAs and proteins [115]. After the twelfth cell cycle, cell divisions become asynchronous, gap phases reappear and zygotic transcription starts. This stage is called the mid-blastula transition or MBT [114].

1.2.1.3. Gastrulation and mesoderm formation

After the blastula stage, gastrulation begins at about stage 10 and ends at stage 13. During gastrulation, a complex set of movements ensues, which rearranges the position of the three germ layers, such that the ectoderm lies on the outside, mesoderm in the middle and endoderm in the inside of the embryo. This process begins when the dorsal lip of the blastopore forms, and then the dorsal marginal zone tissue including both dorsal mesoderm and endodermal cells begin to involute. The polarization of anterior-posterior and ventral-lateral are also determined during this period (Keller 1991). Signalling pathways are also activated to promote cell proliferation and cell fate specification [116].

In Xenopus embryos, mesoderm is induced from cells in the marginal zone (the equator of the sphere) in response to signals secreted from the vegetal hemisphere, converting a band of ectoderm cells to mesoderm. At mid-blastula stage, the maternal

transcription factors, such as VegT and β-catenin, activate the expression of Nodal-related zygotic genes, generating a gradient of Nodal-related molecules expressed in the endoderm. This gradient induces the formation of overlying mesoderm. Low doses of Nodal-related molecules (Xnrs) lead to the formation of ventral mesoderm, while high doses lead to the establishment of Spemann's organizer (Figure 1-6) [117]. After induction, mesoderm is maintained by FGF family members, and is further patterned during gastrulation through both activation and inhibition of BMP signalling [118].

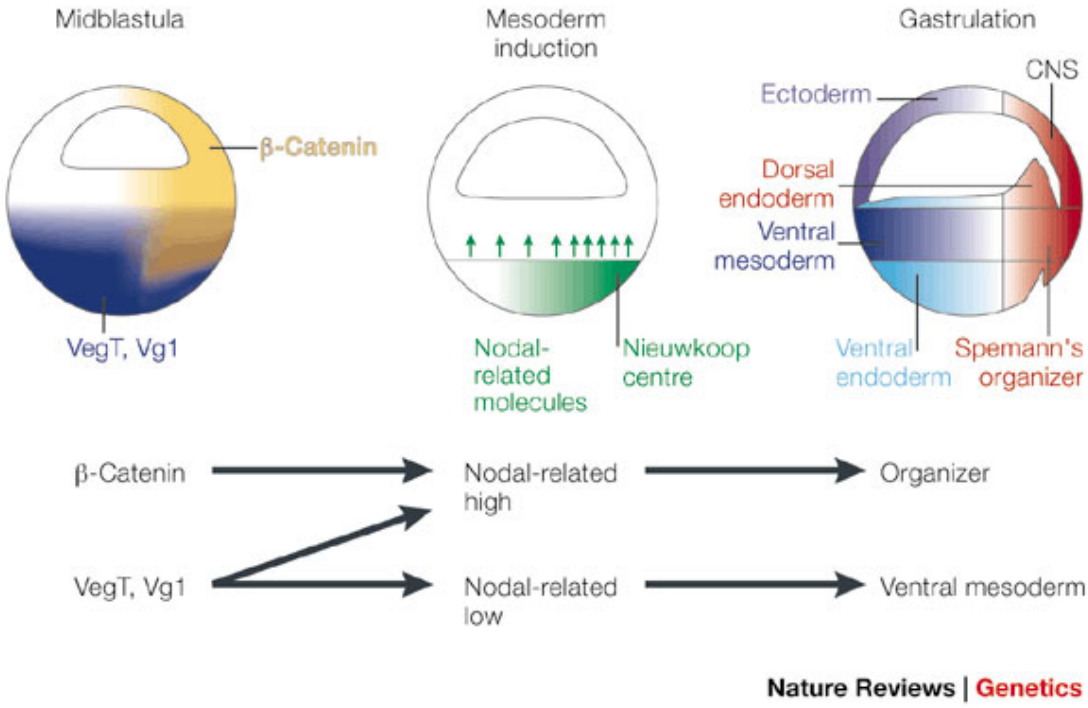

Figure 1-6: Xenopus Mesoderm induction.

The left side figure shows the localization of mesoderm induction related maternal transcription factors at the midblastula stage, in which β-Catenin distributed on the dorsal side of the embryo, VegT and Vg1 are limited at vegetal region. Figures in the middle shows a gradient of Nodal-related molecules expressed in the endoderm, sending signals for mesoderm induction. Nieuwkoop's centre is the region of dorsal endoderm that induces organizer tissue. The right side figure shows at the gastrula stage, the organizer secretes a cocktail of factors that refine the initial patterning. CNS stands for central nervous system. The figure shown here is taken from a review paper published by Edward M. De Robertis et al. [117].

As gastrulation proceeds, the neural ectoderm is induced by the underlying dorsal mesoderm, also called Spemann organiser. A thickened flat region of ectoderm will form all the components of central nervous system and the edges of neural plate will form the neural crest. Neurulation then processes between stages 14 and 20, during which the neural plate folds to form the neural tube [104, 119, 120].

1.2.2. Primary signalling pathways during early embryonic development of *X. laevis*

Embryonic development is a complicated process involving a variety of cellular activities, such as cell division, cell differentiation, cell growth, pattern formation and morphogenesis. These developmental processes need to be accurately regulated to trigger or turn off downstream gene expression, hence ensuring normal embryonic development. Signalling pathways act critically to fine-tune these cellular events in response to extracellular signals and this coordination is of great significance for proper cell fate specification, tissue formation, body patterning and organogenesis. In particular, these important signalling pathways include Wnt/β-catenin signalling, FGF signalling, PI3K/Akt signalling, TGF-β/Nodal signalling and BMP signalling.

1.2.2.1. Wnt/β-catenin signalling pathway

Wnt signalling has long been appreciated to play an important role in both axis determination and patterning of mesodermal tissues in Xenopus. It can be separated into the canonical Wnt signalling (Wnt/β-catenin signalling) and non-canonical Wnt signalling pathways (Figure 1-5), both of which are of significant importance in regulating different aspects of embryonic development. Canonical Wnt signalling is usually activated by Wnt1, Wnt3, Wnt8 and Wnt11 ligands after binding to Frizzled (Fz) receptors and receptor-related protein LRP5/6, ultimately activating β-catenin signalling pathway. Non-canonical Wnt signalling generally functions independently of β-catenin transcriptional activity, and are often activated by another set of Wnt ligands, such as Wnt5. In vertebrates, at least two non-canonical Wnt pathways were described; one is planar cell polarity (PCP) pathway, the other is Wnt/Ca^{2+} pathway, which involves calcium, PKC and G proteins. These non-canonical Wnt pathways have been reported to participate in modulation of developmental processes, such as convergent extension movements, neuronal and epithelial cell migration and cytoskeleton organisation [121-123].

Canonical Wnt signalling plays an important role in a variety of physiological and pathological processes through its capacity to regulate genes involved in cellular specification, proliferation and differentiation. During embryogenesis in Xenopus, Wnt/β-catenin signalling begins very early and persists throughout development, where it is involved in various developmental processes [124]. The first role for Wnt/β-catenin signalling is during the establishment of the dorsal-ventral axis. Depletion of maternal β-catenin results in the loss of dorsal structures. Further evidence for this role comes from ectopic expression of β-catenin in the ventral side, which induces the formation of a secondary axis with full anterior structures [125]. Furthermore, Janet Heasman and colleagues found that one of the Wnt ligands, Wnt11, could specify dorsal axis formation in Xenopus embryos. Through gain and loss of function analyses, they showed that maternal Wnt11 works upstream of β-catenin, and is both necessary and sufficient for axis specification, confirming a role for maternal Wnts in controlling embryonic development [126]. In addition to the regulation of axis formation, Wnt/β-catenin signalling is also involved in anterior-posterior patterning, whereby inhibition of Wnt/β-catenin and BMP signalling at the anterior mesendodermal region is required for Xenopus head formation. Ectopic expression of Wnt8 after MBT causes loss of head, and overexpression of a dominant negative Wnt8 strongly suppresses posterior neural marker expression. Further research also showed that the proteins, FrzB and Dkk, acting as Wnt inhibitors, are expressed in the anterior mesendoderm to inhibit Wnt/β-catenin signalling. These data suggest the importance of Wnt/β-catenin signalling in modulating anterior-posterior patterning in vertebrate embryogenesis.

In 2006, Funato et al. demonstrated that Wnt signalling could be modulated by the redox state. They showed that thiredoxin (Trx) family protein, nucleoredoxin (Nrx) could interact with Dishevelled (Dvl) to regulate canonical Wnt signalling. Overexpression of Nrx suppresses Wnt/β-catenin pathway, whereas inhibition of Nrx induces Wnt/β-catenin downstream gene expression. In addition, H_2O_2 could disassociate the interaction of Nrx and Dvl, enabling β-catenin accumulation, leading to the enhancement of canonical Wnt signalling [127]. These data implicate a role for ROS levels and canonical Wnt signalling via redox-sensitive association of Nrx and Dvl. Another group confirmed this result in mouse intestinal cells. They found that Wnt3a could induce a rapid Noxes dependent superoxide generation, which can inactivate Nrx by oxidation, thereby promoting dissociation of Nrx from Dvl and activating canonical Wnt signalling [128]. However, another group had an opposite results based on *in vitro* experiments of HEK293 cells. They found that H_2O_2 treated cells displayed a reduction of nuclear β-catenin, implicating that extracellular ROS may follow a different

mechanism to negatively regulate canonical Wnt signalling [129]. All of these data demonstrate a role for ROS in regulating Wnt/β-catenin signalling pathway.

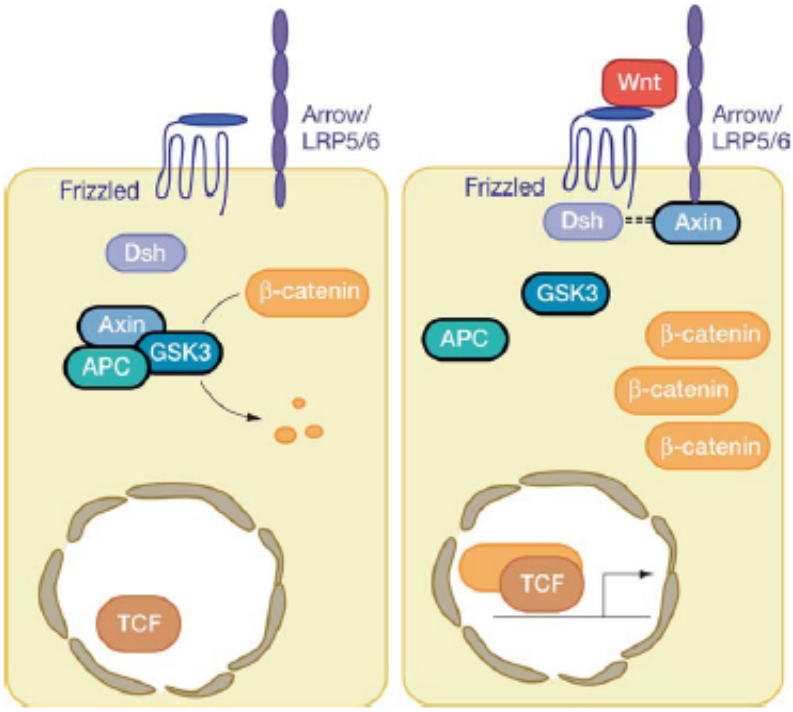

Figure 1-7: The canonical Wnt signalling pathway.

This figure shows the status of Wnt/β-catenin signalling being inhibited (left) and activated (right). When activated, Wnt ligands bind Fz/LRP receptor complexes, which leads to the association of Dishevelled (Dvl) to the complex, ultimately resulting in the stabilisation of β-catenin in the cytoplasm. As the levels of β-catenin rises, it translocates to nucleus and forms a complex with TCF/LEF, thereby promoting the expression of genes that are regulated by TCF/LEF. In contrast, when canonical Wnt signalling is inhibited, cytoplasmic β-catenin is targeted to degradation by the Axin-APC-Gsk3β complex. Negative regulators are outlined in black. Positively acting components are outlined in colour **[130]**.

1.2.2.2. FGF signalling pathway

The fibroblast growth factors (FGFs) are a family of small heparin-binding growth factors. In vertebrates, 22 family members of FGFs have been identified, and can be grouped into seven subfamilies according to their sequence similarities and functional properties. They bind to and activate a conserved family of FGF receptors (FGFRs),

which consist of receptor tyrosine kinases (RTKs) [131]. The activity of FGF signaling is mediated by the binding specificity of ligands and receptors, but is also modulated by additional cofactors. For example, heparin sulfate (HS) glycosaminoglycans (GAGs) can associate with FGFs and FGFRs to form a 2:2:2 FGF-FGFR-HS dimers, which allow the cytoplasmic kinase domains to transphosphorylate one another, thereby activating them [131]. This activation of FGFRs triggers a variety of cytoplasmic signalling cascades, which are involved in a multiple processes, such as embryonic development, tumour growth and wound healing [132, 133]. During embryonic development, FGF signalling functions importantly in induction and maintenance of mesoderm and neuroectoderm, regulation of morphogenetic movements, anteroposterior patterning, somitogenesis and the organogenesis [133]. A brief summary of FGF signalling during Xenopus embryogenesis is given below.

a. FGF signalling in mesoderm formation and gastrulation movements

Early experiments showed that a number of downstream effector proteins of FGF signalling are required for mesoderm development, and inhibition of them can disrupt mesoderm formation, leading to posterior and gastrulation defects. For example, overexpression of a dominant negative FGFR caused specific defects in gastrulation as well as deficiencies in posterior development, and overexpression of wild type FGFR rescued these developmental defects, suggesting that FGF signalling is essential for early embryonic development, especially in the posterior and lateral mesoderm formation [134]. To further distinguish the role for FGF signalling in initial inducing mesoderm formation or maintaining this formation, Fletcher and Harland carried out experiments by repressing FGF signalling before mesoderm induction, and they found that FGF is necessary for both establishment and maintenance of *brachyury* (*bra*) expression and contributes to the development of distinct types of mesoderm [135].

In addition to its role in mesoderm formation, FGF signalling also plays an important role in regulating cell movements during Xenopus gastrulation. It functions by directly modulating cell movements during convergent extension and indirectly mediating through *bra*. Direct modulation was proved by gain of function analyses of *Sprouty2,* an intracellular antagonist of FGF-dependent calcium signalling. Overexpression of *Sprouty2* blocked convergent extension in gastrulation but without affecting mesoderm induction and patterning [136]. For indirect modulation, FGF signalling functions by

controlling the expression of *bra*, which then activates *Wnt11* expression and mediates convergent movements via non-canonical Wnt signalling [132].

b. FGF signalling in axis specification

In addition to its role in regulating mesoderm formation, FGF signalling is also found to mediate the specification of dorsoventral and anteroposterior axes. For specifying the dorsoventral axis, evidence showed that FGF ligands, in particular FGF4, FGF8 and FGF20, are expressed in the animal (dorsal) part but not in vegetal (ventral) part of the marginal zone. Also, FGF dependent activation of Erk is limited in the animal sector of the marginal zone during gastrulation. Moreover, FGF is thought to promote dorsal fates and inhibit ventral fates by limiting the activity and expression of BMP signalling in Xenopus and zebrafish [133, 137]. All of these data suggest a regulatory role of FGF signalling in dorsoventral axis specification. For determination of anteroposterior (AP) axis, FGF has been considered as a regulator of AP axis establishment in Xenopus embryos. It has been found that FGF has a strong posteriorising effect on neuroectoderm in Xenopus, zebrafish, chick and mouse. In addition, *FGF4* and *FGF8* have been reported expressed in posterior mesoderm as endogenous posteriorising factors [132, 133]. Together, these data suggest a role for FGF signalling in modulating axis specification during Xenopus embryogenesis.

1.2.2.3. TGF-β and BMP signalling pathways

Transforming growth factor beta (TGF-β) family consists of two subfamilies: the TGF-β subfamily and the bone morphogenetic protein (BMP) subfamily, both of which are important for Xenopus early embryonic development (Figure 1-6). TGF-β subfamily ligands including TGF-β1, TGF-β2, TGF-β3, Activins and Nodals, have been reported acting as morphogens to turn on the expression of different downstream genes in a concentration dependent manner [138]. The BMP subfamily including BMP2, BMP4 and BMP7, functions in mediating cell fates specification in the neural or other ectodermal derivatives, as well as patterning the ventral and lateral mesoderm [139, 140]. These two pathways share a great similarity in their membrane receptors and follow a similar activation mechanism. Generally, the TGF-β subfamily ligands stimulate phosphorylation of Smad2/3. The BMP subfamily ligands trigger phosphorylation of Smad1/5/8 [141].

In Xenopus embryos, maternally derived transcription factor VegT, cooperates with β-catenin to activate the expression of zygotic genes Vg1 and Xnr. Vg1 and Xnr3 are transcribed and expressed in vegetal pole, which build up a gradient of nodal signal concentrated from dorsal side to ventral side. This graded nodal signal could induce

dose dependent mesendoderm formation, resulting in dorsal specification with higer signal levels [142]. Except for specifying and patterning mesoderm, the nodal signalling pathways are also required for specifying and patterning endoderm, facilitating gastrulation movements and building the left-right asymmetry. While BMP signalling is involved in determination of neural tissue formation from other ectodermal cell fates, and patterning the ventral and lateral mesoderm [138, 141, 143].

A recent study in human lung fibroblasts showed that mitochondria-derived ROS are required for TGF-β mediated gene expression in fibroblasts. Genetically disrupting mitochondrial complex III produced ROS lead to reduction of TGF-β induced profibrotic gene expression [144]. Moreover, blocking mitochondria ROS generation also inhibited *Nox4* expression, which has been reported to be required for TGF-β regulated gene expression [145].

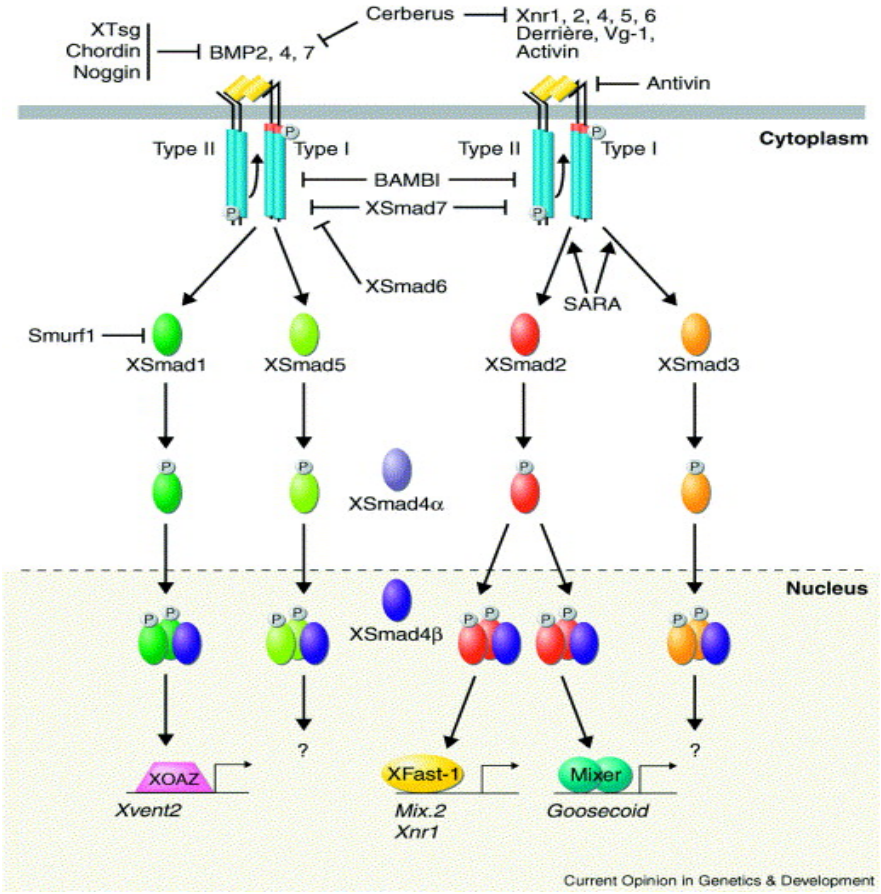

Figure 1-8: TGF-β/Nodal and BMP signalling in early Xenopus development.

This figure shows the signal transduction cascades in BMP signalling (on the left) and the activin signalling (on the right) **[141]**.

1.2.2.4. PI3K/Akt signalling

PI3K signalling plays a pivotal role in cell proliferation, cell growth and survival in response to growth factor, hormone and cytokine stimulation. It consists of two subunits: the p110 catalytic subunit and the p85 regulatory subunit. PI3K can be activated by various growth factors, such as EGF, PDGF, VEGF, etc. [1]. When activated, PI3K catalyses the synthesis of the second messenger PIP_3, which can associate with various proteins containing PH domains, such as PDK and AKT, and activates numerous molecular signals [1]. During early embryogenesis of Xenopus, PI3K/Akt signalling is important for gastrulation, in particular, the catalytic activity of PI3K is required for definition of trunk mesoderm during the blastula stage [146]. In addition, PI3K signalling regulates gastrulation via ErbB signalling [147]. Moreover, Peng et al. reported that ectopic expression of PI3K could induce a second head and axes in Xenopus embryos with enhanced expression of neural markers. Overexpression of an active form of Akt, a major downstream target of PI3K, also induced a duplication of axes and an increased expression of neural markers, suggesting that PI3K regulate axis formation and neurogenesis via Akt. Through further investigation, they found that Akt, transduce this signal via regulating GSK3β, a negative regulator of canonical Wnt signalling, suggesting a connection between PI3K/Akt signalling and Wnt/β-catenin signalling in vertebrate embryonic development (Figure 1-9) [148].

Recent studies have shown that H_2O_2 can directly oxidise and inactivate several phosphatases by oxidising cysteines in their catalytic site, thus modulating the activation state and/or sustained activity of signalling lipids [149]. Among these phosphatases, PTEN can dephosphorylate PIP_3 to PIP_2, thereby functioning as a negative effector of PI3K/Akt signalling [150]. Therefore, PI3K signalling can be regulated by ROS through oxidation of PTEN.

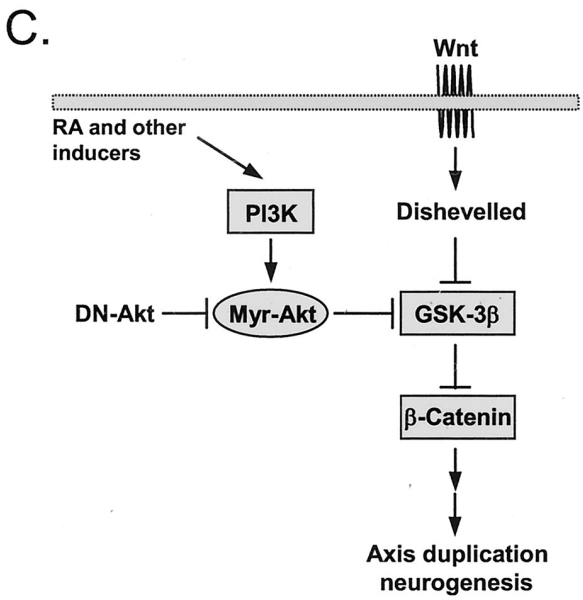

Figure 1-9: PI3K, Akt and Gsk3β in regulating axis formation and neurogenesis in *X. laevis*.

Figure shows that PI3K signalling contributes to axis formation neurogenesis via controlling Wnt/β-catenin signalling with negative regulation of Gsk3β **[148]**.

1.3. Aims of project

As introduced above, ROS have emerged important roles in modulating a number of cellular activities in recent years. However, *in vivo* evidence of ROS regulation is very limited. As an *in vitro* developed vertebrate, Xenopus provides a very good system for research on embryogenesis, which is good for studying ROS regulation in cell proliferation, cell differentiation, cell apoptosis and the signalling transduction. With the HyPerYFP transgenic line, we were able to detect the dynamic of ROS change and manipulate ROS levels during embryonic development. With these approaches, my work is mainly focusing on solving questions in the following three aspects:

1. Function of ROS during early embryonic development:
- The change of ROS levels during embryonic development
- Whether ROS play a role in regulating embryonic development

2. Upstream of ROS
- The source of ROS in oocytes and embryos

3. Downstream of ROS
- ROS regulation on downstream signalling pathways during embryonic development

Chapter 2: Materials and Methods

2.1. Experimental animals

Adult wild-type *Xenopus laevis (X. laevis)* frogs (Nasco) as well as HyPerYFP transgenic line frogs were used for experiments. They were raised in tanks with a water temperature of 16 ºC - 19 ºC and a population density of 5 L water per frog. Transgenic HyPerYFP frogs were generated via restriction enzyme mediated integration (REMI) [64], using SwaI and a CMV:HyPerYFP plasmid [151].

2.1.1. Superovulation of the female *X. laevis*

Adult female frogs were stimulated to lay eggs by injection of 500I.U. hCG into dorsal lymph sac at about 12 hours before egg collection. To ensure a large yield of eggs, female frogs were pre-primed with 500I.U. PMSG by dorsal lymph sac injection at 2-5 days before injecting hCG. After hCG injection, frogs were incubated in a separate tank with 5 L water at 15 ºC – 23 ºC overnight, waiting for next day's egg collection. In order to keep good quality and activity of the eggs, once frogs start laying eggs, they were transferred into 1 x MMR incubation butter until collection ended.

hCG: *Human Choriogonadotropin, CHORULON® 1500I.U, Intervet.*
PMSG: *Pregnant mare serum gonadotrophin, 5000I.U, Intervet.*

2.1.2. Artificial fertilisation of *X. laevis* eggs

The first step in artificial fertilisation is preparation of testis. A male frog was anaesthetised by injection of 40% MS222 into dorsal lymph sac. The frog should be observed as completely motionless before being killed. Then, two testes were taken out from the abdominal cavity and were stored separately in 20 mL L15 at 4 ºC for maximal 10 days.

The next step is to prepare eggs and do artificial fertilisation. Eggs from *X. laevis* were collected, removed from extra water and placed in proper culture plates. Then, sperm solutions were prepared by cutting off one piece of testis and homogenising it with proper amount of 1 x MMR in Eppendorf tubes. Generally, 1/5 testis is enough to fertilise 300-400 eggs. Next, sperm solutions were pipetted out and spread evenly on eggs. After 5 minutes, 0.1 x MMR was added into the plates with eggs and sperms. Then successfully fertilised eggs could be recognised by cortical rotation and pigmentation contraction after 30 minutes post fertilisation.

1 X MMR: *0.1 M NaCl, 2 mM KCl, 1 mM MgCl2, 2 mM CaCl2, 5 mM HEPES, regulate pH to 7.5 and store at room temperature.*
40% (w/v) MS222: *dissolve 400 mg MS222 with 1 mL ddH_2O, store at -20 ºC*.
MS222: *E10505, Sigma-Aldrich.*

2.1.3. Dejellying *X. laevis* eggs

2% L-cysteine with proper culture medium was used for removing the jelly coat from eggs. For fertilised eggs, 2% L-cysteine with 0.1 x MMR was used, while for immature oocytes or pre-activation eggs, 2% L-cysteine with 1 x OR2 was employed. Usually, eggs / oocytes were incubated with 2% L-cysteine for 5-10 minutes to remove the jelly coat, and washed three times for further manipulation.

2% (w/v) L-cysteine: *dissolve 2 g L-cysteine with 100 mL 0.1 x MMR or 1 x OR2, regulate pH to 7.8 with 10 M NaOH and store at room temperature.*
L-Cysteine hydrochloride monohydrate: *C7880, Sigma-Aldrich.*

2.1.4. Microinjection

Glass injection needles were employed for injection of *X. laevis* oocytes and embryos. Needles were pulled with Microneedle Puller (Sutter Instrument, model P-87), filled with 1-5 µL mRNA/DNA solution and placed into the holder of injection equipment (Medical System, model Pi-100) prior to injection. Then, desired injection volume was obtained by gradually breaking the needle tips under a stereoscope. Generally, the total volume of solution injected would not exceed 60 nL for *X. laevis* oocytes and 10 nL for *X. laevis* embryos.

In oocytes, mRNAs were injected at 24-48 hours prior to imaging. In embryos, mRNAs or plasmid DNAs were injected at 1 or 2-cell stage, and sometimes, impermeable chemicals (e.g. NAC) were injected into blastocoel at blastula stage. During injection, as well as the first two hours following injection, embryos were incubated in 2% Ficoll buffer and cultured at 15 ºC - 23 ºC until the desired developmental stages.

2% (w/v) Ficoll: *dissolve 2 g Ficoll 400 (Sigma) with100 mL 0.1 x MMR and store at -4 ºC.*
NAC: *to make of 1 M NAC, dissolve 32.6 g NAC with 200 mL ddH_2O, adjust pH to 7.8*

with 10 M NaOH and store at -20 ºC.
NaAc: *to make of 1 M NaAc, dissolve 27.2 g NaAc with 200 mL ddH_2O, adjust pH to 7.8 with 10 M NaOH and store at 23ºC.*

2.1.5. Immature oocytes preparation

Selected female frog was pre-primed with 500I.U. PMSG at 2 days before egg collection. 1 L 0.1% MS222 was prepared for female frog anaesthesia. On the day of egg collection, pre-primed frog was firstly immersed in MS222 solution for 15-30 minutes until immobile, then taken out and placed in dorsal recumbency on a wipe. Next, the frog was incised with two 2 cm incisions on the lower part of abdomen (lateral and symmetrically to the midline), and so did the muscle layer, until the exposure of ovaries. Then ovaries were collected, cut into 1 cm x 1 cm pieces, and washed 4-5 times until blood was washed away. To ensure the quality of oocytes, manual defolliculation was carried out, after which the separated oocytes were cultured in 16 ºC incubator until further manipulation [152].

1 x OR2: *dilute from 10 x OR2 (A+B) stock, adjust pH to 7.5 and store at 16 ºC.*
10 x OR2 solution A: *dissolve NaCl 48.221 g, KCl 1.864 g, $CaCl_2{\cdot}2H_2O$ 1.47 g, $MgCl{\cdot}6H_2O$ 2.03 g, HEPES 11.915 g, NaOH 1.52 g with 1 L ddH_2O, autoclave and store at room temperature for use.*
10 x OR2 solution B: *dissolve Na_2HPO_4 1.42 g with 1 L ddH_2O, autoclave and store at room temperature for use.*
1x calcium-free OR2: *prepare a 10 x OR2 solution A without addition of $CaCl_2{\cdot}2H_2O$, dilute with 10 x OR2 solution B to make 1 x calcium-free OR2, adjust pH to 7.5 and store at 16 ºC.*
0.1% (w/v) MS222: *dissolve 1 g MS222 powder in 1 L water, adjust pH to 7.5 and store at 16 ºC.*

2.1.6. Immature oocytes injection and maturation

Immature oocytes were prepared as described in 2.1.1.4 and injected with proper amount of mRNA at 24-48 hours before use. Then the injected oocytes underwent an *in vitro* maturation with 2 μM progesterone at 16 ºC, at about 12 hours prior to use. Successfully matured oocytes could be identified with a white spot at the animal cap, which associateed with the germinal vesicle break down.

2 μM progesterone: *1: 5000 dilute from 10 mM progesterone stock.*
Progesterone: *P0130, Sigma-Aldrich. Dissolve 31.45 mg progesterone with 10 mL EtOH to make a 10 mM stock, aliquot to 1 mL and store at -20 ºC for use.*

2.2. mRNA preparation

2.2.1. DNA linearization

Relevant plasmids (listed below) were first linearized by proper restriction enzymes to generate DNA templates for mRNA synthesis. After an overnight incubation with restriction enzyme at 37 ºC, linearized DNA was purified via QIAquick Spin column (QIAGEN) and tested via electrophoresis agarose gel. After measuring concentration with NanoDrop, DNA templates were stored at -20 ºC for use.

Table 2-1: mRNAs used for injection

mRNAs used	Plasmid	Origin	Enzyme used for digestion and mRNA synthesis	Injection amount
HyPer	pCS2+HyPerYFP	A gift from Mitchison lab	Not1, SP6	20 ng per oocyte
SypHer	pCS2+SypHer	Addgene 48250	Not1, SP6	20 ng per oocyte
R-geco	pCS2+r-geco	A gift from Dorey lab	Not1, SP6	20 ng per oocyte
mCherry	pCS2+mCherry	A gift from Nancy lab	Not1, SP6	20 ng for oocytes
IP_3 phosphatase	pCS107-IP_3 Phosphatase	EST clone Tegg120m23	Asc1, SP6	20 ng per oocyte
Nox5-alpha	pCS2+ nox5-alpha	Shoko cloned from trop testis	Not1, SP6	20 ng per oocyte
Nox5-DN	pCS2+CMV-dnNox5	A gift from Lambeth lab	Asp718, SP6	20 ng per oocyte
Mito-HyPer	pCS2+mitoHyPer	A gift from Belousov lab	Not1, SP6	20 ng per oocyte
Wnt8	pCS107-wnt8	A gift from Gurdon lab with vector pSP64T, originally from Moon lab	Asc1, SP6	50 pg per embryo
β-gal	pCS107-β-gal	Siwei Zhang cloned	Asc1, SP6	50 pg per embryo

2.2.2. mRNA synthesis

Capped mRNA was transcribed using the mMESSAGE mMACHINE SP6 kit (Ambion) according to manufacturer's protocol. At the end of transcription, 1 μL TURBO™ DNase (2 U/μL) was added to the reaction buffer and incubated for 15 minutes to remove the

remaining DNA. Next, synthesised mRNA was purified using MEGAclear kit (Ambion) following manufacturer's instructions and dissolved in proper amount of Nuclease-free water for further steps. Synthesised mRNA was then adjusted to 1 µg/µL and stored at -80 ºC for use. The quality of the RNA products could be checked via electrophoresis agarose gels.

TURBO^{TM} DNase: *AM2239, Applied Biosystem.*
mMESSAGE mMACHINE SP6 Transcription Kit: *AM1340, Ambion.*
MEGAclear Transcription Clean-up Kit: *AM1908, Ambion.*

2.3. Inhibitor treatment in *X. laevis* oocytes and embryos

For experiments using *X. laevis* oocytes, defolliculated or dejellied oocytes were pre-incubated with different inhibitors for 20 minutes before activation / fertilisation and were continually treated with inhibitors till collection or experiments complete. For experiments using *X. laevis* embryos, embryos were treated with inhibitors either from 2/4-cell stage or mid-blastula stage until collection or experiments finish. Drugs and inhibitors used are listed below.

A23187: *C7522, Sigma-Aldrich. Dissolved in EtOH for a 10 mM solution. Store at -20 ºC for use.*
Antimycin-A: *A0149, Sigma-Aldrich. Dissolve 5 mg with 1 mL DMSO, aliquot and store at -20 ºC for use.*
EGTA: *E3889, Sigma-Aldrich. Make 1M EGTA with ddH_2O and store at room temperature for use.*
Diethyl Malonate: *W237507, Sigma-Aldrich. Store at room temperature.*
DMSO: D8414, Sigma-Aldrich. Store at room temperature.
Ryanodine**:** *1329, Tocris. Dissolve in DMSO to make a 150 mM solution and store at -20 ºC for use.*
Rotenone: *R8875, Sigma-Aldrich. Dissolved in DMSO to make a 1 mM solution, aliquot and store at -20 ºC for use.*
Oligomycin A: *75351, Sigma-Aldrich. Dissolve 5 mg with 1 mL DMSO, aliquot and store at -20 ºC for use.*
Sodium azide: *08591, Sigma-Aldrich. Store at 4 ºC for use.*

2.4. Measurement of ATP level in *X. laevis* oocytes and embryos

Intracellular ATP levels in oocytes and embryos were measured with an ATP Determination Kit. Based on requirement of firefly luciferase for ATP to produce light (emission maximum ~560 nm at pH 7.8) from reaction, the ATP level can be quantified (Figure 2-1A). For each single measurement, an ATP standard curve was set up using a series of ATP solutions with known concentration (Figure 2-1B). ATP assay was then performed following manufacturer's instructions and read with a luminometer. After subtracting background, the ATP concentrations from samples could be calculated using the established standard curve and relevant read out values.

For sample collection, 3 x 20 Xenopus oocytes or embryos (before stage 14) at particular stages were collected and homogenised with 180 µL 1 x PLB (taking the volume of an oocyte or embryo before stage 14 as 1 µL, total volume is 200 µL), and centrifuged at maximum speed for 10 minutes at 4 ºC. 10 µL supernatant was taken out, mixed with 990 µL ddH_2O and stored at -80 ºC until use. 1 unit/mL apyrase was employed in this assay as a negative control. Biological triplicates and Technical duplicates were performed in each experiment in order to get reasonable results.

ATP Determination Kit: *A22066, Invitrogen.*
Apyrase from potato: *A6536, Sigma-Aldrich.*
1 x PLB: *dilute from 5 x PLB, E1910, Promega.*
Luminometer: *Mithras LB 940 Multimode Microplate Reader, Berthold.*

A

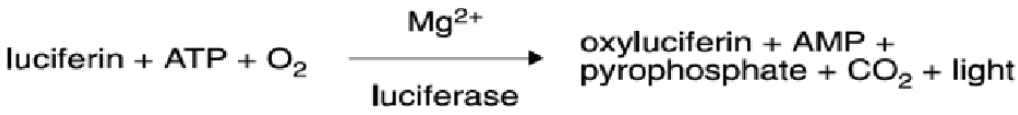

B

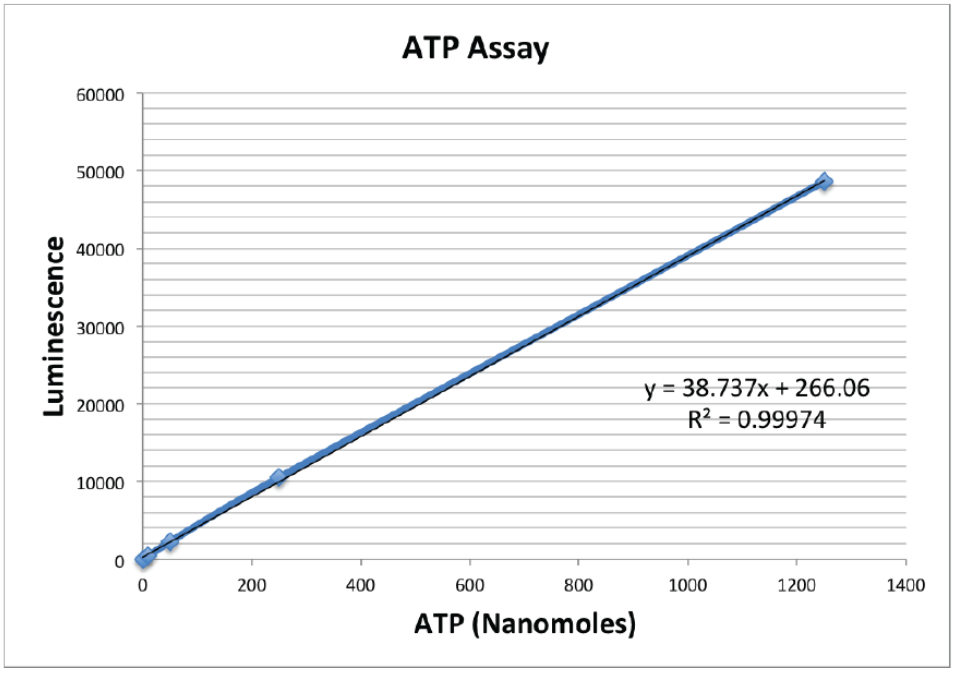

Figure 2-1: Principles of ATP assay system.

(A) Equation of ATP assessment. (B) An example of ATP standard curve generated using 0, 10 nM, 50 nM, 250 nM, 1250 nM ATP solutions.

2.5. TOPFlash Assay

TOPFlash is a T-cell factor (TCF) reporter plasmid consisting of seven copies of TCF binding site upstream of the Thymidine Kinase (TK) minimal promoter and luciferase open reading frame. After injection, the luciferase reporter vector will go into the nucleus and when β-catenin translocates into the nucleus, the TCF/LEF transcription factor will be activated and induce the change of luciferase signal. This method has been used to investigate the activation of canonical Wnt signalling pathway.

Plasmids TOPFlash (100 pg) and pTK-Renilla (50 pg, endogenous control) were co-injected with 50 pg β-gal or wnt8 mRNA into 1-2 cell stage *X. laevis* embryos. The injected embryos were then treated with inhibitors or re-injected with antioxidants (NAC) at mid-blastula stage (NF St. 8.5), and collected for luciferase analysis at gastrula stage (NF St. 10.5/11). Ten embryos (collected in triplicates of 10) from each

group were collected and homogenised with 200 µL 1 X PLB, and centrifuged at 4 °C, 16,000 rcf for 10 minutes to separate clear lysate from precipitated yolk. Then, 50 µL clear lysate was aliquot into 96-well plate and analysed with the DLR system for luciferase activity (Promega).

Dual-Luciferase Reporter Assay System Kit (DLR): *E1910, Promega*.
Luminometer: *Mithras LB 940 Multimode Microplate Reader, Berthold*.

Table 2-2: Constructs used for injection

Constructs	Origin	Injection amount
M50 TOPFlash	A gift from Moon lab	100 pg per embryo
pTK-Renilla	A gift from Niehrs lab	50 pg per embryo

2.6. Western blot

Western blot has been used to detect specific components of signalling cascades at the translational level. In my study, I use this method to detect the activity of relevant signalling pathways under different ROS levels.

2.6.1. Sample preparation

Five to ten embryos were collected from each condition at NF St. 11 and removed from excessive lipid content. Then these embryos were immediately cooled in dry ice and stored at -80 °C till extraction. For each 5 embryos collected, 60 µL protein extraction buffer was prepared freshly and used for homogenisation and protein extraction. The homogenised lysates were then centrifuged at 4 °C, 16,000 rcf for 15 minutes to separate clear lysate from precipitated yolk, after which 50 µL of clear lysate was aspirated and immediately mixed with equal volume of 2 x SDS loading buffer. Next, mixed samples were boiled at 98 °C in a PCR machine for 3 minutes and stored at -20 °C until use.

2.6.2. Western blot running

Generally, 10 µL protein extract was loaded on each well of an 8% SDS-PAGE gel, and ran at 120 V, 45 mA for 1.5 hours. After running, resolved proteins were transferred onto PVDF membranes by semi-dry transfer machine at 30 V, 50 mA per gel for 1.5 hours. After protein transfer, the membranes were blocked with either 5%

milk or 5% BSA (according to requirement of antibody) for 30-60 minutes and incubated with primary antibodies at 4 °C overnight. Antibodies were used at a dilution of 1:10,000 (phospho-Erk), 1:1,000 (phospho-Akt), 1:1,000 (phospho-Smad1), 1:1000 (phospho-Smad2) and 1:100,000 (α-Tubulin). Secondary antibodies were used at a dilution of 1:40000 (anti-Rabbit) or 1:100000 (anti-Mouse), and incubated with 1 x TBST for 1 hour at room temperature. Signals were detected using Immobilon™ Western HRP substrate on X-ray films. After detection, stained antibody could be stripped down from PVDF membrane by incubation with stripping buffer for 20 minutes at room temperature. Then PVDF membranes were washed twice with 1 x TBST, re-incubated with 5% milk for 30 minutes and stained with control antibody (if using anti-α-Tubulin, stain for 1 hour at room temp). Next, the membrane was washed 3 times with 1 x TBST, stained with secondary antibody for 1 hour at room temperature and detected for signals with Immobilon™ Western HRP substrate on an X-ray films.

2.6.3. Solutions and antibodies

Buffer for protein extraction: *100 µL 1 M NaF, 50 µL 200 mM NaPi, 50 µL 10% NP40, 20 µL 1 M Tris pH 8.0, 20 µL 1.25M β-glyceropyrophosphate, 20 µL 1 M NaVO3, 10 µL 0.5M EGTA, 4 µL 0.5M EDTA, 2 µL 20 µM Calyculin A, 50 µL Protease Inhibitor Cocktail, 50 µL PhosStop, add ddH_2O to 1 mL, put on ice and use immediately.*

Stacking gel solution: *18.75 mL 40% Acrylamide, 10 mL 2% bis-acrylamide, 18.75 mL 1 M Tris pH 6.8, add ddH_2O to 150 mL and store at 4 °C for use.*

Resolving gel solution: *3 mL 40% Acrylamide/bis-acrylamide, 4 mL 2.8 M Tris pH 8.8, add ddH_2O to 15 mL.*

1 x TBST: *dilute from 10 x TBS and add 0.1% Tween®20.*

10 x TBS: *1 M Tris (pH 8) 100 mL, 5 M NaCl 300 mL, ddH_2O 600 mL.*

5 % (w/v) BSA blocking buffer: *dissolve 5 g Bovine Serum Albumin in 100 mL 1 x TBST.*

5 % (w/v) Milk blocking buffer: *dissolve 5 g Skim Milk Powder in 100 mL 1 x TBST.*

2 X SDS loading buffer: *20% SDS 4 mL, 1 M Tris (pH 6.8) 2 mL, Glycerol 4 mL, BME 0.4 mL, 10 mg Bromophenol Blue.*

1 x SDS running buffer: *dilute from 10 x Tris/Glycine/SDS Buffer (161-0732, BIORAD).*

Bromophenol Blue*: B0126, Sigma-Aldrich.*

Tween®20: *P9416, Sigma-Aldrich.*

Bovine Serum Albumin: *A7906, Sigma-Aldrich.*

Skim Milk Powder: *70166, Sigma-Aldrich.*

Acrylamide/bis-acrylamide, 40% solution: *A7168, Sigma-Aldrich.*

Protease Inhibitor Cocktail: *cOmplete, EDTA-free, 04693132001, Roche.*
PhosSTOP: *phosphatase inhibitor cocktail tablet, 04906837001, Roche.*
Immobilon PVDF membrane: *IPVH00010, Millipore.*
Immobilon™ Western HRP substrate: *WBKL0500, Millipore.*
Stripping buffer: *21059, Thermo Scientific.*
Anti-phospho-Akt (Ser473) (193H12) antibody: *4051, Cell Signalling.*
Anti-phospho-ERK 1/2 monoclonal antibody: *M7802, Sigma-Aldrich.*
Anti-α-Tubulin antibody: *9026, Sigma-Aldrich.*
Anti-phospho-Smad1 (Ser463/465) - Smad5 (Ser463/465) - Smad8 (Ser426/428) antibody: *9511, Cell Signalling.*
Anti-phospho-Smad2 (Ser465/467) antibody: *05-953, Millipore.*

2.7. Total RNA extraction and detection

2.7.1. Total RNA extraction

Five to Ten *X. laevis* embryos were collected, removed from excessive medium and kept in 200 µL RNAlater prior to RNA extraction. Usually, collected embryos were homogenised with a pestle within 24 hours and harvested via RNeasy Mini Kit (QIAGEN) following manufacturer's instructions (indeed, collected embryos with RNAlater can be stored at room temperature for one week, or 4 °C for one month, or -20 °C / -80 °C for archival storage). Then, extracted RNA was eluted with 30 µL nuclease-free water, tested for concentration and stored at -80 °C until use.

2.7.2. Reverse Transcription of cDNA

The cDNA synthesis was performed with the High-Capacity RNA-to-cDNA Synthesis Kit (Applied Biosystems) following manufacturer's protocol. Reaction products (20 µL) were diluted to 200 µL with nuclease-free water and stored at -20 °C until use.

2.7.3. Real-time PCR

Real-time PCR reactions were performed using SYBR Green PCR Master Mix (Applied Biosystems) and StepOne+ machine. Primers were designed and tested for melting curve profiles prior to use in experiment. Expression values were generated using the ΔΔCT method and *rpl8* was used as an endogenous control for normalisation.

2.7.4. Reverse transcription PCR

Total RNA was extracted and reverse-transcribed to cDNA as described above. Ex-Taq polymerase was employed. After 36-cycle amplification, reaction products were checked using 1% electrophoresis gel.

Ex-Taq: *Takara.*
RNAlater: *AM7020, Ambion.*
RNeasy Mini Kit: *74104, Qiagen.*
High-Capacity RNA-to-cDNA^{TM} Kit: *4387406, Applied Biosystems.*
SYBR Green Real-Time PCR Master Mix: *4385612* Applied Biosystems.

2.7.5. Primers

Table 2-3: Primers used for qPCR and RT- PCR

Primer name	Primer sequence
ef1α-F	TGGACACGTAGATTCTGG
ef1α-R	CAGCAACAATCAGGACAG
nox5-F	GAGCCTGCTAACTAAGCTTGAG
nox5-R	AAGGTCTAATGCCATCTGCAGG
duox1-F	TCATGAGTTCCAGGCTGCTG
duox1-R	CACAAACGATAAGCTGGCCAG
duox2-F	GGATCCAAGTATCTCCCCAG
duox2-R	GGTAAGCCTAGGTCTCTTGC
rpl8-F	CACGTGTCCGTGGTGTGGCT
rpl8-R	CGACCAGCTGGGGCATCTCT
bra-F	GGGACCCCACCGAGAAGGAG
bra-R	GGATCCAGGCCCGACATGCT
fgf20-F	CCCCTCCGACCTCTCCCATC
fgf20-R	TGATCCTGCCGAGTGCCCTG

2.8. In situ hybridisation

2.8.1. Preparation of Digoxigenin (Dig) labelled RNA probe

Plasmid DNA was linearized by appropriate restriction enzymes and *in vitro* transcribed to RNA labelled with Dig. A volume of 20 µL reaction solution was set up as follows: 2.0 µg linearized plasmid DNA, 1 x transcription buffer, 0.5 mM Dig-labelled NTPs, 20 U RNA inhibitor and 20 U SP6, T3, or T7 RNA polymerase (Promega), and incubated for 2 hours at 37 °C. Then, the reaction buffer was continually treated with 10 U TURBO DNase for 10 minutes at 37 °C to remove DNA templates, and purified with Micro Bio-spin column according to manufacturer's protocol. Finally, obtained probes were checked using electrophoresis agarose gel, diluted with hybridisation buffer to 1 µg/mL and stored at -20 °C for use.

Table 2-4: Probes used for in situ hybridisation

Probes used	Plasmid	Origin	Enzyme used for digestion and probe synthesis
brachyury	pXT1-brachyury	Jim Smith	Bgl II, T7
cyba	pCS107-cyba	EST clone TTpA018c02	Cla I, T7

2.8.2. Whole mount in situ hybridisation

Embryos were collected at desired developmental stage (NF St. 11) and fixed with fresh 1 x MEMFA for 1 hour at room temperature in 20 mL glass vials. Next, samples were washed three times (10 minutes each) with 100% methanol and stored at -20 °C until use.

Generally, in situ hybridisation could be performed in 3 days. On the first day, samples were placed into separate mesh basket sitting in a 40-well Intavis rack in a bath containing 100 mL 100% methanol. For best results, place no more than 15 embryos in the same mesh basket. Then, samples were re-hydrated with a gradually decreasing methanol gradient (75%, 50%, 25% methanol with H_2O) for 5 minutes and treated with 5 µg/mL proteinase K solution for 10 minutes at room temperature. Then samples were rinsed twice for 5 minutes in 5 mL triethanolamine (TEA) solution (0.1 M pH 7.8). In the end of second wash, adding 12.5 µL acetic anhydride to each basket and rock for 5 minutes, then adding another 12.5 µL acetic anhydride and rock for another 5 minutes. Next, samples were washed twice 5 minutes in 1 x PBST and fixed again with 4% formaldehyde in 1 x PBST. After re-fixation, samples were washed 5 times with 1 x PBST, transferred to individual plastic tubes containing 0.5-1 mL hybridisation buffer and pre-hybridised for 4 hours at 60 °C in a shaking incubator. After pre-hybridisation, the hybridisation buffer was replaced by probe solutions and embryos were incubated with probes overnight at 60 °C.

On the second day of in situ hybridisation, embryos were transferred back to hybridisation buffer and incubated for 10 minutes at 60 °C shaker. Then embryos were washed 3 times in pre-heated 2 x SSC at 60 °C for 20 minutes each, followed by 2 times wash in 0.2 x SSC, 20 minutes each, at 60 °C. After that, embryos were cooled down to room temperature and washed with 1 x MAB. Then, samples were blocked with 1 x MAB+ 2% BM and 2% HTLS for 1 hour and probed with 0.5 mL anti-Dig-POD (1:1000) diluted in blocking buffer for 4 hours at room temperature. Embryos were then

washed in 1 x MAB for 5 minutes three times and stored in 1 x MAB solution overnight at 4 °C.

Next day, wash samples five times in 1 x MAB at room temperature, 20 minutes per wash. After final wash in 1 x MAB, embryos were transferred into freshly made alkaline phosphatase buffer and washed twice. BM purple substrate was used for chromogenic reactions. When the chromogenic reaction developed sufficiently, embryos were washed again in 1 x MAB overnight to eliminate any residual substrate and bleached in bleaching buffer with light. After rehydration, embryos were re-fixed in MEMFA and imaged by a Leica M165FC stereoscope with colour CCD module attached.

2.8.3. Reagents and materials used for in situ hybridisation

1 x PBST: *dilute from 10 x PBS plus 0.1% Tween®20.*

10 x PBS: *NaCl 80 g, KCl 2 g, Na_2HPO_4 14.4 g, KH_2PO_4 2.4 g, add ddH_2O to 1 L and adjust pH to 7.5. Autoclave and store at room temperature for use.*

1 X MEMFA (MOPS, EGTA, Magnesium sulphate, Formaldehyde): *0.1 M MOPS, 2 mm EGTA, 1 mm MgSO4, 3.7% formaldehyde. Regulate pH to 7.4 and store at 4 ºC.*

Alkaline phosphatase buffer: *100 mM Tris pH 9.5, 50 mM $MgCl_2$, 100 mM NaCl, 0.1% Tween®20.*

Hybridisation Buffer: *50% formamide (Ambion), 5 x SSC, 1 mg/mL Torula RNA (Sigma), 100 µg/mL heparin (Sigma), 1 x Denhardt's solution (Sigma), 0.1% Tween®20, 0.1% CHAPS (Sigma).*

2 x SSC: *300 mM NaCl, 30 mM sodium citrate. Prepare a 20 x stock solution, adjust pH to 7.0 with NaOH and sterilize by autoclaving.*

Bleaching buffer: *methanol: 30% H_2O_2: formamide = 7: 3: 0.5 (v/v/v).*

BM Purple: *11442074001, Roche.*

30% Hydrogen peroxide solution: *H1009, Sigma-Aldrich.*

RNase cocktail: *purchased from Ambion. The solution contains 500 U/mL RNase A and 20,000 U/mL RNase T1.*

1 x MAB: *100 mM maleic acid, 150 mM NaCl. Prepare a 2 x stock, regulate pH to 7.5 with NaOH and sterilise by autoclaving.*

DIG-11UTP: *11209256910, Roche.*

Anti-DIG-HRP (Anti-DIG-POD): *11207733910, Roche.*

10% Blocking Medium (BM): *Roche.*

10% Heat-treated lamb serum (HTLS): *Sigma.*

Proteinase K Solution: *20 mg/mL, Ambion.*

2.9. Imaging and data processing

2.9.1. Imaging and detection of H_2O_2

HyPerYFP probe was used for assessment of H_2O_2 related ROS [59]. Imaging was performed using a Nikon TE2000 PFS microscope, a mercury illumination source, and a Cascade II EMCCD camera (Photometric) with excitation filters BP430/24 nm and BP500/20 nm, emission filter BP535/30 nm. HyPerYFP ratios were generated by ImageJ after subtracting, smoothing, and dividing the 500 nm to 420 nm excitation images [60].

2.9.2. Imaging and detection of calcium

R-GECO probe was used for detection of calcium signal during oocyte activation. Images were captured via a Swept Field confocal (Nikon) using a [10 x Plan Fluor] objective on an inverted TE2000 microscope, equipped with a perfect focus system to eliminate focus drift. The settings were as follows, pinholes [46 µm], scan selection [Galvano], format [512 x 512]. Images DsRed were excited with the 543 nm laser lines and acquired on a Cascade 512B EM CCD camera (Photometrics) through the Elements Software (Nikon). For laser induced wound: settings were as below: laser wavelength [561 nm], laser power [40], pulse [10], images were then captured immediately after laser activation.

2.10. Statistical analysis

For all experiments, statistical analysis was performed using GraphPad Prism™. For analysing one-factor data from three or more groups, one-way ANOVA was used. Non-parametric one-way ANOVA (Kruskal-Wallis test), which does not assume Gaussian distribution, was used for analysing most of the data in this thesis. However, in some cases if the data failed Kruskal-Wallis test but are following a Gaussian distribution, parametric one-way ANOVA was applied. For analysing one-factor data from two samples, t-test was used. Mann-Whitney test that does not assume Gaussian distribution was used for two-sample analysis in most of the cases. Unpaired t-test was used for analysing data from real-time PCR. For comparing differences between groups with two factors, two-way ANOVA was used. In addition, a detailed method for each experiment's statistical analysis has been described individually in relevant figure legend. Error bar equals to standard error of mean and "*" indicates $P<0.05$, "**" indicates $P<0.01$, "***" indicates $P<0.001$ and "****" indicates $P<0.0001$.

Chapter 3: ROS are required for Xenopus early embryogenesis

3.1. Introduction

ROS play an essential role in wound healing and tail regeneration [60, 63], however, the mechanism of how ROS regulate regeneration and if ROS play a role in early embryonic development are still elusive. It has been reported by Warburg et.al, that fertilisation process is accompanied with a respiratory burst in sea urchins [97]. We then wonder whether there is also an oxidative burst associating with fertilisation in higher organisms, and whether the oxidative environment is essential for embryonic development. Therefore, the aims of this chapter are to test whether an H_2O_2 oxidative burst occurs following Xenopus egg fertilisation, how ROS level change throughout the various stages of embryonic development and what the role of ROS play during early embryogenesis.

3.2. Result

3.2.1. Using HyPerYFP as a tool to measure intracellular ROS levels in *X. laevis*

To clarify the role of ROS in embryonic development, an effective assay for monitoring intracellular ROS levels is needed. As previously described by Nick R. Love et al. [63], a widely used genetic ROS sensor, HyPerYFP has been employed and introduced into *X. laevis*. This variant of YFP consists of a prokaryotic OxyR domain and is especially sensitive to hydrogen peroxide (H_2O_2) over other ROS [59]. Once oxidised, it induces a reversible conformational change, which can be marked and reflected by two excitations of fluorescence. Thus, we can easily monitor H_2O_2 or closely related ROS levels *in vivo* by calculating the ratio of HyPer-oxidised and HyPer-reduced [59]. Nick R. Love and Yaoyao Chen expressed this HyPerYFP in *X. laevis* and established a transgenic line that can ubiquitously express HyPerYFP in cytoplasm, therefore, making the visualisation of ROS in oocytes and embryos possible.

Since there is no previous report of expressing HyPer in Xenopus oocytes and embryos, a test was set up to confirm whether HyPerYFP readout could respond to H_2O_2 (Figure 3-1). *X. laevis* oocytes were collected, incubated with an increasing concentration of H_2O_2 and tested for ratiometric changes in HyPer. As shown in figure 3-1, we could see a gradual enhancement of HyPerYFP signal following addition of H_2O_2, which confirmed the HyPerYFP could act as readout of increasing H_2O_2 levels in oocytes. Images were taken at 5 minutes after addition of H_2O_2 and processed with

ImageJ to obtain the HyPer ratio. The ratiometric HyPerYFP signals were further transferred into a colour metric scale, such that a blue or green colour represents a lower HyPer ratio and a more reduced state of the oocyte or embryo, while an orange or red colour represents a higher HyPer ratio and a more oxidative state of the oocyte or embryo. After this step, the data were quantified by normalising each group to either untreated oocytes or their control group to remove any experimental differences. After normalisation, higher ratio represents a more oxidative state, while lower ratio represents a more reduced state.

Figure 3-1. Using HyPerYFP as a tool to measure H_2O_2 related ROS in *X. laevis* oocytes.

Panels show HyPerYFP images of an oocyte from a transgenic HyPerYFP female, after exposure to an increasing concentration of H_2O_2. Grey images are from the separate channel of 500 nm and 430 nm, respectively. Scale bar is 200 micron.

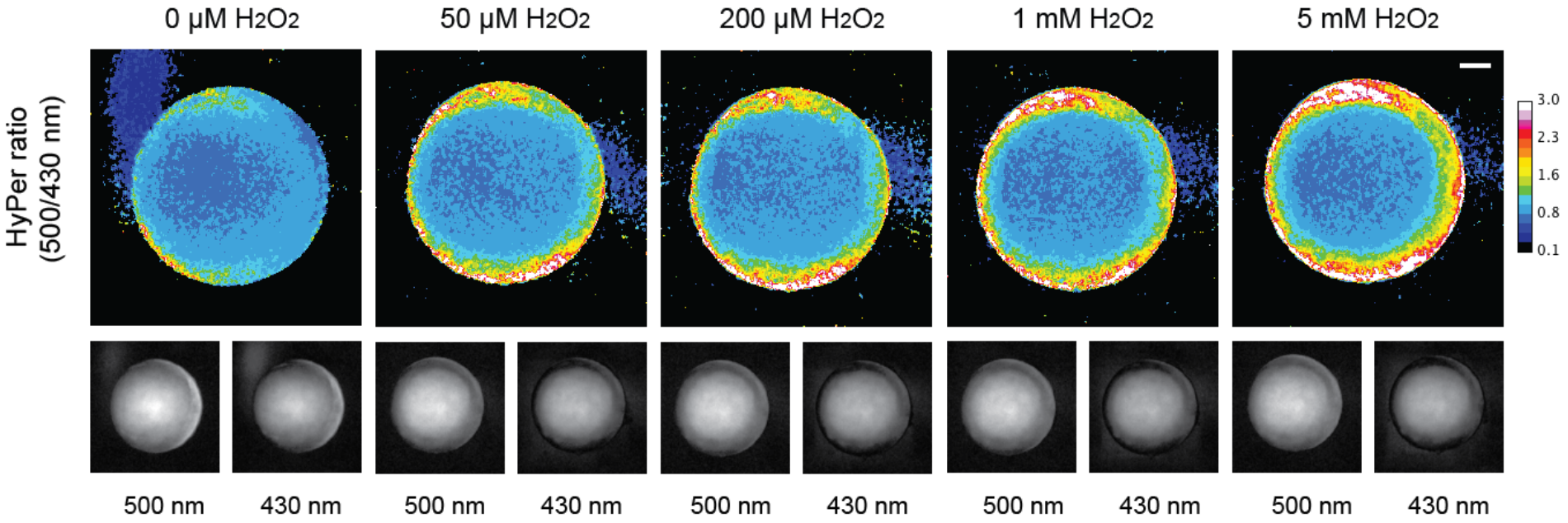

Figure 3-1: Using HyPerYFP as a tool to measure H2O2 related ROS in *X. laevis* oocytes.

3.2.2. ROS burst post fertilisation and high ROS levels are sustained throughout embryogenesis in *X. laevis*

To elucidate whether ROS contribute to early embryonic development, ROS level was measured at different developmental stages using transgenic eggs and embryos of *X. laevis*. Eggs were collected from female frogs expressing HyPerYFP and artificially fertilised for observation. By imaging HyPerYFP signal during fertilisation, we were able to capture the oxidative burst of ROS occurring within minutes following fertilisation (Figure 3-2. A-B). In particular, the unfertilised eggs exhibited a low level of ROS, starting an increase in their intracellular H_2O_2 or ROS levels from 10 minutes post fertilisation, and rising progressively to 1.5 ~2 folds in the first hour post fertilisation (Figure 3-2. A-B).

Although HyPerYFP is able to detect changes in ROS levels, it is also sensitive to changes in pH [59]. In order to exclude the possibility that the elevation of HyPer ratio post activation is due to an increase in pH levels, rather than a rising of intracellular H_2O_2. We overexpressed a pH sensitive construct, SypHer, to monitor the pH fluctuation during fertilisation. SypHer is a mutated form of HyPer with an inactivated H_2O_2-sensing domain and can be used as a ratiometric pH sensor [61]. Since we do not have a transgenic line expressing SypHer in our lab, in order to observe the pH change during fertilisation, we overexpressed SypHer in oocytes, in vitro matured them and did prick activation to mimic the fertilisation process (Figure 4-1). Immature oocytes were injected with 20 ng SypHer mRNA, subsequently matured and prick activated. However, we only detected a very slight change in pH in prick activated oocytes, which is consistent with a previous report published in 1990s, reporting a very mild increasing pH during fertilisation from 7.33 to 7.67 (Figure 3-2. C-D). Besides, it is also important to note that HyPer ratio would not be significantly affected by pH under 8 [59]. These results suggest that the observed elevation of HyPer ratio is coming from a change of intracellular ROS levels but not the change of pH.

Figure 3-2. A production of ROS following fertilisation in *X. laevis* embryos.

(A) This panel shows an increasing levels of ROS (H_2O_2) inferred by HyPer ratio (500/430 nm) in the first 55 minutes post fertilisation. Images were captured before fertilisation, labelled as 0 and every 10 minutes after fertilisation. Data were analysed and processed with imageJ. Figures under different time point are derived from one representative embryo. Scale bar equals 200 micron. (B) A temporal quantification of normalised HyPer ratio of A, which shows a significant difference of ROS levels between unfertilised eggs and fertilised eggs. One-Way ANOVA was used for statistical analysis. Error bars represent a standard error of mean (S.E.M, n=10) and *** indicates a P value less than 0.001 (***, P<0.001). (C) Panels represents the pH fluctuation inferred by SypHer ratio (500/430 nm) in the first 80 minutes post activation in a mature oocyte of *X. laevis*. Images were captured before fertilisation, labelled as 0 and every 20 minutes after fertilisation. Data were analysed and processed by imageJ. Figures under different time point are derived from one representative embryo. Scale bar equals 200 micron. (D) A temporal quantification of normalised SypHer ratio of C. One-Way ANOVA was used for statistical analysis. Error bars represent S.E.M, ** indicates P < 0.01, n=28. Results are from one representative experiment.

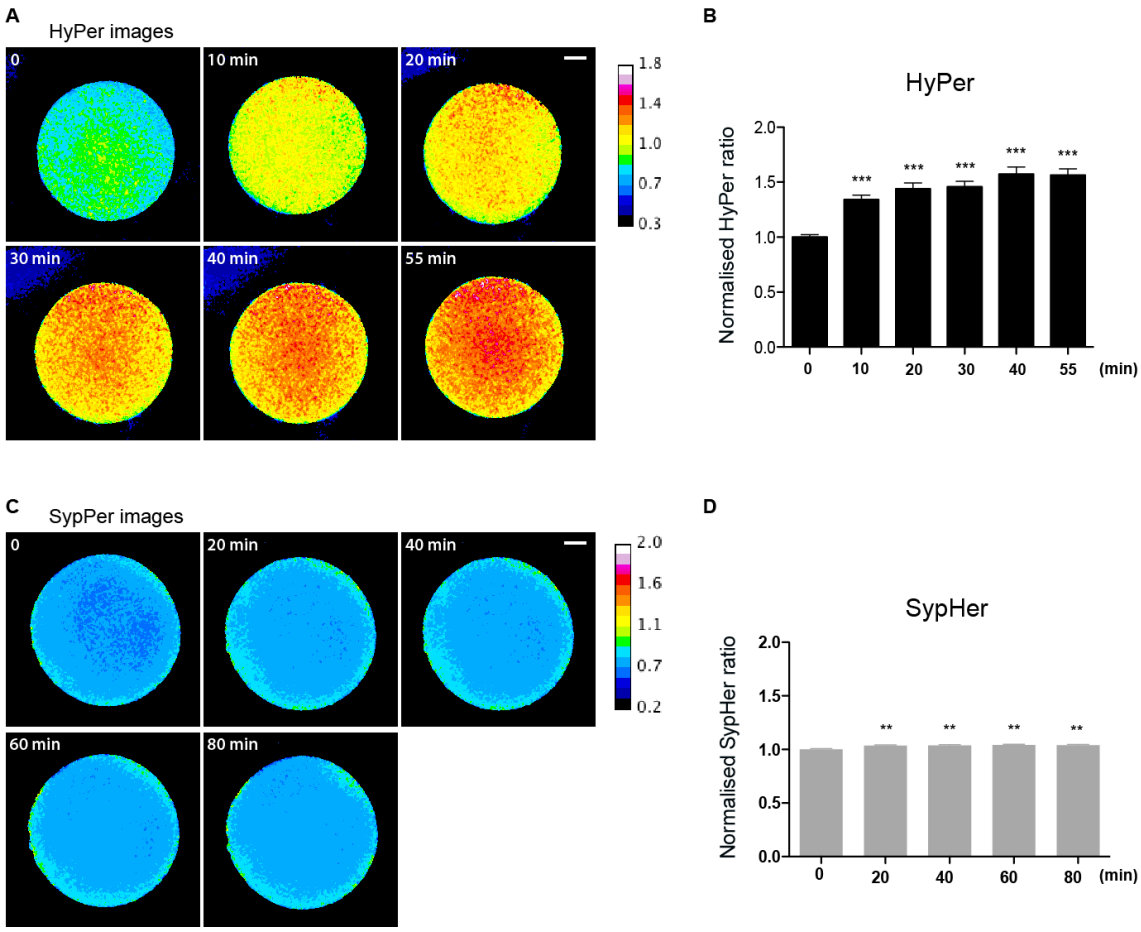

Figure 3-2: A production of ROS following fertilisation in *X. laevis* embryos.

In addition to HyPerYFP results, parallel test has also been done using Amplex Red in combination with horseradish peroxidase (HRP) to confirm the increase in H_2O_2 (ROS) following fertilisation. As introduced in Chapter 1, in the presence of HRP, Amplex Red can react with H_2O_2 in a 1:1 stoichiometry to produce fluorescent resorufin, which has an excitation maximum at 570 nm and an emission maximum at 585 nm (Figure 3-3. A). We then activated *X. laevis albino* eggs with injection of Amplex Red (control) and Amplex Red plus HRP, and took for image immediately. In consistent with data obtained from HyPerYFP, an enhanced fluorescence was observed in eggs co-injected with Amplex Red and HRP, whereas no obvious change of fluorescent intensity was detected in the control group (Figure 3-3. B). Together, these data conclude that fertilisation induces a H_2O_2 oxidative burst in Xenopus eggs, and is, to the best of our knowledge, the first time this has been shown using a vertebrate species.

We next sought to determine whether the fertilisation-induced H_2O_2 change were transient or were they sustained throughout development. Interestingly, we found that embryos sustained elevated levels of H_2O_2 throughout the early stages of development, which were kept high through the cleavage stages, blastula stages and gastrula stages, only to begin decreasing at the neurula stage, until reaching a very lower level of around 0.4 (less than one third of that in an unfertilised egg) at tadpole stages (Figure 3-4. A-B). Taken together, these data demonstrated the early embryogenesis in *X. laevis* is associated with an oxidative environment, similar to that found in regenerating tails [63], suggesting an important role of oxidation or ROS during early phases of Xenopus development.

Figure 3-3. Amplex Red assay shows an increase of H_2O_2 in activated oocytes.

(A) Conversion of Amplex Red into resorufin with consumption of H_2O_2 in presence of HRP. (B) Representative images of fluorescent change in eggs injected with Amplex Red or Amplex Red plus HRP, showing an increase of fluorescent intensity in oocytes co-injected with 100 pm Amplex Red and 0.2 unit/L HRP. Images were captured immediately after injection (labelled as time 0) and every 2 minutes thereafter. Presented images were taken from particular time point of a movie. Scale bar is 1 millimetre. This work is finished in assistance of Dr. Shoko Ishibashi, who helped injection and imaging. I processed the data with image J and made it a figure.

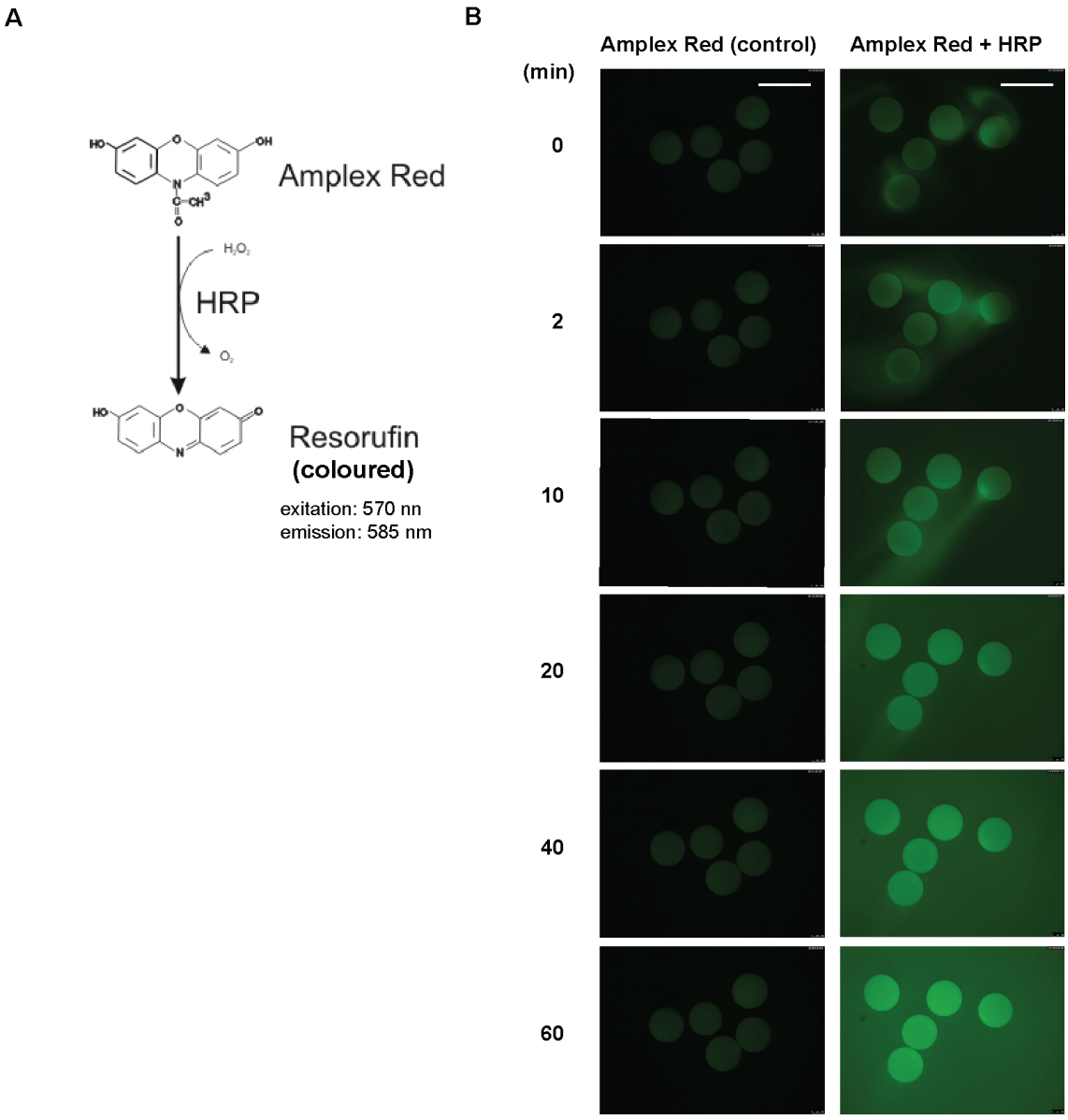

Figure 3-3: Amplex Red assay showing an increase of H_2O_2 in activated eggs.

Figure 3-4. ROS sustain the process of embryogenesis in *X. laevis*.

(A) This figure shows a time course of embryonic oxidative state in *X. laevis*. ROS (H_2O_2) level marked by HyPer ratio (500/430 nm) first ascends post fertilisation, then maintains through gastrula stage, and starts to descend in neurula stage. Panels of St. 26, St. 32 and St. 40 were stitched together from multiple images due to the growing size of embryos. Images shown in this figure are derived from same embryo. Scale bar is 200 micron. (B) Quantification of normalised HyPer ratio during embryonic development of *X. laevis*. Kruskal-Wallis was used for data analysis and n number is displayed on the top of each bar. Error bars state S.E.M, * stands for $P<0.05$ and *** stands for $P<0.001$. Data are from two biological replicates.

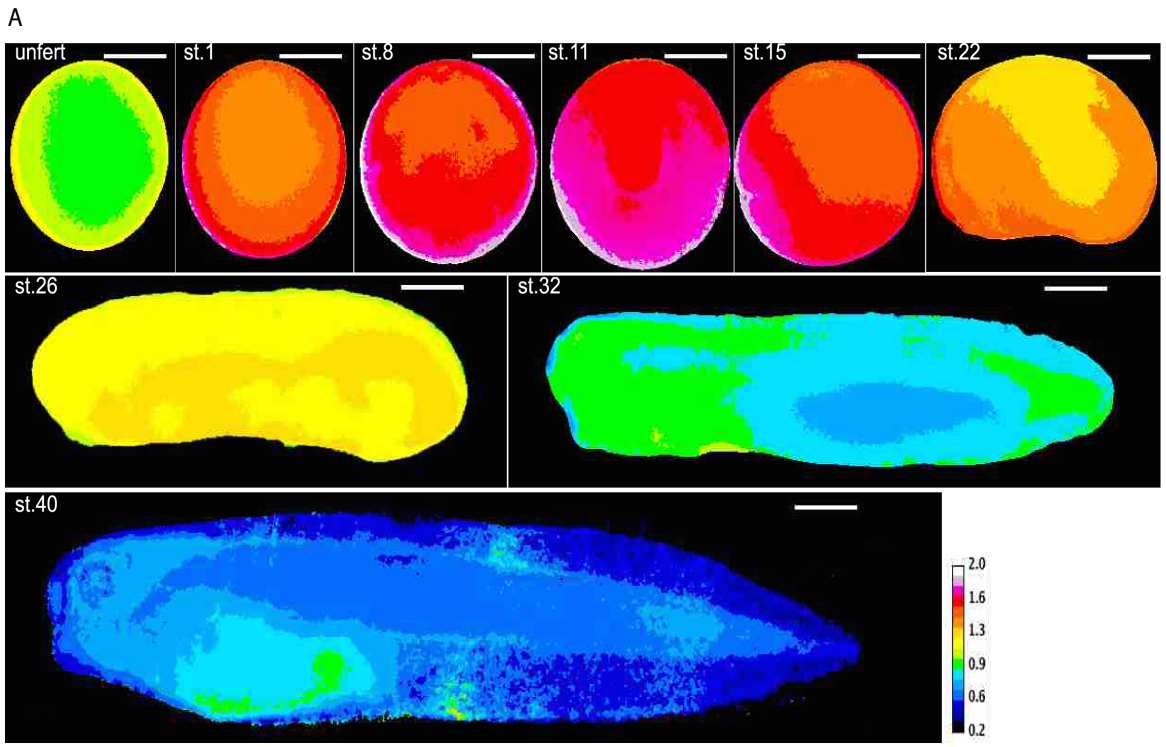

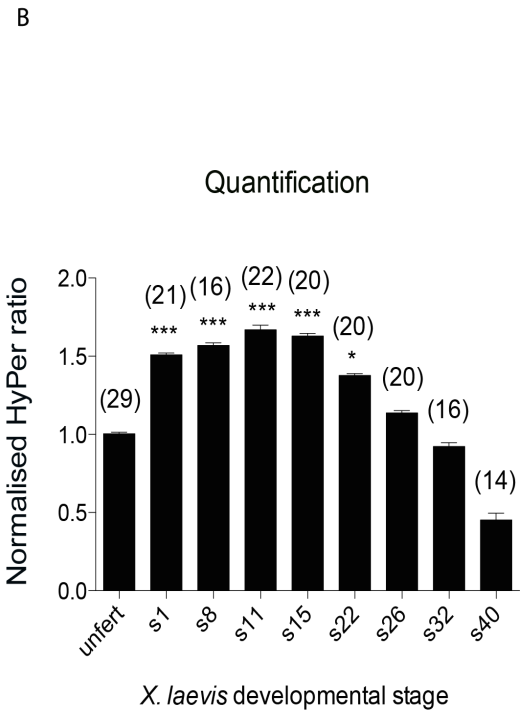

Figure 3-4: ROS sustain the process of embryogenesis in *X. laevis*.

3.2.3. Lowering embryonic ROS by the antioxidant NAC impairs mesoderm formation

To determine any role of ROS during early embryogenesis, we next sought to perform loss of function experiments using antioxidant treatments. N-acetyl-cysteine (NAC) is a precursor of glutathione, and has been commonly used to minimise oxidative stress in cells [153, 154]. In addition, a report published in 1996 described that injection of NAC into blastocoel of mid-blastula stage embryos could cause a severe developmental defect in *X. laevis* embryos. However, the effect of NAC on lowering ROS in *X. laevis* embryos and the molecular mechanisms of this phenotype were not stated [155]. Since we sought to use NAC as a means to decrease intracellular ROS levels in embryos, we first confirmed that NAC injection could lower H_2O_2 related ROS levels (Figure 3-5. B-E). Embryos expressing HyPerYFP were collected and injected with 10 mM NAC at blastula stage and tested for HyPerYFP signal. Sodium acetate (NaAc) was used as a control of NAC. Consistent with the previous report [155], NAC injected embryos could not go through gastrulation, leading to severe developmental defects (Figure 3-5. A), including enlarged cement glands and failure in axis elongation. Since cement gland is originated from ectoderm [156] and axis elongation is derived from mesoderm [157], and since *bra* is critical for gastrulation, we then asked whether mesoderm induction was affected in NAC injected embryos and the expression of Xenopus mesodermal marker gene *brachyury* (*bra*) was tested. We found a decrease of *bra* expression in NAC injected embryos by in situ hybridisation (Figure 3-5. F), and this result was further confirmed by qPCR of *bra* (Figure 3-5. G), both of which demonstrated that NAC significantly inhibited the induction of mesoderm in *X. laevis* embryos. Importantly, the decreased expression of *bra* in qPCR of NAC injected embryos was partially rescued via the addition of exogenous H_2O_2 to the culture media (Figure 3-5. G), which suggested the importance of oxidative state to mesoderm formation.

Figure 3-5. Anti-oxidation via NAC impairs embryonic mesoderm formation.

(A) Embryonic phenotypes of control (NaAc) and NAC treated embryos. The number of embryos exhibited the phenotype showed in figures in contrast with the total number of injected embryos was listed at the bottom. (B) HyPer images of embryos injected with NAC at stage 11, and its quantification (C), control n=21, NAC n=16. Mann-Whitney test was used for statistical analysis, **** denotes P<0.0001. (D) HyPerYFP imaging of embryos injected with NAC at s14 and its quantification (E), control n=12, NAC n=12. Mann-Whitney test was used for statistical analysis, **** denotes P<0.0001. (F) Xenopus *bra* expression in NAC treatments, evidenced by in situ hybridisation, n=6. (G) Real-time PCR (qPCR) measurements of *bra* expression following the indicated treatments, n=3. Unpaired t-test was used for statistical analysis, error bars indicate S.E.M and * denotes P<0.05, ****denotes P<0.0001.

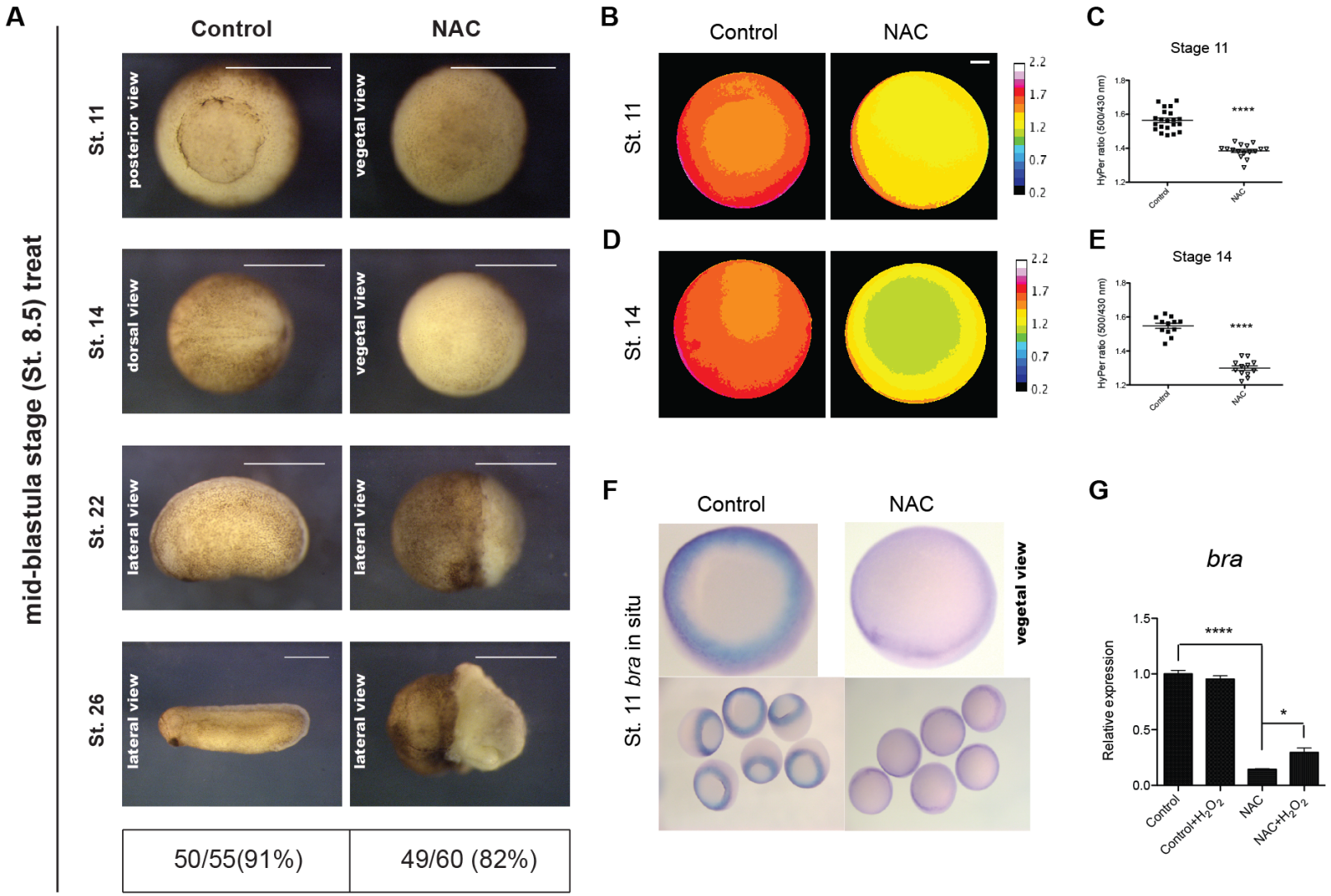

Figure 3-5: Anti-oxidation via NAC impairs embryonic mesoderm formation.

3.2.4. Embryonic ROS regulate PI3K/Akt activation

Next, we sought to identify the molecular mechanisms underlying the loss of mesoderm formation in embryos injected with NAC, which was showing reduction of ROS. FGF signalling has long been recognised as an essential signalling pathway for promoting mesoderm formation and previous work has shown that PI3K/Akt signalling participates in embryonic mesoderm formation [146]. Besides, several studies have described a role for ROS in activating PI3K/Akt signalling [158]. Thus, we first examined whether PI3K/Akt signalling was properly activated in NAC injected embryos. Using western blot analysis of an antibody for the activated version of Akt, we found that NAC mediated anti-oxidation dramatically declined phosphorylated Akt (pAkt) levels, whereas the total Akt (pan-Akt) level was not affected (Figure 3-6. A), demonstrating the loss of pAkt was not due to the general loss of Akt protein. We then wonder whether the loss of pAkt in NAC treated embryos is due to the lowering of ROS. To answer this question, we employed H_2O_2 and menadione. H_2O_2 is one of the major reactive oxygen species and menadione has been reported as a ROS inducer through redox cycling [159]. Importantly, we found that addition of exogenous H_2O_2 or menadione successfully rescued the NAC induced loss of pAkt (Figure 3-6. B), indicating that ROS could modulate mesoderm formation by controlling PI3K/Akt signalling during Xenopus embryogenesis. Interestingly, a study published in 2010 in human embryonic stem cells (hESCs), also reported that lowering ROS by scavengers could decrease Akt phosphorylation levels and block them from differentiation into mesoderm [160]. Taken together, these data suggested a conserved role of ROS in promoting mesoderm formation from Xenopus embryonic cells to pluripotent human ESCs.

Since the Erk/MAPK acts in concert with the PI3K/Akt pathway during Xenopus mesoderm induction, we next examined whether Erk/MAPK signalling was also affected in NAC treated embryos and found that neither the phosphorylated Erk (pErk) nor the total Erk (pan-Erk) protein level was affected by this treatment (Figure 3-6. A).

Figure 3-6. Anti-oxidation via NAC impairs Akt phosphorylation.

(A) Representative western blot figures showing that the inhibition of ROS production inhibits Akt phosphorylation. Embryos were treated with 1 mM H_2O_2 or injected with 10 mM NAC or NaAc (control) at stage 8.5 and analysed by western blot at stage 11 with antibodies specific to pAkt, pErk pan-Akt and pan-Erk. (B) Akt phosphorylation was recovered after addition of exogenous H_2O_2 (1 mM) or menadione (4 μM), to the culture medium of embryos at stage 8.5 and analysed by western blot at stage 11. Experiments were repeated three times.

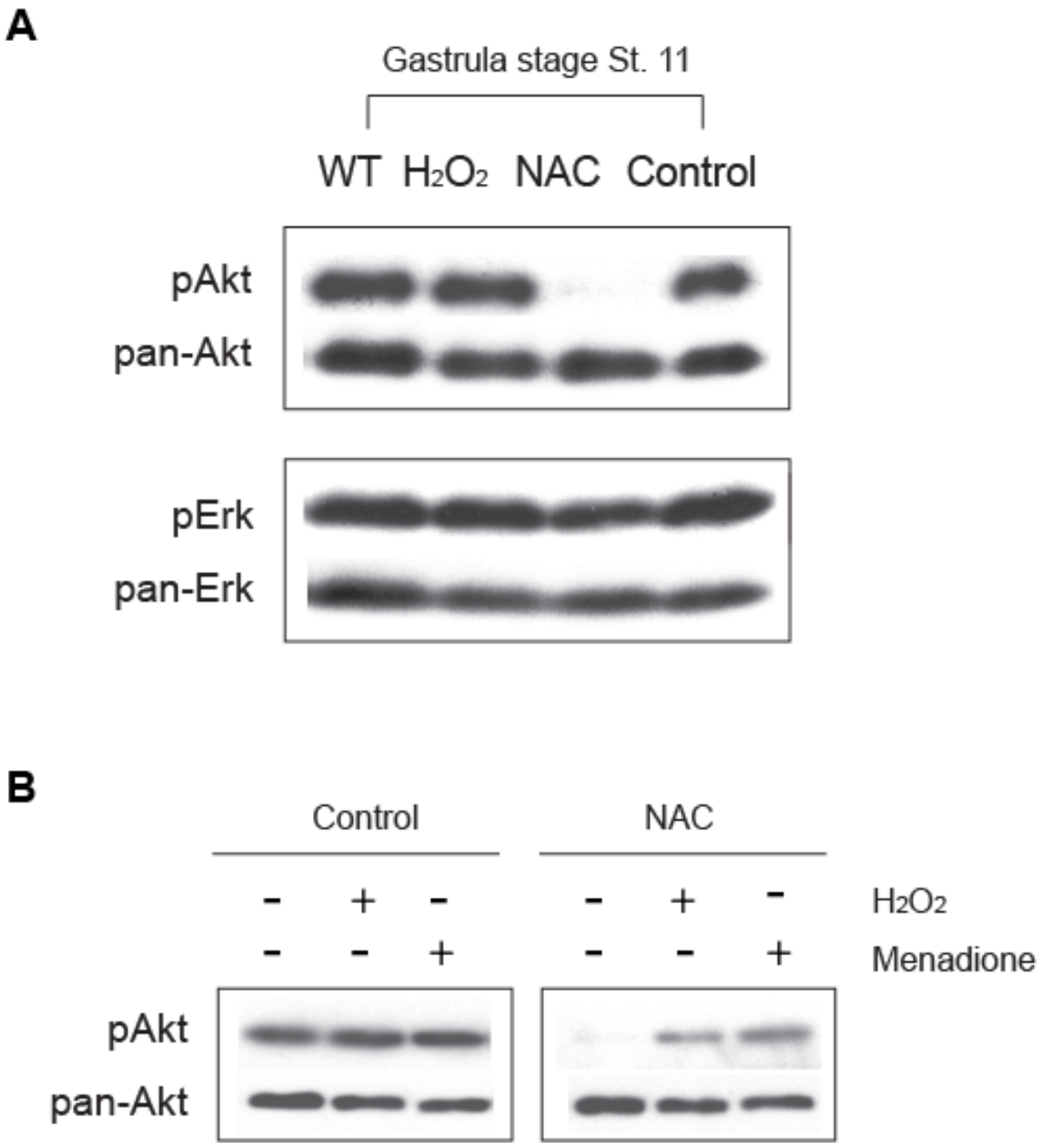

Figure 3-6: Anti-oxidation via NAC impairs Akt phosphorylation.

3.2.5. Embryonic ROS regulate TGF-β/Nodal signalling

Because of the importance of Smads proteins in patterning mesoderm during Xenopus development [139, 140, 161, 162], we next assessed the expression of TGF-β/Nodal and BMP signalling in NAC injected embryos. TGF-β/Nodal activation was found to be completely inhibited in NAC injected embryos, evidenced by western blot detection of phosphorylated Smad2 (pSmad2), whereas the BMP signalling was not affected, as assessed by phosphorylated Smad1 levels (pSmad1) (Figure 3-7. A). Notably, the loss of pSmad2 caused by NAC could be rescued by exogenous H_2O_2 or menadione (Figure 3-7. B), suggesting that a role of ROS in maintaining TGF-β/Nodal signalling during Xenopus embryogenesis.

It is also important to ascertain that NAC induced decline of ROS did not cause a global, unspecific inhibitory effect on all embryonic signalling pathways. Indeed, pErk and pSmad1 activation were not affected by NAC treatment, which confirmed that intracellular ROS are required for activation of a subset of signalling pathways involved in mesoderm formation, but not all of them.

Figure 3-7. Anti-oxidation via NAC impairs Smad2 phosphorylation.

(A) Representative western blot figures showing that the inhibition of ROS production inhibits the phosphorylation of Smad2 (pSmad2). Embryos were treated with 1 mM H_2O_2 or injected with 10 mM NAC or NaAc (control) at stage 8.5, and analysed with antibodies specific to pSmad1, pSmad2 and α-tubulin at stage 11. (B) Regain of pSmad2 levels after addition of exogenous H_2O_2 (1 mM) or menadione (4 μM) to the culture medium of embryos at stage 8.5, and anaylsed with antibodies at stage 11. Results were repeated three times.

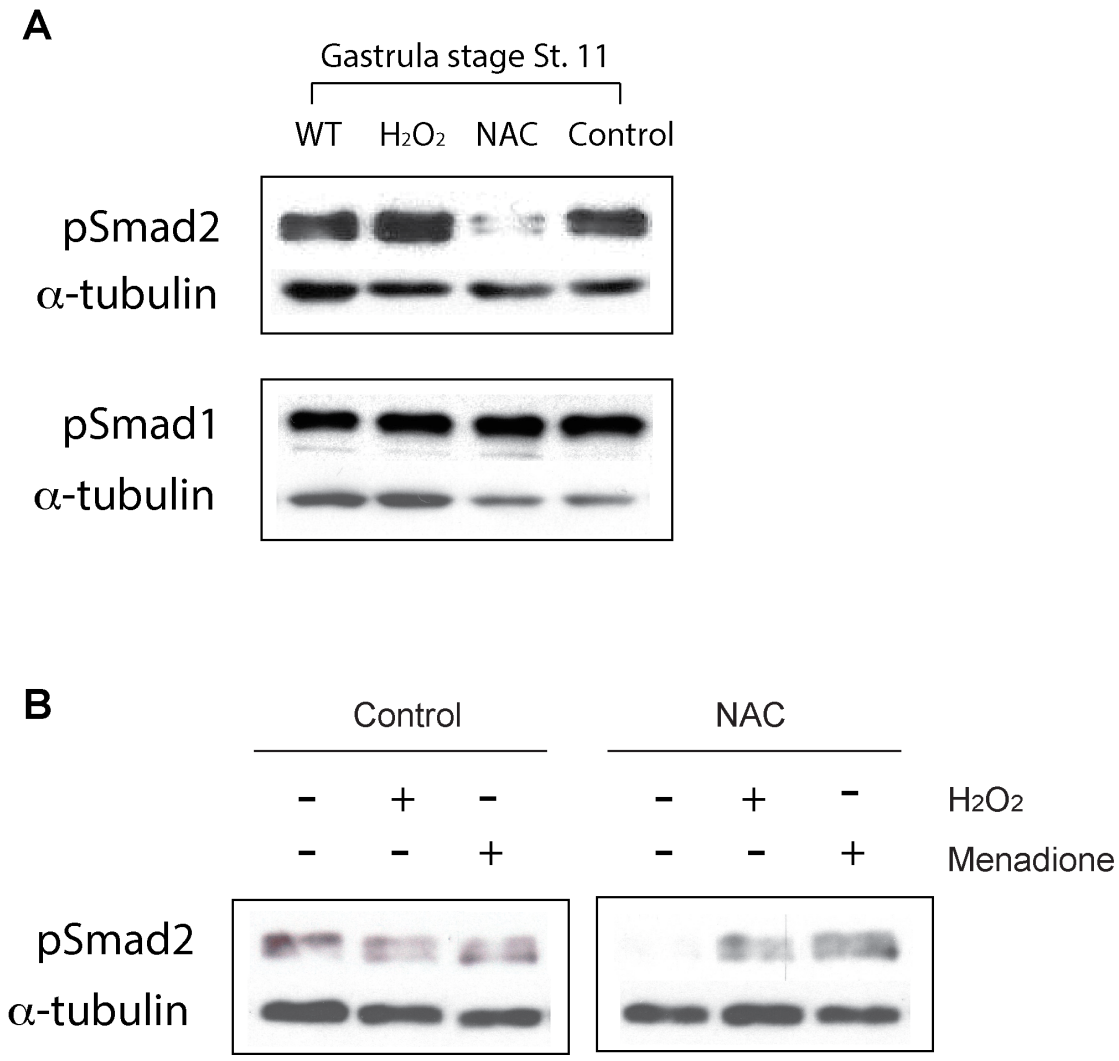

Figure 3-7: Anti-oxidation via NAC impairs Smad2 phosphorylation.

3.2.6. Embryonic ROS modulate Wnt/β-catenin signalling

Another important signalling pathway for mesoderm specification is Wnt/β-catenin signalling, which is required for axis formation and anterior-posterior patterning of Xenopus embryos [163-165]. Besides, there are several publications demonstrating ROS regulation of Wnt/β-catenin signalling pathway, as reviewed in Chapter 1. We then wonder whether early embryonic ROS could regulate Wnt/β-catenin signalling during mesoderm formation. To address this, we carried out a series of experiments in gastrula stage embryos using TOPFlash assay, a technique quantifying TCF/LEF mediated expression of luciferase. Once canonical Wnt signalling was activated, there would be an increase in luciferase expression, which could catalyse the substrate reaction with generation of fluorescence. The intensity of fluorescence can then be read out by a luminometre, which reflects the activity of canonical Wnt signalling. Embryos incubated with H_2O_2 from the blastula stage (St. 8.5) were found a significant increase of endogenous Wnt/β-catenin signalling by gastrula stage, as evidenced by TOPFlash assay (St. 10.5-11) (Figure 3-8. A). In the contrast, NAC injected embryos displayed a reduction in Wnt/β-catenin signalling (Figure 3-8. A). Furthermore, the lowering effect caused by NAC was also seen after hyper-activation of Wnt/β-catenin via the overexpression of *Wnt8* mRNA in embryos as assayed by TOPFlash (Figure 3-8. B). Besides, a partial restoration was seen after incubating embryos with exogenous H_2O_2 or menadione (Figure 3-8. C). We next sought to confirm the loss of Wnt/β-catenin signalling in NAC injected embryos using an alternative method. Since Xenopus *fgf20* is expressed in early embryogenesis under the control of Wnt/β-catenin pathway and acts as a major transcriptional target of β-catenin [166], we performed a test of *fgf20* expression in gastrula stage embryos using qPCR and found that NAC injected embryos possessed a significantly lowered level of *fgf20* (Figure 3-8. D). These data show that embryonic ROS also play an essential role in control of embryonic Wnt/β-catenin pathway.

Figure 3-8. ROS modulate early embryonic Wnt/β-catenin signalling.

(A) H_2O_2 could modulate embryonic Wnt/β-catenin signalling. Xenopus embryos were injected with TOPFlash plasmids and then incubated with 1 mM H_2O_2 or injected with 10 mM NAC or NaAc (control) at blastula stage. Ten embryos of each group were collected at the gastrula stage for luciferase analysis, n=4. (B) Anti-oxidation via NAC significantly lowered the artificial induced Wnt signal. TOPFlash plasmids were co-injected with 50 pg of *Wnt8* or *β-gal* (control) mRNA into Xenopus embryos, which were incubated with 1 mM H_2O_2 or injected with 10 mM NAC or NaAc (control) at stage 8.5, and collected for luciferase analysis at stage 10.5-11, n=3. (C) Addition of 1 mM H_2O_2 or 4 μM menadione can partially rescue the NAC induced loss of Wnt/β-catenin signalling, n=3. Mann-Whitney test was used for statistical analysis in (A), (B) and (C). (D) Real-time PCR (qPCR) of *fgf20* in 10 mM NAC or NaAc (control) injected embryos; unpaired t-test was used for statistical analysis, n=3. All error bars denote S.E.M, * indicates $P<0.05$, ** indicates $P<0.01$ and *** indicates $P<0.001$.

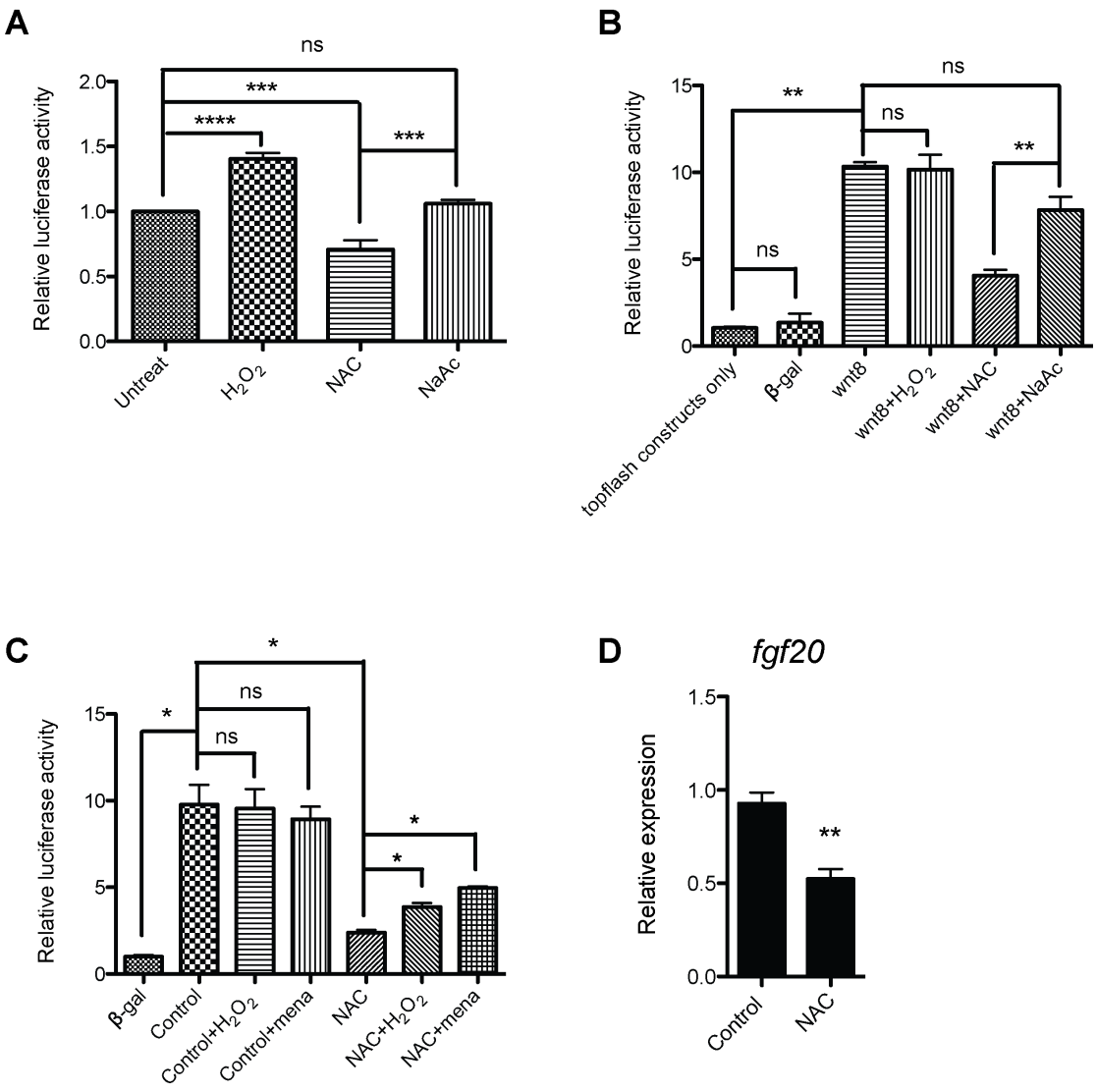

Figure 3-8: ROS modulate early embryonic Wnt/β-catenin signalling.

3.2.7. Embryonic ROS levels are not derived from NADPH oxidases (Noxes)

We next sought to ask what produce ROS in embryos. Since NADPH oxidases (Noxes) have been reported as a major source of ROS, we next tested whether embryonic ROS were generated by Noxes. To answer this, we first tested whether Noxes encoding genes were expressed in early embryos. As introduced in Chapter 1, the Noxes are following different activation mode to generate ROS, in which Nox5, Duox1 and Duox2 containing an EF-hand domain and can be activated by calcium independent of other components; while Nox1 to Nox4 need to form a complex with a core component $P22^{Phox}$ to be activated [22]. Thus, we tested the expression of *nox5, duox1, duox2* and the $P22^{Phox}$ encoding gene *cyba*'s *expression* in early embryos. Different stages of embryos along with early embryogenesis were collected, homogenised and extracted total RNA for reverse transcription polymerase chain reaction (RT-PCR). However, we were unable to detect any expression for *nox5*, *duox1* and *duox2* during Xenopus early embryonic development (Figure 3-9. A). Although *cyba* that encodes the core component of Nox1-4, expressed at early neurula stage evidenced by RT-PCR (Figure 3-9. A-b) and in situ hybridisation (Figure 3-9. B), when addition of DPI, a common Noxes inhibitor to the embryos, no reduction of ROS was detected (Figure 3-9. C, D), and embryos treated with DPI developed normally. These data suggested that NADPH oxidases are not responsible for ROS production during early Xenopus development.

Figure 3-9. NADPH oxidases are not essential for ROS generation in Xenopus early embryonic stage.

(A) RT-PCR of main Nox family genes in Xenopus embryos. (a) RT-PCR of some Nox family genes using Xenopus testis cDNA. (b) RT-PCR of *cyba*, (c) *nox5*, (d) *duox1*, (e) *duox2* in early stage Xenopus embryos. (B) In situ images of *cyba*, n=11. (C) HyPer imaging of DPI treated embryos and its quantification (D) at St. 11 and St. 14, n=12. Mann-Whitney test was used for statistical analysis and error bars mean S.E.M.

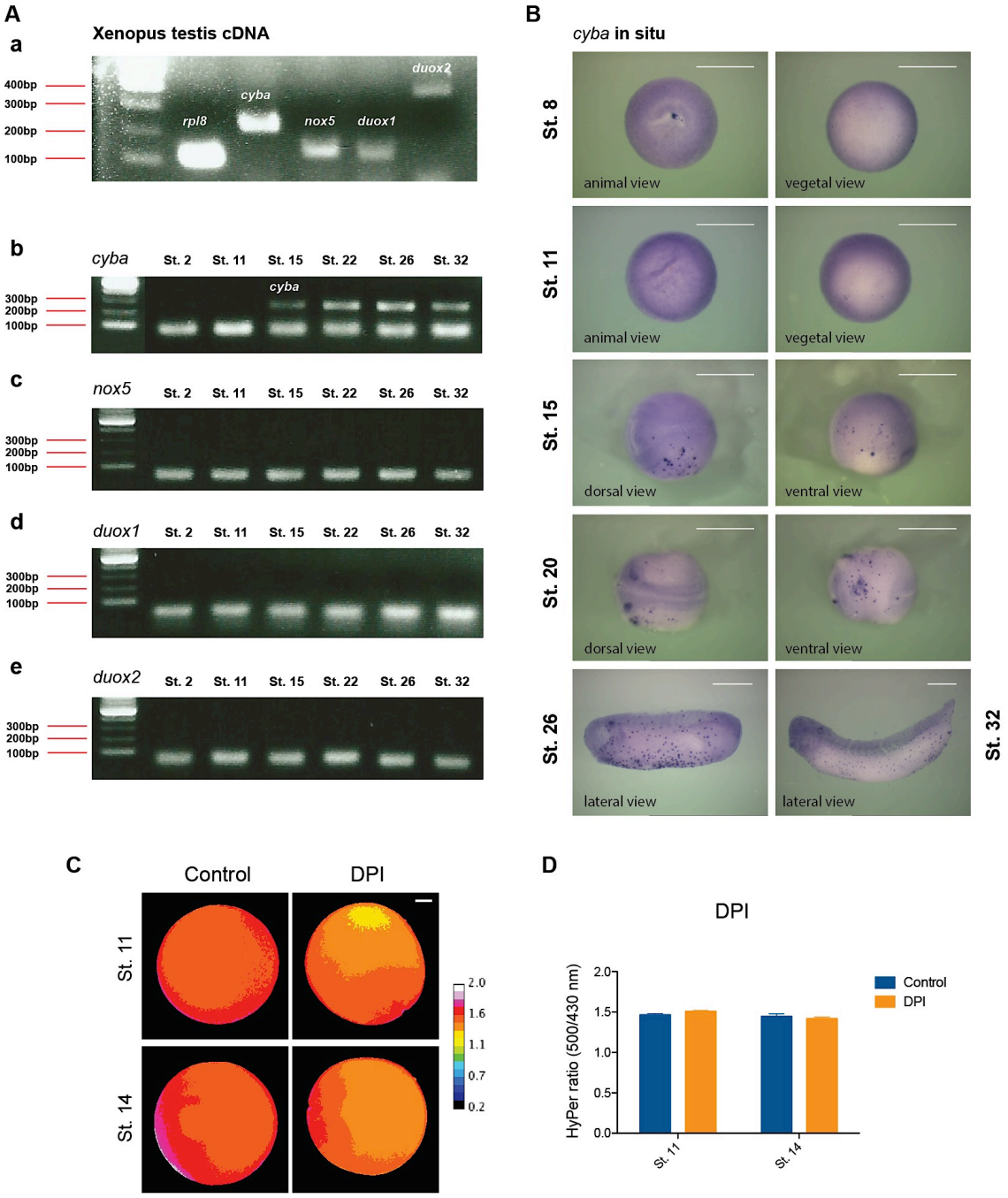

Figure 3-9: NADPH oxidases are not essential for ROS generation in Xenopus early embryonic stage.

3.3. Summary

ROS regulation is becoming a hot topic in recent years, as second messengers in cells, ROS functioning by direct modification of DNAs, proteins and molecules, thus to transduce signals and modulate a variety of biological processes. In the early of last century, Otto Warburg discovered an oxidative burst in sea urchins [97], this phenomenon was confirmed by Foerder et al. in 1978 [167], after this, many studies were carried out to confirm this phenomenon, but the role of this fertilisation-induced ROS in embryogenesis is still not clear [98, 99]. In this chapter, we showed that fertilisation induces a burst of ROS, which is sustained throughout early embryogenesis in *X. laevis*. This finding of fertilisation-induced ROS production in Xenopus eggs is consistent with that seen in the sea urchin [97, 167] and devil stinger [98], suggesting an evolutionary conserved elevation of ROS post fertilisation.

Research in vertebrate also shed lights on the role of ROS in wound healing and regeneration. A ROS burst was observed in both *zebrafish* and Xenopus, immediately after wounding [60, 63], and a sustained production of ROS is crucial for Xenopus tadpole's tail regeneration [63]. Love et al. also showed that disruption of this ROS level resulted in reduced numbers of proliferating cells and impaired tail regeneration. Through further investigation, they showed that this increased ROS levels were essential for the activation of Wnt/β-catenin signalling, hence turning on the expression of *fgf20*, and ensuring proper tail regeneration [63]. However, except canonical Wnt signalling, the interaction of other signalling pathways with ROS during tail regeneration was less touched. Besides, whether ROS are consistently required for the activation of Wnt signalling or only in need during tail regeneration are unknown. In addition, the ROS levels during vertebrate development and other possible functions of ROS are still unraveled.

In this chapter, I first showed that an increase in ROS levels following egg fertilisation in *X. laevis*, which sustained throughout the early embryogenesis, and go down gradually after neurula stage. Lowering ROS levels by antioxidant NAC impairs mesoderm formation, and interferes with some important signalling pathways, suggesting this elevated embryonic ROS play a role during early embryonic development, probably by modulation of signalling pathways. Here we studied the role of ROS on regulating the signalling pathways required for Xenopus mesoderm formation. Through gain and loss of function analyses, we show that a regulatory role of ROS in PI3K/Akt, TGF-β/Nodal, and Wnt/β-catenin signalling during Xenopus early embryogenesis. Although previous studies suggested that ROS could fine-tune

different signalling pathways to regulate cell proliferation, cell differentiation and cell death, most of them were carried out *in vitro* and based on cancer or disease systems. Using *X. laevis* as a model system, we provide evidence for ROS function in early embryogenesis *in vivo*, which are the first time to show that physiological fertilisation induced ROS are critical for early embryonic development in a vertebrate. Moreover, the consistency of ROS regulation of canonical Wnt signalling in both tail regeneration and embryonic development, also suggested a conserved role for ROS modulation across vertebrate embryogenesis to wound healing and regeneration. All these findings will promote the studies of oxidative dependent signalling transduction, not only in embryonic development, but also in a variety of biological processes.

However, one question we have not addressed in this chapter is the molecular source of the Xenopus oxidative H_2O_2 burst. In fact, cellular ROS can be derived from a variety of sources, including mitochondria, the enzymatic oxidation of NADPH and metabolic reactions [7, 168-170]. In sea urchins, Wong and Creton et.al showed that the dual oxidase class of NADPH-oxidase enzymes were important for the oxidative burst. Love et al. also showed that Noxes contribute to ROS production in Xenopus regenerating tadpoles [63]. But what I found here is that the Nox family genes did not transcribed in early stage embryos until the early neurula stage, from where *cyba* was detected. However, even *cyba* started to be transcribed, we did not detect any its biological function in maintaining ROS levels at this stage, based on the pharmacology experiment of DPI. Therefore, the function of Noxes and their contribution to intracellular ROS levels in *X. laevis* embryos remain to be discovered. Another question we did not address here is the interaction between ROS and the signalling pathways. How do ROS regulate the signalling pathways, directly or indirectly? Although many literatures suggested potential ROS targets, such as Nrx [171], further investigation is needed.

Chapter 4: IP_3R-derived calcium activates ROS production during egg activation / fertilisation

4.1. Introduction

In last chapter, we observed the burst of ROS post fertilisation and examined the role of this ROS during early embryogenesis of *X. laevis*. However, the origin of ROS is unravelled. To better understand the physiological significance of fertilisation induced ROS, it is important to trace the origin of ROS, so that we may be able to modulate its production. Previous research reported that sperm entry induces a calcium wave in the sea urchin [172], then this phenomenon was also observed in oocyte or egg activation from plants to humans [173]. Since ROS are also generated post activation, we wondered whether calcium might act upstream of ROS production. To observe the calcium oscillations, a genetically encoded fluorescent protein, named R-GECO [174] was used. This R-GECO was developed from random mutagenesis of GCaMP3 accompanied by high-throughput *in vitro* screening, besides, with a replacement of circularly permuted GFP to an mApple fluorophore. It has a maximum excitation around 550 nm and a maximum emission around 600 nm, and could have a 16-fold increase in fluorescent intensity in response to calcium. With this indicator, we were able to observe the calcium wave in Xenopus oocytes.

4.2. Results

4.2.1. ROS production is following calcium release post activation in mature oocytes but not immature oocytes

As introduced in Chapter 1, stage VI oocytes of Xenopus that arrested at prophase of meiosis I are considered as immature oocytes and cannot be activated or fertilised. But after stimulation with progesterone, immature oocytes are induced to progress through meiosis until they are arrested once again at metaphase of meiosis II, where they are considered as mature oocytes or eggs. At this point, the mature oocytes or eggs are ready to be activated or fertilised. It is well known that the transition of oocyte to egg encompasses a sequence of events, which prepare the egg for fertilisation and subsequent development, including the acquired capacity for the egg to generate a calcium wave following fertilisation or activation [110, 175]. If ROS generation is depending on the calcium wave, we would predict that ROS generation would occur only in activated or fertilised mature oocytes / eggs, but not in immature oocytes, where a calcium wave does not occur.

To test this hypothesis, ovaries were collected, and immature oocytes were isolated, manually defolliculated and injected with mRNAs encoding a calcium indicator and HyPerYFP (Figure 4-1. A). The injected oocytes were then separated into two groups; one group was matured by the addition of progesterone and the other group was not. After the group was allowed to mature, the oocytes were activated by a laser or pricking. As expected, mature oocytes showed a cortical contraction and cortical rotation upon prick activation; whereas immature oocytes had no response to activation (Figure 4-1. B). We next examined the state of calcium oscillation and ROS production upon activation in both mature and immature oocytes. R-GECO [174] was used as a calcium indicator and HyPerYFP was used as a ratiometric sensor of ROS levels. Defolliculated oocytes were injected with 20 ng R-GECO mRNA and cultured in 1 X OR2 medium prior to calcium imaging. As control, 20 ng mCherry mRNA was also injected. In addition, 20 ng HyPerYFP mRNA was injected for ROS ratiometric imaging. Half of the injected oocytes underwent an overnight *in vitro* maturation with progesterone and successfully matured oocytes were identified by the appearance of a white spot at the animal pole, which signified the breakdown of germinal vesicle. The selected matured oocytes, together with immature oocytes were then taken for imaging.

Consistent with previous reports, the mature oocytes exhibited a calcium wave soon after activation (Figure 4-2. B). This calcium increase in mature oocytes could last for 10 minutes (data not show). In contrast, in immature oocytes, only a local calcium puff appeared post activation, which diminished within a minute following activation (Figure 4-2. A). The same result was also found for ROS levels as assessed by HyPerYFP ratiometric imaging, in which ROS levels was only found to be elevated after activation in mature oocytes (Figure 4-2. C, E), but not in immature oocytes (Figure 4-2. C, D).

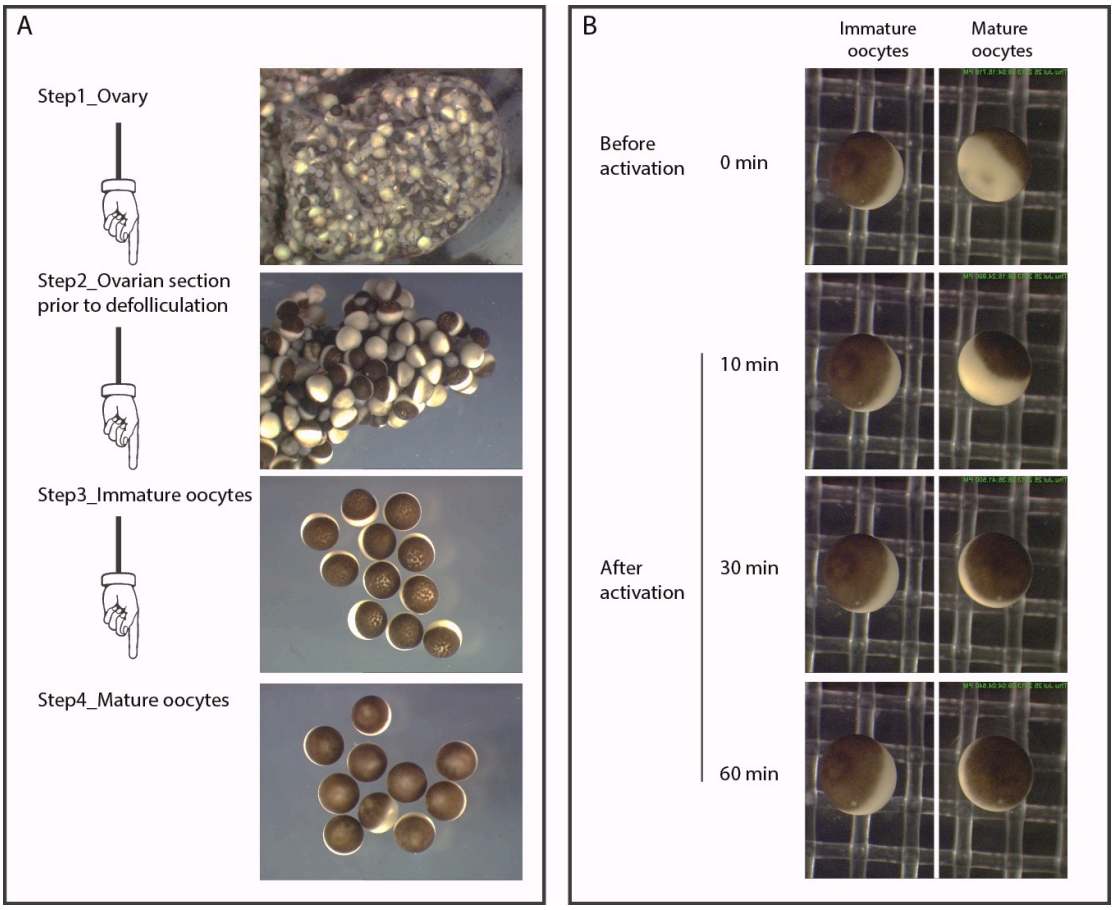

Figure 4-1: *X. laevis* oocyte manipulation and activation.

(A) A flow chart depicts the main procedures of oocyte manipulation. (B) Panels show a representative time course of prick induced oocyte activation in immature oocyte (left) and mature oocyte (right). Mature oocyte (right) undergoes a cortical orientation and pigmentation contraction after 10 minutes post prick activation, which has not been detected in immature oocyte (left).

Figure 4-2. Calcium release and ROS production in activated oocytes

(A) Panels show a time course of calcium waves inferred by R-GECO post activation in immature oocyte and mature oocyte (B) of *X. laevis***.** Images were captured every 15 seconds post activation and time 0 represents before activation. (C) Panels show images of intracellular ROS state as assessed by HyPerYFP ratio (500/430 nm) in immature oocytes and mature oocytes. Images were captured before activation, marked as time 0, and every 20 minutes post activation. Scale bar equals 200 micron. (D) Temporal quantification of ROS production inferred by normalised HyPerYFP ratio in immature oocytes and mature oocytes (E), Kruskal-Wallis test was used for statistical analysis, Error bar indicates S.E.M, *** states $P<0.001$, mature oocytes n=28, immature oocytes n=33. Figure A, B and C show a representative sample of activated oocytes, separately. Data are from two independent experiments.

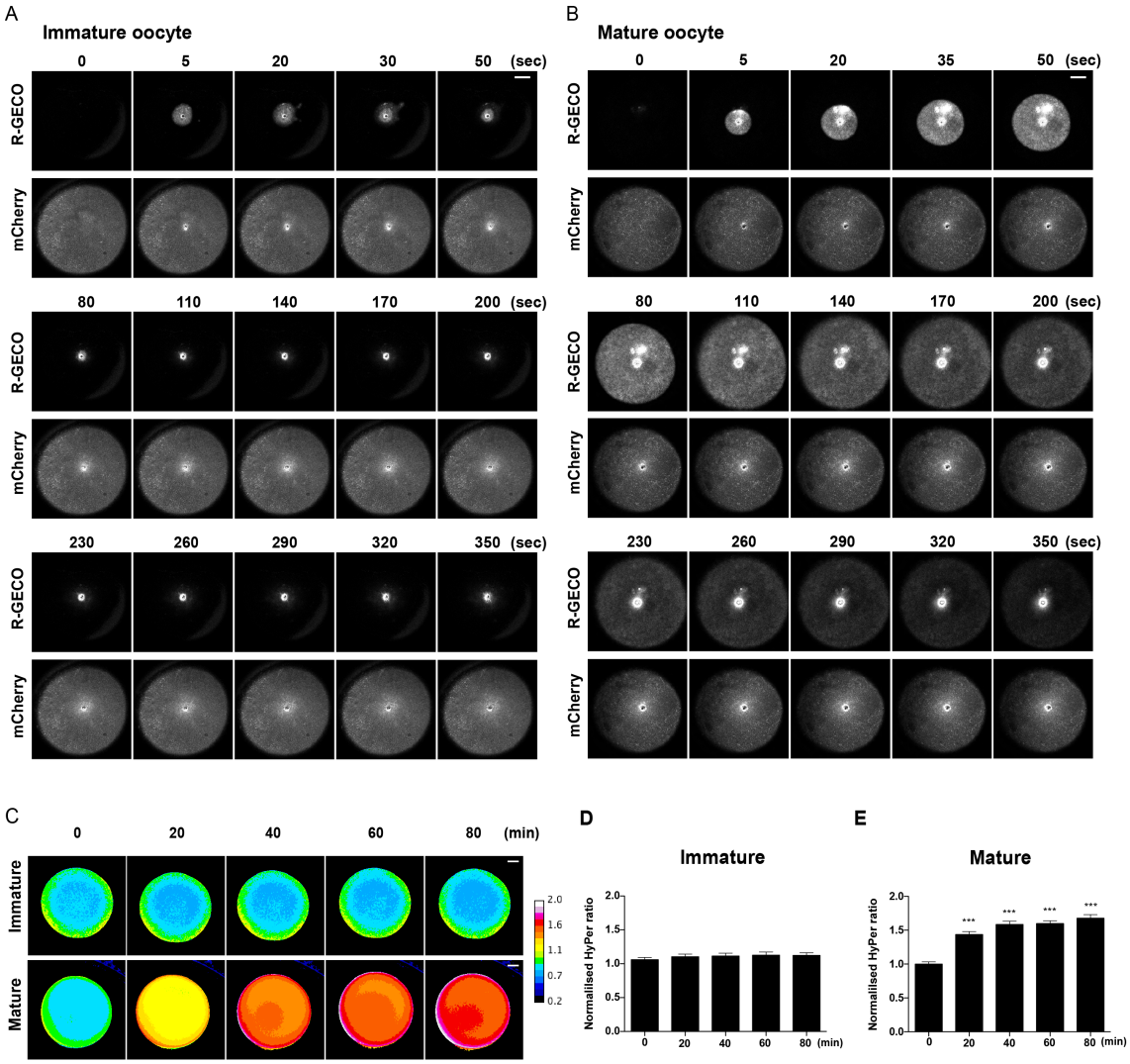

Figure 4-2: Calcium release and ROS production in activated oocytes.

4.2.2. ROS production is calcium dependent

Having shown that ROS production is associated with a lasting increase of calcium levels in mature oocytes following activation, which is not seen in immature oocytes, we next endeavoured to identify if we could induce the production of ROS, by using other means of generating calcium responses in the oocytes. We therefore used the calcium ionophore, A23187, to test whether it could also stimulate ROS production in the oocytes. It had previously been shown that A23187 could mimic activation in mature oocytes [176]. We therefore injected immature oocytes with 20 ng R-GECO or 20 ng HyPerYFP mRNA. As done in the previous experiments, some of these oocytes were left to remain immature, while others were matured *in vitro* with progesterone. When we added 10 uM A23187 to the immature oocytes, we did not see a calcium wave or ROS production in the immature oocytes (Figure 4-3. A, B, F, H). However, 10 uM A23187 did induce a calcium wave in the mature oocytes, and this calcium response was also associated with an increase in ROS levels in the mature oocytes (Figure 4-3. A, B, E, G, H). The response we found in mature oocytes to 10 uM A23187 was essentially the same as we saw following laser activation or prick activation (Figure 4-3. A, B, C, G). Given that the ionophore was dissolved in EtOH, we used EtOH alone as control for these experiments, and these showed no increase in calcium or ROS levels even in mature oocytes (Figure 4-3. A, B, D).

The fact that addition of A23187 to immature oocytes had no effect on ROS generation can be explained by the fact that a calcium wave cannot be mobilised in immature oocytes, even after adding the ionophore. This also suggests that ROS requires a sustained increase in intracellular calcium, which is only afforded by activating a calcium wave.

Figure 4-3. A23187 induces a calcium wave and a ROS production in mature oocytes but not in immature oocytes.

(A) Panels show calcium waves post activation in mature oocytes (upper three) and immature oocytes (bottom). Time 0 is before activation or addition of A23187 and EtOH, then images were taken every 15 seconds afterwards. (B) A change of ROS level proved as assessed by HyPerYFP (500/430nm) post activation in mature oocytes and immature oocytes. Images were taken before activation (set as time 0) every 20 minutes post activation. Figures in A and B show a representative sample of each condition separately. Scale bar equals 200 micron. (C) Quantification of normalised HyPerYFP ratio in prick activated mature oocytes, n=34. (D) Quantification of normalised HyPerYFP ratio in EtOH treated mature oocytes, n=33. (E) Quantification of normalised HyPerYFP ratio in A23187 activated mature oocytes, n=32. (F) Quantification of normalised HyPerYFP ratio in A23187 treated immature oocytes, n=34. Kruskal-Wallis test was used in C, D, E, F. Error bar indicates S.E.M, ** states $P<0.01$, *** states $P<0.001$. (G) Quantification of normalised HyPerYFP ratio in prick activated and A23187 activated mature oocytes, prick activated n=34, A23187 activated n=32. (H) Quantification of A23187 induced ROS as assessed by normalised HyPerYFP ratio in mature oocytes and immature oocytes, mature oocytes n=32, immature oocytes n=34. Two-way ANOVA was used for statistical analysis. Error bar indicates S.E.M, **** implies $P<0.0001$. Data are from three independent experiments.

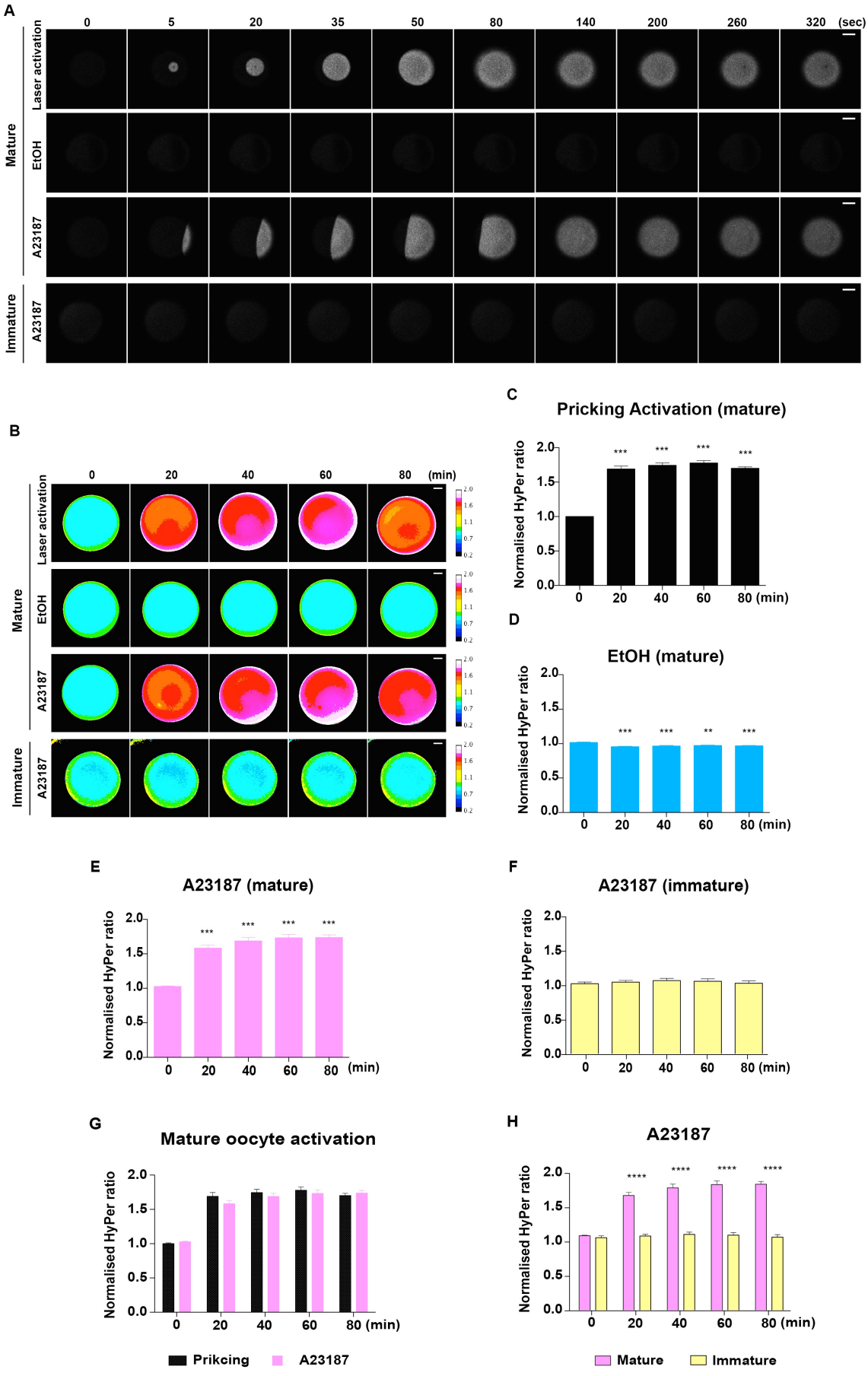

Figure 4-3: A23187 induces a calcium wave and a ROS production in mature oocytes but not in immature oocytes.

Next we blocked calcium release in mature oocytes with the calcium chelator, EGTA. Oocytes were either injected with 20 ng mRNA of calcium indicator R-GECO or 20 ng HyPerYFP mRNA and matured by progesterone as before. Then, matured oocytes were incubated with calcium-free OR2 containing 100 uM EGTA for five minutes and activated by laser. Control group oocytes were treated with calcium-free OR2 for five minutes without EGTA then activated by laser. As anticipated, we observed no calcium wave in EGTA incubated oocytes (Figure 4-4. A), and according to our hypothesis, we also saw no ROS production in these oocytes (Figure 4-4. B, D). While the control group, which was not incubated with EGTA, generated a calcium wave and a ROS production (Figure 4-4. A, B, C). These results suggest that calcium acts upstream of ROS production.

Figure 4-4. EGTA blocks calcium release and ROS production in activated mature oocytes of *X. laevis*.

(A) Calcium wave assessed by R-GECO in control and EGTA treated mature oocytes post activation. Images were taken every 15 seconds post activation and before activation was set as time 0. Figures show a representative sample of control and EGTA treated oocytes, respectively. (B) ROS status inferred by HyPerYFP ratio (500/430 nm) of control and EGTA treated mature oocytes after activation. Images were taken before activation (marked as time 0) and every 20 minutes post activation. Scale bar equals 200 micron. (C) Quantification of normalised HyPerYFP ratio in control and EGTA (D) incubated mature oocytes. Kruskal-Wallis test was used for statistical analysis, control n=20, EGTA n=24. Error bar indicates S.E.M, *** implies $P<0.001$. Data are from three independent experiments.

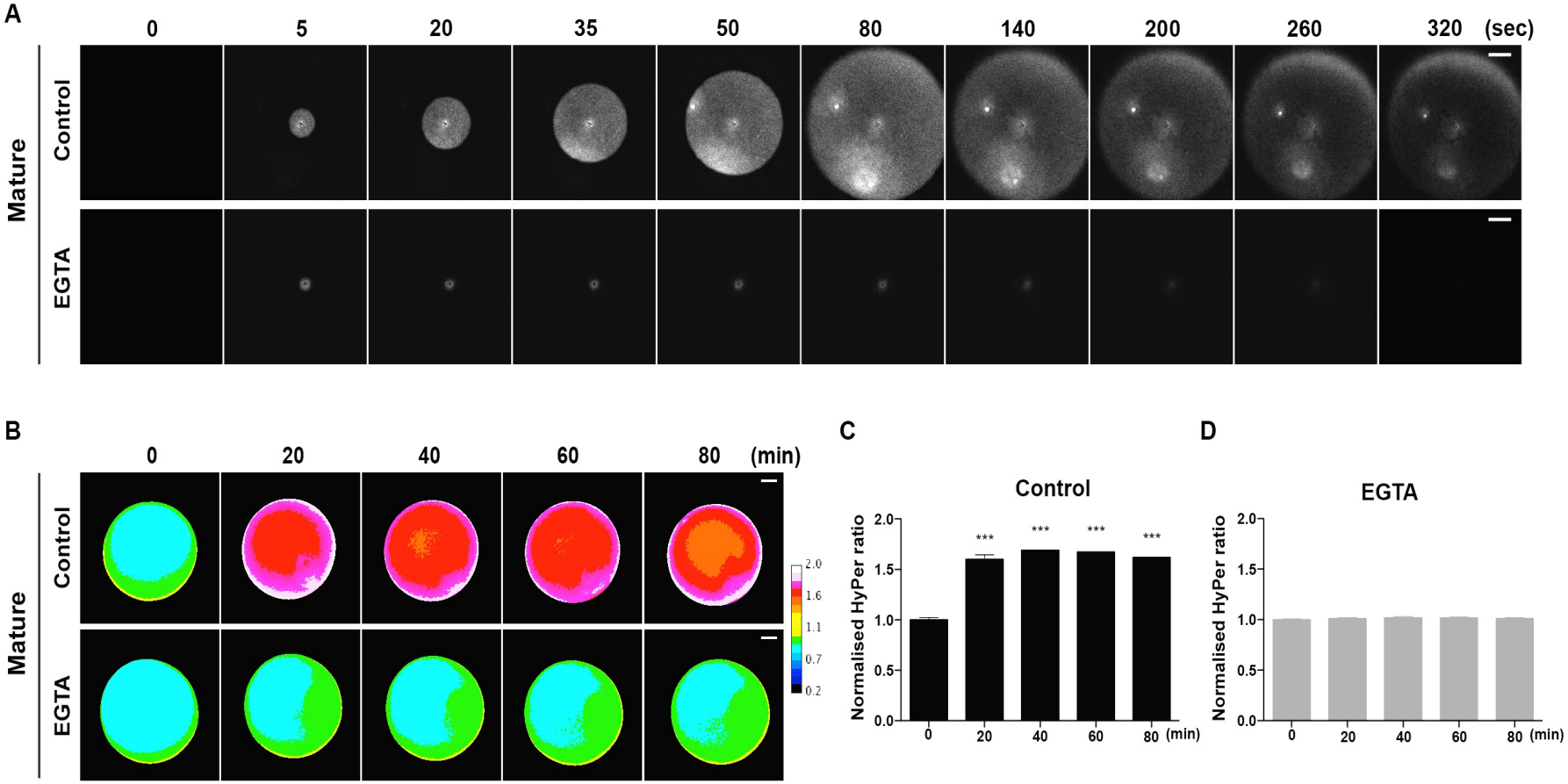

Figure 4-4: EGTA blocks calcium release and ROS production in activated mature oocytes of *X. laevis*.

4.2.3 ROS production is downstream of IP3 receptor following fertilisation

It has long been known that the fertilisation induces a calcium wave, and that this wave is dependent on the release of intracellular calcium stores in endoplasmic reticulum (ER). Inositol 1,4,5-trisphosphate (IP_3) receptors (IP_3R) and ryanodine receptors (RyRs) are calcium channels localised in the ER and they are responsible for the release of the intracellular calcium stores [177]. We then asked which calcium channel might be responsible for the fertilisation / activation dependent wave of calcium that acts upstream of ROS production in Xenopus. Since IP_3 has been shown to contribute to calcium release following fertilisation [178, 179], we tested whether IP_3 was required for induction of the calcium wave and subsequent ROS production. To do this we cloned and overexpressed a construct encoding the IP_3 phosphatase, which dephosphorylates IP_3 to inositol 1,4-bisphosphate (IP_2) and inositol monophosphate (IP_1), thereby inactivating its ability to activate and open the IP_3R channel in the ER. To do this, we injected immature oocytes with 20 ng IP_3 phosphatase mRNA plus mRNAs encoding the calcium indicator R-GECO or HyPerYFP respectively. These oocytes where then matured with progesterone, activated and then imaged for calcium and ROS levels. For control experiments, the R-GECO and HyPerYFP mRNAs were injected without including the IP_3 phosphatase mRNA. No calcium wave was observed in IP_3 phosphatase injected oocytes post activation (Figure 4-5. A), and consequently, no ROS production was observed in these oocytes as well (Figure 4-5. B, D). In contrast, control oocytes exhibited both a calcium wave and ROS production, following activation (Figure 4-5. A, C). These results suggest that IP_3 and IP_3R are necessary for the activation of calcium wave and ROS generation following activation in Xenopus.

We then asked whether the RyR pathway, which has also been shown to be involved in intracellular calcium release following fertilisation in fish and echinoderm egg [184], might also be involved in calcium release and ROS production in Xenopus. To test the role of RyR in calcium dependent ROS generation, we treated activated mature oocytes with ryanodine, which is an antagonist of RyRs [182] and delay calcium wave in *X. laevis* embryos [183]. A gradient of concentrations from 30 uM to 1.5 mM of ryanodine were tested, but none of them was found to inhibit the calcium wave (Figure 4-5. E) or ROS generation in our activated oocyte assay system (Figure 4-5. F). Data showed in Figure 4-5 E-F are from 1.5 mM ryanodine treated oocytes. Although the evidence is not sufficient enough to rule out RyRs' role during calcium dependent ROS production, it suggests that the prominent role for IP_3R in activating calcium release and ROS production in mature oocytes.

Figure 4-5. IP_3 phosphatase inhibits calcium release and ROS production in activated mature oocytes of *X. laevis*.

(A) Panel shows calcium release post activation in a representative sample of control and IP_3 phosphatase injected oocytes, respectively. Images were captured every 15 seconds after activation, and before activation was set as time 0. (B) HyPerYFP ratio (500/430 nm) images of control and IP_3 phosphatase injected oocytes post activation. Images were captured every 20 minutes after activation, and before activation was set as time 0. (C) Quantification of ROS generation post activation in control group, evidenced by normalised HyPerYFP ratio, n=17. (D) Quantification of normalised HyPerYFP ratio of IP_3 phosphatase injected oocytes post activation, n=25. Data are from two independent experiments, Kruskal-Wallis test was used for statistical analysis, error bar indicates S.E.M, * implies $P< 0.05$, *** implies $P<0.001$. (E) Calcium release post activation in control and ryanodine treated oocytes. (F) HyPerYFP ratio (500/430 nm) of control and ryanodine treated oocytes post activation. (G) Quantification of normalised HyPerYFP ratio of control (n=8) and ryanodine (n=8) incubated oocytes post activation. Data are from one attempt of experiment but similar results were obtained in repeated experiments. Two-way ANOVA was used for statistical analysis. Error bar denotes S.E.M. Scale bar is 200 micron.

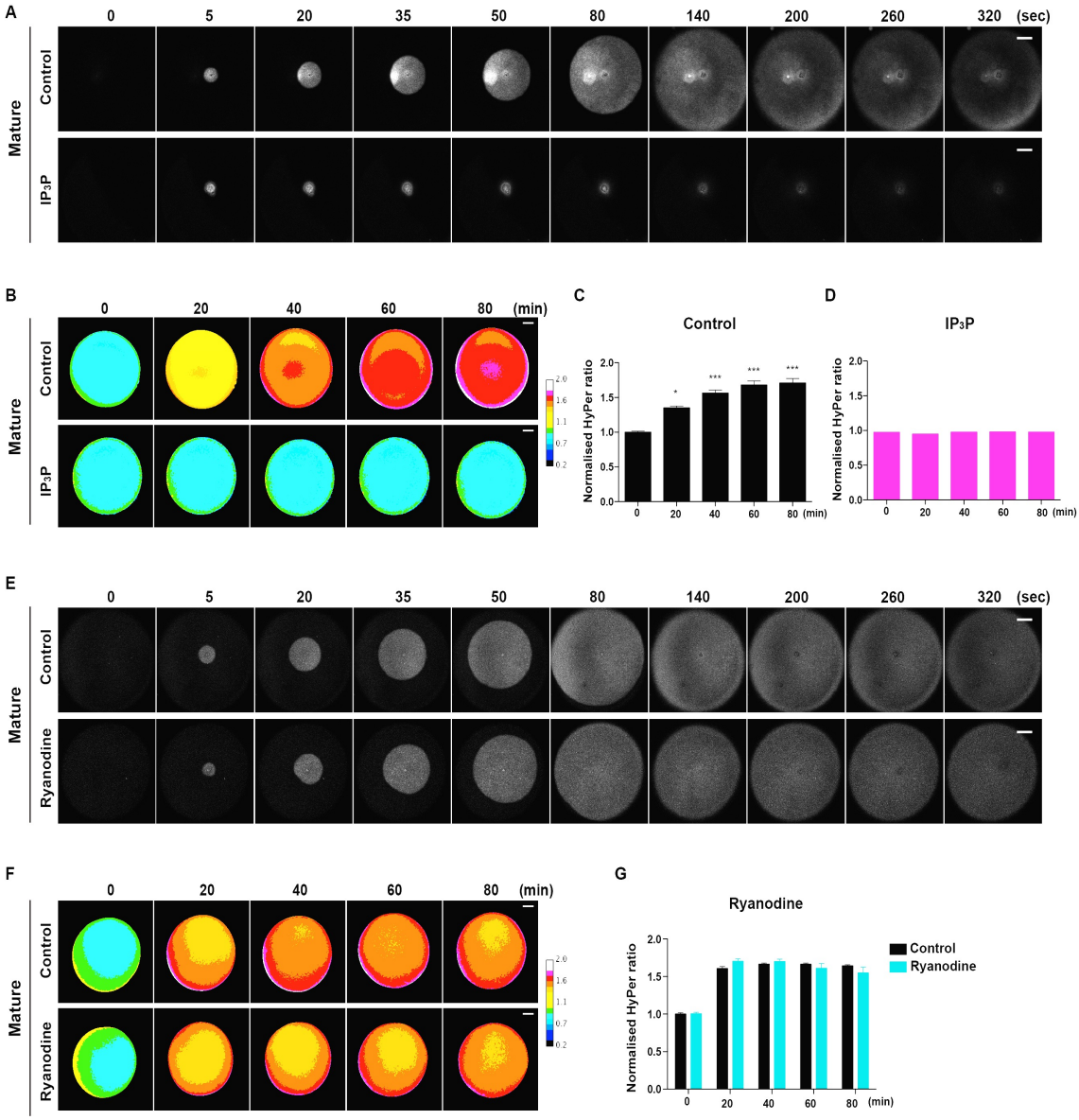

Figure 4-5: IP_3 phosphatase inhibits calcium release and ROS production in activated mature oocytes of *X. laevis*.

4.3. Summary

This chapter explored the relation of activation induced calcium wave and ROS production. I found that the initial burst of ROS following egg activation / fertilisation is calcium dependent and mediated by IP_3R but not RyR channel.

As mentioned previously, most calcium signals that rely on calcium release from internal stores. During fertilisation, IP_3Rs dominant the calcium wave in most species, while RyRs were only reported a substantial contribution in fish and echinoderm eggs [184]. In Xenopus fertilisation process, IP_3R is considered to be the channel releasing calcium from ER and this is also confirmed in my study. The rapid increase in intracellular calcium is thought to activate a series of cellular activities, such as cell proliferation, cell death and cell migration that essential for early embryonic development [184]. As second messengers, ROS have also been reported to regulate various cellular processes (see introduction). My study here provided direct evidence to link ROS and calcium, that ROS production is downstream of calcium signal. However, a question we did not answer here is how does this calcium signal lead to ROS production? Potential candidate would be some ROS generation enzyme that containing a calcium-bind domain or any possible ROS sources that could respond to calcium signals.

Chapter 5: Mitochondria generate ROS post egg activation / fertilisation

5.1. Introduction

In last chapter, we found out that the burst of ROS post egg activation / fertilisation is calcium dependent and downstream of IP_3 in *X. laevis*. However, the source of ROS is still uncovered. To better understand the role of ROS in early embryonic development and to find out the cascades of ROS regulation, it is necessary to figure out the endogenous source of ROS that initiates ROS burst post fertilisation and maintains ROS levels during Xenopus embryonic development. As introduced in chapter 1, there are many organelles and enzymes producing ROS, among which mitochondria and Nox family enzymes are considered to be the main sources of ROS in cells. In this chapter, I will test the major ROS generators to determine their contribution to ROS production in Xenopus oocytes and embryos.

5.2. Results

5.2.1. ROS production post activation is not NADPH oxidase dependent

We next investigated if one of the important sources of ROS, the NADPH oxidases (Noxes) are responsible for the increase in ROS levels, following fertilisation / activation. In 2004, Julian L. Wong et al. reported a dual oxidase Udx1 dependent oxidative burst in sea urchin following fertilisation [185]. We wondered whether Nox family might be responsible for the dramatic increase in ROS levels we found in Xenopus. Importantly, there are several NADPH oxidase members, which contain an N-terminal EF-hand region and can be activated by cytosolic calcium elevation namely Nox5, Duox1 and Duox2 [22]. We therefore tested whether the genes encoding these Noxes were expressed maternally in mature oocytes / eggs, and therefore, were present at the right time to be involved in ROS production, following fertilisation. We isolated mRNA from St. VI mature Xenopus oocytes and we performed RT-PCR with primers specific to *nox5, duox1 and duox2* (Figure 5-1. A). These results showed that only one of the calcium regulated NADPH oxidases is expressed in the mature oocyte, namely *nox5*. To ask whether Nox5 (or any other NADPH oxidase in the egg) might be responsible for ROS production following fertilisation, we incubated mature eggs during activation with diphenyleneiodonium (DPI) and apocynin (APO), two potent inhibitors of NADPH oxidases, including Nox5 [39, 186, 187]. Eggs from HyPerYFP transgenic females were collected, dejellied, and pre-incubated with 10 uM DPI and 1 mM APO for 15 minutes before activation. 0.1% DMSO was used as control. We found no difference in the level of ROS produced in the HyPerYFP transgenic eggs when they

were incubated with DPI or APO, versus the controls (Figure 5-1. B, C, D). These inhibitor studies suggest that ROS production following activation / fertilisation is not dependent on NADPH oxidase activity.

To further test whether Nox5 might play a role in ROS production following activation / fertilisation, we performed a series of *nox5* gain and loss of function experiments. Since the functional domain of Nox5 is highly conserved from human to frog, human derived full length NOX5 (NOX5-α) and a dominant negative form of NOX5 (NOX5-DN) were expressed in Xenopus oocytes [30]. 20 ng mRNA encoding NOX5-α, together with 20 ng HyPerYFP mRNA were injected into immature oocytes. The same amount of mCherry and HyPerYFP mRNAs were also injected in immature oocytes as control. Then the injected oocytes were *in vitro* matured with progesterone and activated by pricking and imaged. We found no significant increase in ROS production when wild-type human NOX5-α was overexpressed in the oocytes (Figure 5-1. E, F). In addition, when we overexpressed the dominant negative version of NOX5 (NOX5-DN), it failed to decrease the level of ROS production in the activated mature oocytes (Figure 5-1. E, G). These results suggest that Nox5, in particular, and NOX family members in general are not responsible for calcium-dependent ROS burst following fertilisation. This led us to consider other possible sources of ROS in the mature oocytes.

Figure 5-1. Role of Nox family members in ROS burst post activation of *X. laevis* oocytes.

(A) Detecting the expression of calcium activated Nox family encoding genes by RT-PCR. This is a representative example of the two independent experiments. (B) HyPerYFP (500/430 nm) ratios images of Noxes inhibitors DPI and APO. Images were taken every 20 minutes after activation and before activation is marked as time 0. The images presented for each condition are derived from same oocyte. (C) Quantification of normalised HyPerYFP ratio of control (n=29) and DPI (n=29) treated mature oocytes post activation. Data are from three independent experiments. (D) Quantification of normalised HyPerYFP ratio of control (n=43) and APO (n=42) treated oocytes post activation. Data are from four biological replicates. (E) ROS levels as evidenced by HyPerYFP (500/430 nm) ratios in *nox5-α* and *nox5-DN* injected mature oocytes after activation. (F) Quantification of normalised HyPerYFP ratio of control (n=35) and *nox5-α* (n=36) injected oocytes post activation. Results are from biological triplicates. (G) Quantification of normalised HyPerYFP ratio of control (n=19) and *nox5-DN* (n=25) injected oocytes after activation. Results are from biological duplicates. Two-way ANOVA was used for statistical analysis of C, D, F and G. Error bar denotes S.E.M. Scale bar is 200 micron.

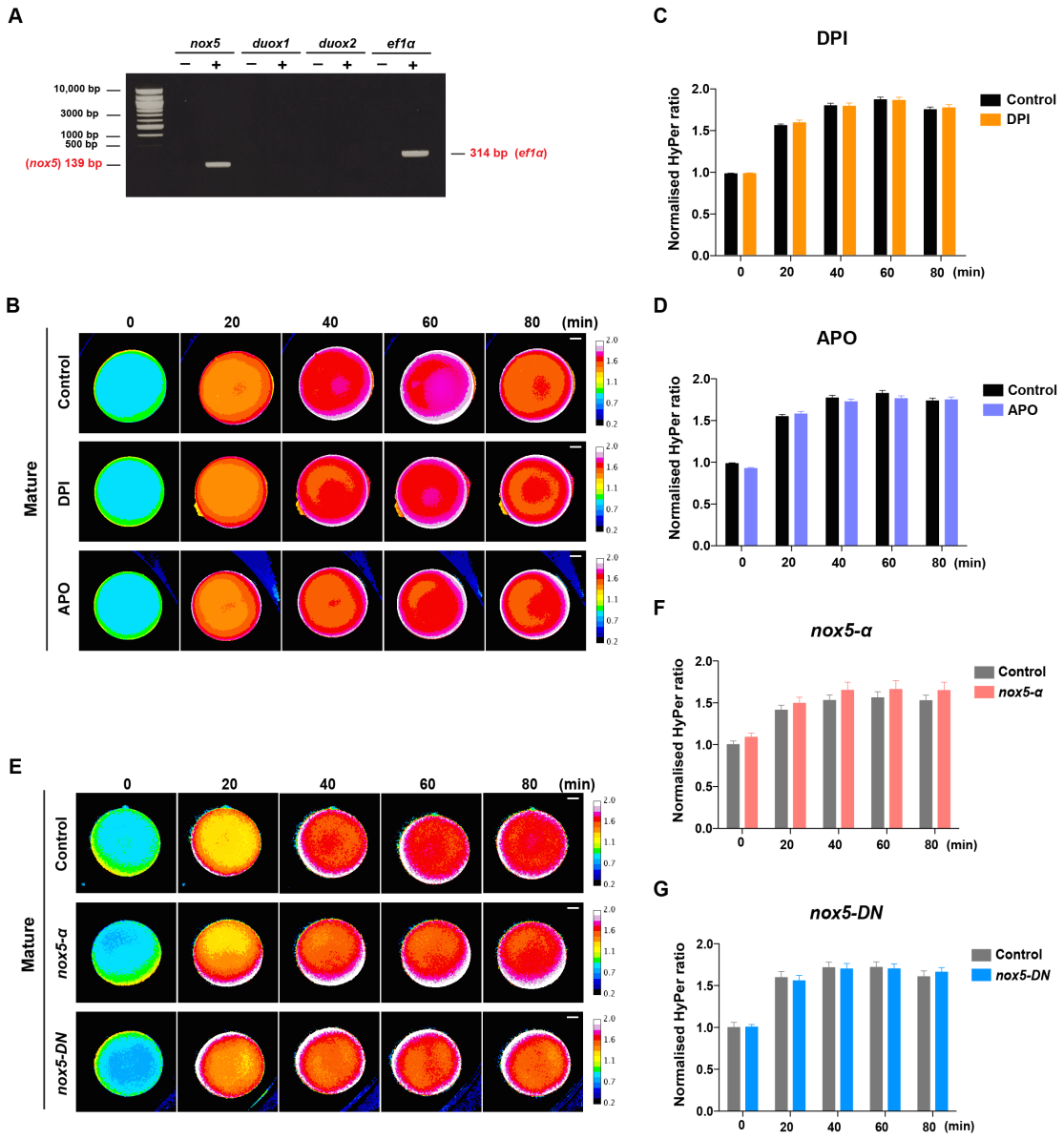

Figure 5-1: Role of Nox family members in ROS burst post activation of *X. laevis* oocytes.

5.2.2. ROS production is dependent on the mitochondrial respiratory chain

Although our data shows that calcium is responsible for stimulating ROS generation following fertilisation or egg activation in *X. laevis*, the origin of ROS remains unknown. Given that mitochondria has long been acknowledged as an important source of ROS [8], we decided to ask whether mitochondrial activity might be responsible for the increase in ROS levels we are seeing. In particular, we wondered whether the calcium release, downstream of IP_3R in ER, might enter into mitochondria through mitochondrial calcium uniporter (MCU), and trigger the mitochondrial respiratory chain to generate ROS [188]. To test this hypothesis, mitochondrion specific antioxidants mitoQ and mito-Tempo were added to mature oocytes, to see whether this might affect ROS production. Both of mitoQ and mito-Tempo contain a lipophilic cation triphenylphosphonium (TPP) moiety, which helps them pass lipid bilayers and accumulate several hundred-fold within mitochondrion [189-191]. MitoQ is a derivative of coenzyme Q and conjugated with TPP and while mito-TEMPO is a piperidine nitroxide combined with TPP. Both of them are known as mitochondria-targeted antioxidants [189-191]. Matured oocytes from HyPerYFP transgenic females were collected, dejellied and pre-incubated with 10 uM mitoQ or mito-TEMPO for 20 minutes before activation. Then oocytes were imaged before pricking activation and every 20 minutes after activation. 10 uM Decyl-TPP that includes the same TPP moiety but has no antioxidant activity was used as control. However, neither mitoQ (Figure 5-2. A, B) nor mito-TEMPO (Figure 5-2. C, D) decreased ROS production post activation.

Figure 5-2. Mitochondria-target antioxidants could not block ROS production in *X. laevis* oocytes.

(A) HyPerYFP ratio (500/430 nm) images of control and mitoQ treated oocytes. Images were taken before activation (time 0) and every 20 minutes after activation. (B) Quantification of normalised HyPerYFP ratio of control (n=21) and mitoQ (n=23) treated oocytes. Results are from biological duplicates. (C) HyPerYFP ratio (500/430 nm) images of control and mito-TEMPO, images were taken before activation (time 0) and every 20 minutes after activation. (D) Quantification of normalised HyPerYFP ratio of control (n=11) and mito-TEMPO (n=11) treated oocytes. Results presented here are from one of two repeated experiments. Two-way ANOVA was used for statistical analysis of B and D. Error bar denotes S.E.M. In each condition of figure A and C, HyPerYFP images from time 0 to time 80 are derived from same oocyte separately. Scale bar is 200 micron.

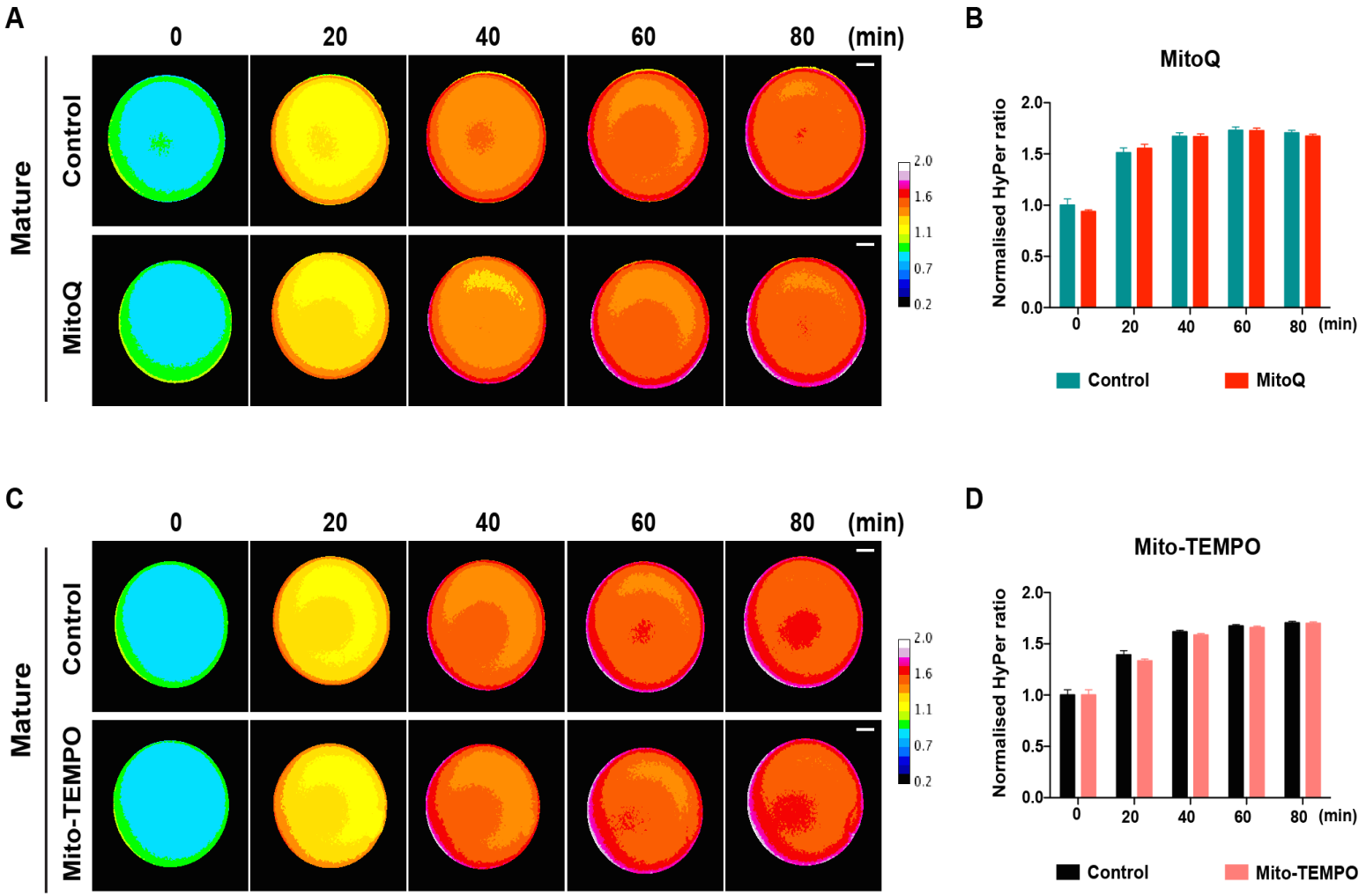

Figure 5-2: Mitochondria-target antioxidants could not block ROS production in *X. laevis* oocytes.

To investigate whether or not mitochondria were involved in ROS production we then turned to several mitochondrial inhibitors, which would be expected to inhibit the electron transport chain and thus affect mitochondria-dependent ROS production (Figure 5-3). Rotenone was used to block electron transport from iron-sulfur centre (Fe-S) to ubiquinone at mitochondrial complex I. Malonate binds the active site of the succinate dehydrogenase (mitochondrial complex II), hence working as a competitive inhibitor of the enzyme. Antimycin A (Antimycin) inhibits the oxidation of ubiquinone in the mitochondrial complex III by binding to Qi site of the cytochrome C reductase. Sodium azide acts in a similar fashion to cyanide, by inhibiting the Hem groups of cytochromes in mitochondrial complex IV. Finally, oligomycin blocks the proton channel of complex V, hence functions as an inhibitor of ATP synthase.

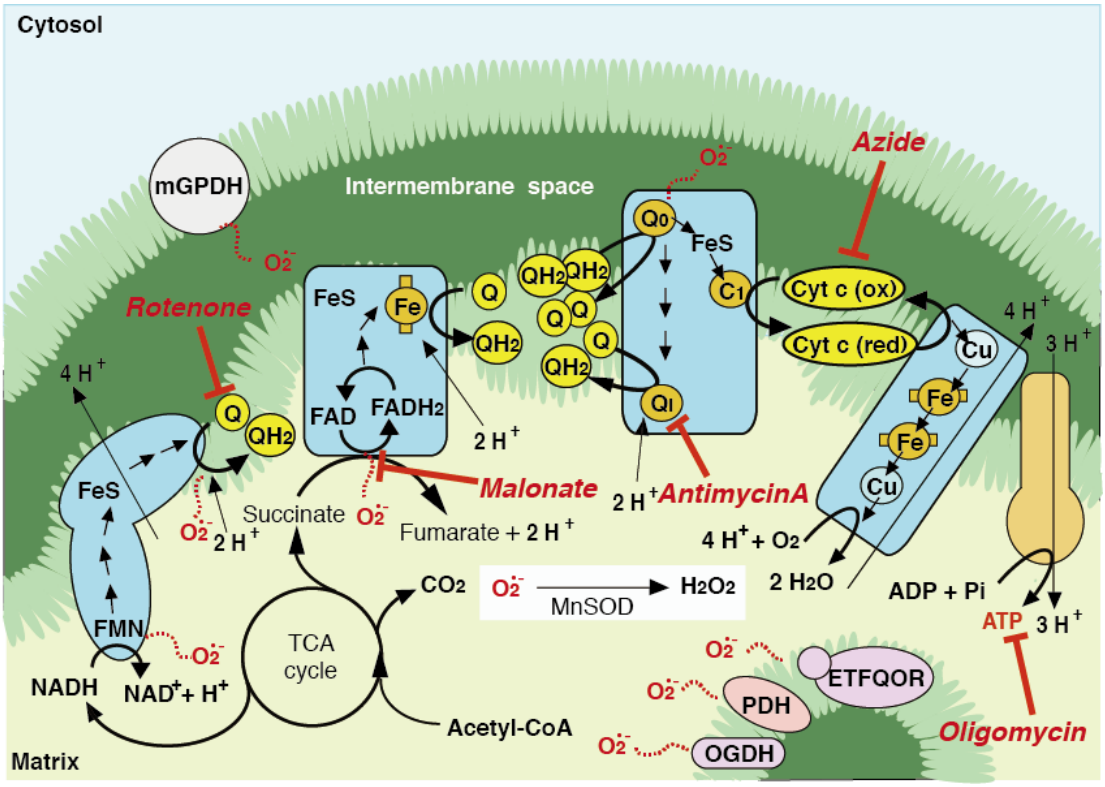

Figure 5-3: Reaction sites of mitochondrial respiratory chain inhibitors.

This figure shows the targeting sites of mitochondrial inhibitors. Inhibitors are labelled bold in red colour and followed by a red arrow pointing to the reaction site, respectively. This figure was generated by Dr. Shoko Ishibashi.

Mature oocytes (eggs) were collected from transgenic HyPerYFP female and incubated with mitochondrial inhibitors for assessment. Mitochondrial complex I inhibitor rotenone showed no detectable change of ROS levels relative to controls, following activation, as evidenced by the HyPerYFP ratio (Figure 5-4. A, B). Interestingly, activated eggs incubated with inhibitors of mitochondrial complex II, III and IV exhibited a significant lower level of ROS production than controls. In particular, eggs treated with the complex II inhibitor malonate, at 5 mM concentration displayed a significantly lower ROS level, both pre and post-activation (Figure 5-4. C, D). In addition, activated eggs treated with 10 uM antimycin (Figure 5-4. E, F) or 1 mM sodium azide (Figure 5-4. G, H) also displayed significantly lower ROS levels than controls. Given that we were concerned that the decrease in ROS level might be due to depletion of ATP levels, we also tested whether oligomycin, potent inhibitor of the ATP synthase, affected ROS production following activation, and we found that activated eggs treated with 6.5 uM oligomycin showed no observable effect on ROS production relative to controls (Figure 5-4. I, J). These data suggest that ROS production, following egg activation / fertilization depends on mitochondrial ROS production, in particular downstream of complex II, III and IV.

It is also notably that malonate treated activated eggs exhibited a decrease in ROS levels before activation, suggesting that ROS production from the mitochondrial complex II is required for maintaining the low, but detectable ROS level in unfertilised eggs.

To further confirm these results, we also employed a mitochondrial specific HyPer, named mito-HyPer, which contains a triphenylphosphonium cation component that can drive accumulation of HyPerYFP within mitochondria [61]. Given that we did not have a transgenic line expressing this construct maternally, we injected immature *X. laevis* oocytes with 20 ng mito-HyPer mRNA, matured with progesterone and activated them by pricking prior to HyperYFP imaging. Our data show that the mitochondrially localised HyPerYFP responded in similar fashion to the inhibitors as we saw using the cytoplasmic HyPerYFP transgenic eggs (Figure 5-5), confirming that the initial oxidative burst following fertilisation is generated by complex II, III, IV from mitochondria.

Figure 5-4. Mitochondrial respiratory chain inhibitors suppressed ROS production in mature oocytes of *X. laevis*.

(A) Oxidative state evidenced by HyPer (500/430 nm) of rotenone treated oocytes. Images were captured before activation (time "0") and every 20 minutes after activation. (B) Quantification of normalised HyPer ratio of rotenone treated oocytes post activation, control n=34, rotenone n=36. (C) Oxidative state of malonate treated oocytes post activation and its quantification of normalised HyPer ratio (D), control n=46, malonate n=45. (E) HyPer images of antimycin treated oocytes post activation and its quantification of normalised HyPer ratio (F), control n=43, antimycin n=46. (G) HyPer images of sodium azide treated oocytes post activation and its quantification (H), control n=20, sodium azide n=25. (I) HyPer images of oligomycin treated oocytes post activation and its quantification (J), control n=43, oligomycin n=42. Two-way ANOVA was used for statistical analysis. Error bar denotes S.E.M, **** states $P<0.0001$. In figure A, C, E, G and I, HyPer images from time "0" to time "80" are derived from same oocyte separately. Scale bar is 200 micron. Data above are from four experimental replicates.

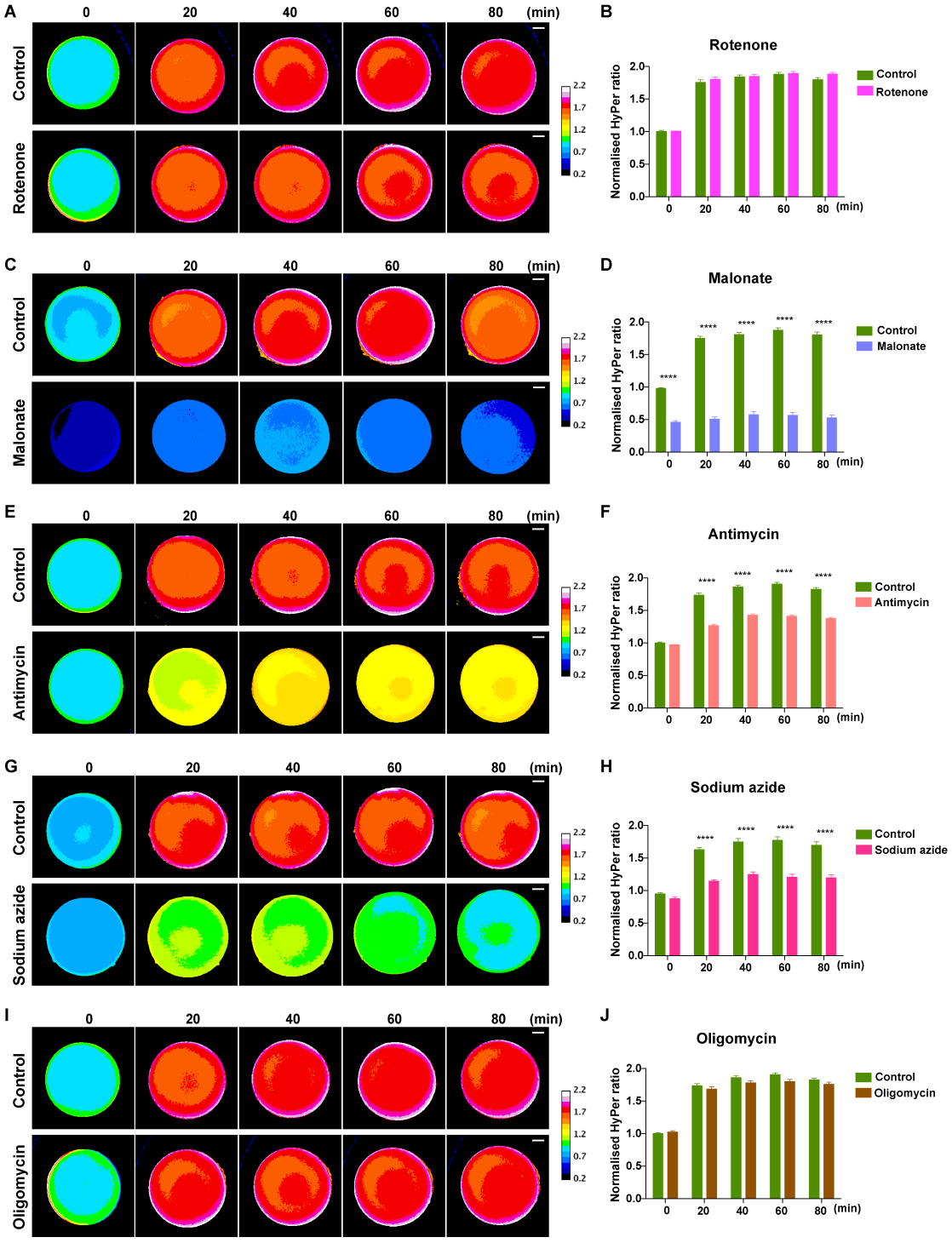

Figure 5-4: Mitochondrial respiratory chain inhibitors suppressed ROS production in mature oocytes of *X. laevis*.

Figure 5-5. A decrease of ROS production detected by mito-HyPer in mature oocytes post activation.

(A-E) Plots show quantification of ROS levels, as evidenced by mito-HyPer (500/430 nm) after incubating activated mature oocytes with different mitochondrial inhibitors. For ratio analysis, images were captured before activation (time "0") and every 20 minutes after activation. (A) Quantification of normalised mito-HyPer ratio of control (n=28) and rotenone (n=28) treated oocytes post activation. (B) Quantification of normalised mito-HyPer of malonate treated oocytes post activation, control n=28, malonate n=27. (C) Quantification of normalised mito-HyPer of antimycin treated oocytes post activation, control n=28, antimycin n=26. (D) Quantification of normalised mito-HyPer of sodium azide treated oocytes post activation, control n=28, sodium azide n=28. (E) Quantification of normalised mito-HyPer of oligomycin treated oocytes post activation, control n=47, oligmycin n=40. Data were analysed using two-way ANOVA, error bar denotes S.E.M, ** states P<0.01, ***states P<0.001 and **** states P<0.0001.

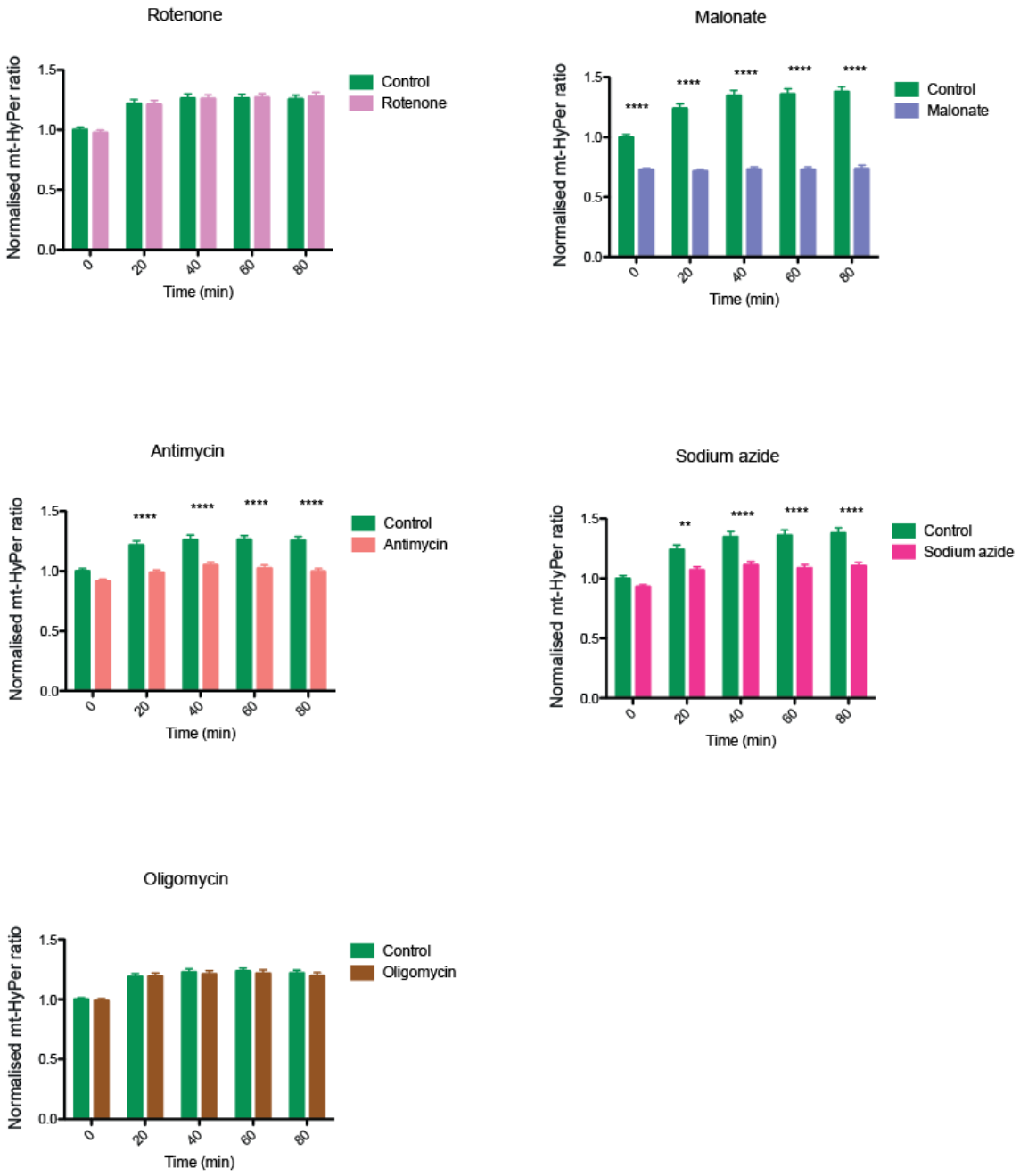

Figure 5-5: A decrease of ROS production detected by mito-HyPer in mature oocytes post activation.

Given that we had seen no effect on ROS production in activated eggs, even when they were treated with oligomycin (the ATP synthase inhibitor), we reasoned that this lack of an effect could have been due to oligomycin not working. Therefore we decided to test ATP levels in activated eggs treated with the mitochondrial inhibitors, including oligomycin. Mature oocytes / eggs were pre-treated with mitochondrial inhibitors and prick activated. In each treatment, 20 eggs were collected before activation (time 0), 30 minutes and 60 minutes after activation. In each test, a gradient of known ATP concentrations were performed to calibrate the ATP assay. Additionally, 1 unit/ml Apyrase (an ATPase) was used to ensure that the signal measured was ATP, and not an artifact from another nucleotide. Concentrations of mitochondrial inhibitors were used as before. Intriguingly, we observed no significant effect on ATP levels, after addition of any of the mitochondrial inhibitors (Figure 5-6. A-E), except for oligomycin (Figure 5-6. E). These data suggest that the respiratory chain of mitochondria is not required to maintain ATP levels in activated eggs, raising the question of what is responsible for ATP synthesis in post-fertilisation eggs? The answer is likely to be glycolysis. In 2012, Agathocleous et al. reported that in embryonic Xenopus retina cells, the dividing progenitor cells mainly rely on glycogen to fuel aerobic glycolysis for ATP production, rather than the classical oxidative phosphorylation inside mitochondrion, which demonstrates the importance of the coordination of glycolysis versus oxidative phosphorylation, though a process referred to as the Warburg Effect in normal development [192]. Intriguingly, our data showed that treatment with oligomycin resulted in a significant increase in ATP levels in post-activated eggs. This result was totally the opposite of what we expected, as we envisioned a significant decrease in ATP levels, after treating the eggs with oligomycin. This result can be explained by taking two considerations. One is the data from the other mitochondrial inhibitors suggest that the respiratory chain of mitochondria are not involved in maintaining ATP levels in activated eggs, thus inhibiting the ATP synthase, would at best, be expected to have no effect on ATP levels. However, the fact that we see an increase in ATP levels suggest that perhaps, the ATP synthase is working backwards in post-activated eggs, such that ATP is being hydrolysed to ADP, in order to maintain the H^+ gradient across the mitochondrial membrane, and this consumption is being inhibited, thus resulting in higher ATP levels in the eggs. This is an extremely interesting possibility, which has been seen in bacteria, were ATP is consumed in order to maintain the proton gradient, which is necessary to assist the transport of metabolites across the membrane [193]. Perhaps the mitochondria in early embryos also run the ATP synthase backwards in order to maintain the H^+ gradient for efficient transport of metabolites across the mitochondrial membrane as well. This intriguing possibility deserves further investigation.

We were also concerned that the mitochondrial inhibitors might impair the fertilisation / activation induced calcium wave, and thus disrupt ROS production in this manner. To determine whether this might be the case, we injected immature oocytes with mRNAs encoding R-GECO, matured them with progesterone and pretreated the mature oocytes with mitochondrial inhibitors for 20 minutes before laser activation. The imaging data showed that there was no significant difference detected in the experimental groups containing the inhibitors and those in the control group (Figure 5-7. A-F), suggesting that the mitochondrial inhibitors had no effect on the initiation of the calcium wave, post-activation. Therefore this result confirmed that the effect of the mitochondrial inhibitors on ROS production was not due to inhibition of the calcium wave.

Figure 5-6. Mitochondrial respiratory chain inhibitors did not lessen intracellular ATP.

(A) ATP level was measured with rotenone, malonate (B), antimycin (C), sodium azide (D) and oligomycin (E) treated oocytes before activation (time “0”) and every 30 minutes after activation. Mann-Whitney test was used for statistical analysis at each time point, n=5, error bars mean S.E.M, * denotes $P<0.05$, ** denotes $P<0.01$. Data are from three independent experiments.

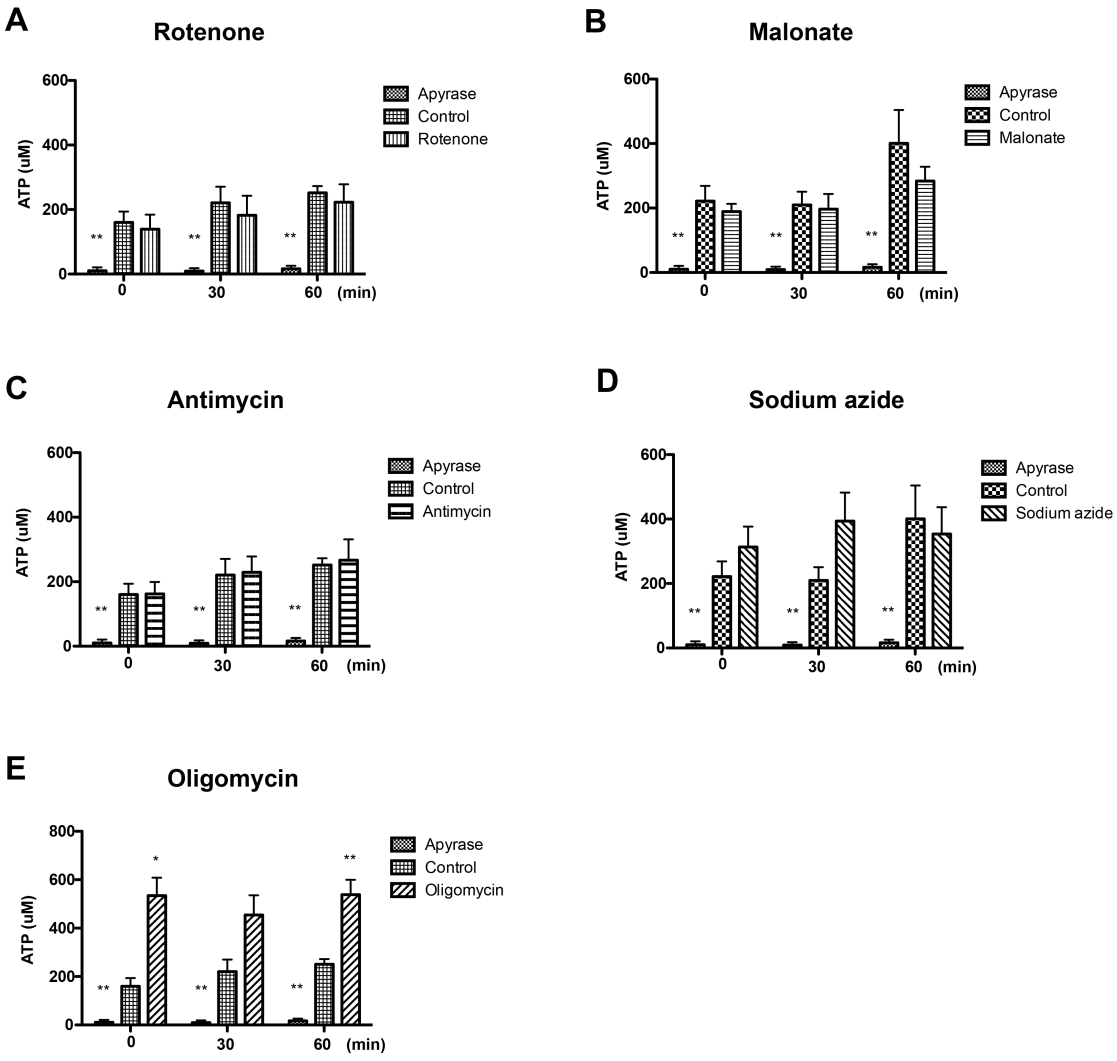

Figure 5-6: Mitochondrial respiratory chain inhibitors did not lessen intracellular ATP.

Figure 5-7. Mitochondrial respiratory chain inhibitors did not affect calcium oscillation in activated mature oocyte.

(A) Panels show calcium wave (inferred by R-GECO) post activation in rotenone, malonate (B), antimycin (C), sodium azide (D) and oligomycin (E) treated oocytes. Images were captured before activation (time “0”) and every 15 seconds after activation. A representative sample was shown in each condition. Scale bar equals 200 micron. (F) Quantification of R-GECO labeled calcium intensity (normalised). Kruskal-Wallis test was employed for statistical analysis at each time point, n=6, error bar means S.E.M. Data are from one of the biological duplicate experiments.

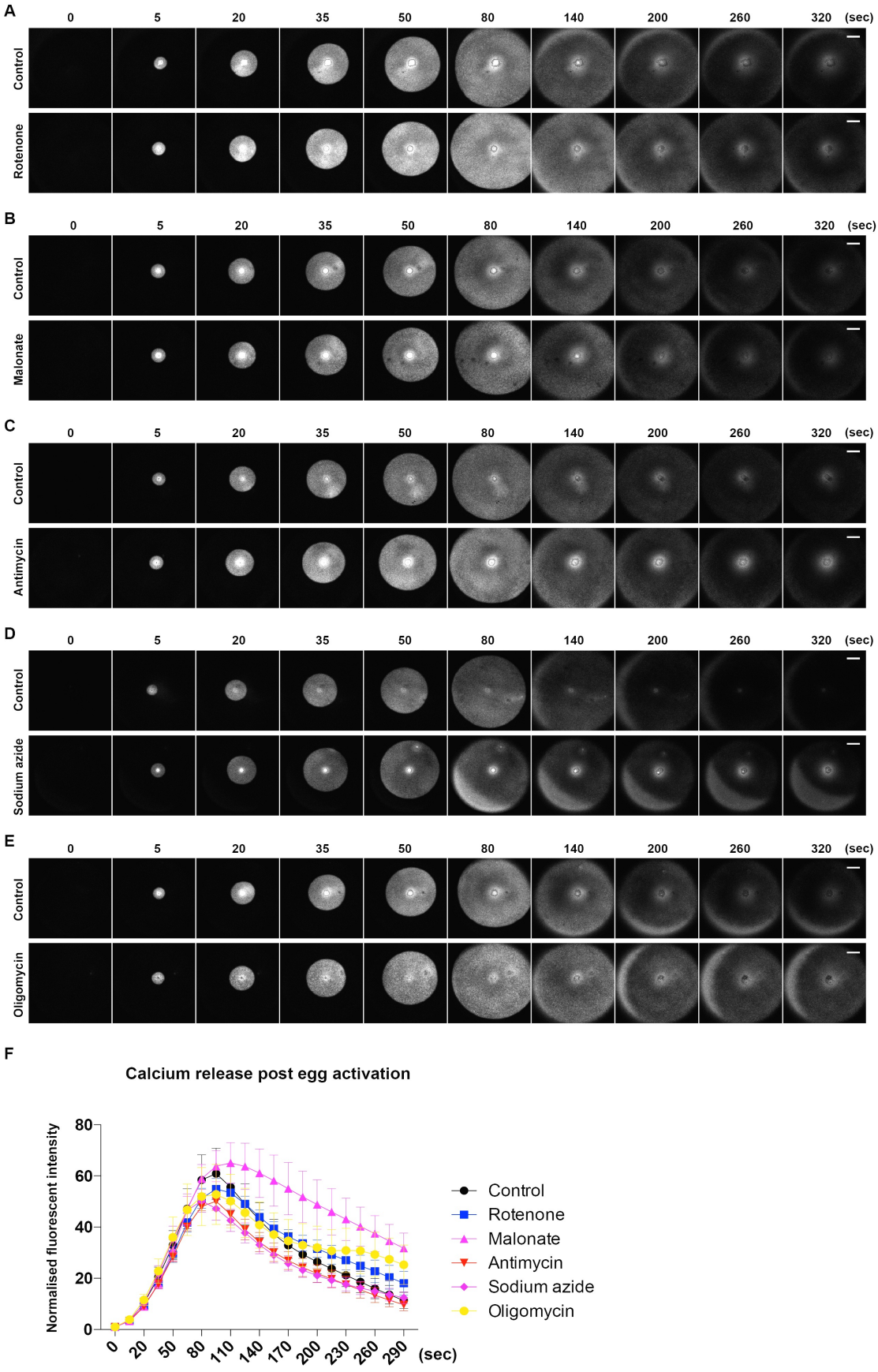

Figure 5-7: Mitochondrial respiratory chain inhibitors did not affect calcium oscillation in activated mature oocyte.

5.2.3. Effect of mitochondrial membrane potential on ROS generation

In respiring mitochondria, when electrons go through the electron transport chain, there are protons pumping from the matrix to the inter-membrane space, thus creating an electrochemical gradient which build up the inner mitochondrial trans-membrane potential (ΔΨm). Studies have shown that ROS generation could be dramatically regulated by the amplitude of ΔΨm in mitochondria [194]. To figure out the role of ΔΨm in fertilisation induced ROS production, we examined a mitochondrial uncoupler, FCCP, which could specifically increase the proton permeability thus destroying the mitochondrial ΔΨm. Mature Xenopus oocytes expressing HyPerYFP were collected from transgenic females and incubated with 10 μM FCCP for imaging. 0.1% DMSO was used as control. As expected, a sharp decline of ROS production was observed in FCCP treated embryos evidenced by HyPerYFP (Figure 5-8. A, B), which was further confirmed by mito-HyPer (Figure 5-8. C). Like in the case of treating pre-activated eggs with malonate, we observed a significant decrease in ROS levels even before activation, suggesting that the ΔΨm is required to maintain ROS levels in resting, pre-fertilised eggs.

Since FCCP could disconnect the electron transport chain from ATP formation, an ATP assay was also performed in FCCP treated oocytes. However, there was no decrease of ATP level was observed in FCCP treated oocytes, and indeed, we saw an increase level of ATP after oocyte activation (Figure 5-8. D). This result is similar to that obtained after oligomycin treatment, where an increase in ATP levels was also observed. We next tested whether FCCP treated oocytes displayed an effect in the calcium wave following activation, and we found no significant difference in the treated oocytes compared to control oocytes (Figure 5-8. E). These results suggest that ROS production after egg activation / fertilisation requires an established mitochondrial membrane potential.

Figure 5-8. Role of FCCP on ROS production.

(A) Panel shows representative HyPerYFP (500/430 nm) images of FCCP treated oocytes, which captured before activation (time 0) and every 20 minutes after activation. (B) Quantification of normalised HyPerYFP ratio of A, control n=22, FCCP, n=21. (C) Quantification of mito-HyPerYFP ratio in FCCP treated oocytes, control n=19, FCCP, n=10. (D) Intracellular ATP level of FCCP treated oocytes, n=3. (E) Status of calcium activity of FCCP treated oocytes post activation, control n=6, FCCP n=5. Mann-Whitney test was used for statistical analysis and error bars indicate S.E.M.

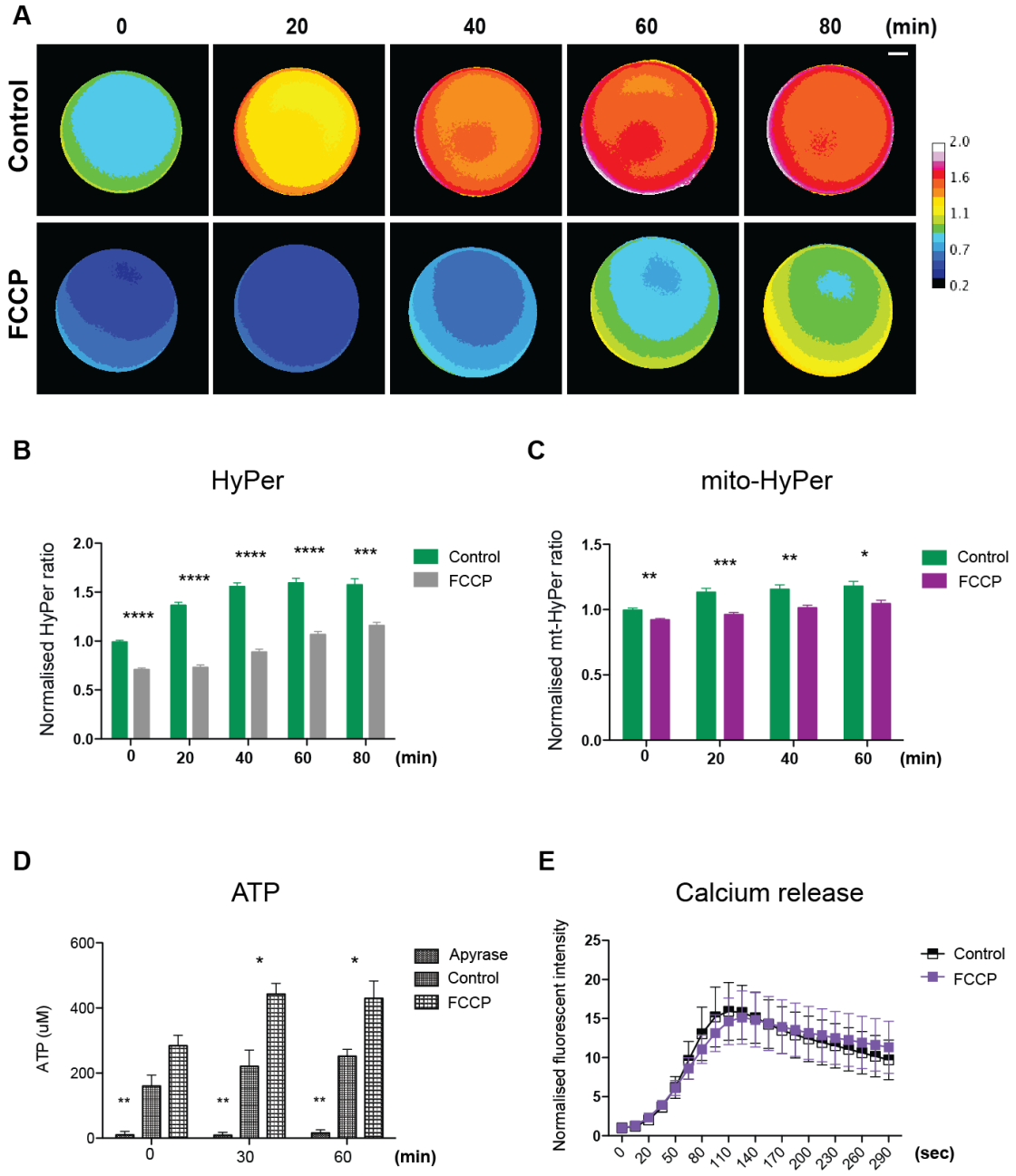

Figure 5-8: Role of FCCP on ROS production.

5.2.4. Lowering ROS using mitochondrial respiratory chain inhibitor causes cell cycle arrest

To address the role of ROS during early embryogenesis, we next sought to inhibit the mitochondrial respiration and then follow the embryos through development. For this, 2/4-cell stage embryos were treated with mitochondrial inhibitors and they were observed at St. 6.5 (early blastula) and St. 10 (early gastrula) of development (Figure 5-9. A). DMSO was used as control for rotenone, antimycin and oligomycin, while H_2O was used as control malonate and sodium azide. After treatment, rotenone treated embryos were found to arrest at the 4-cell stage (Figure 5-9. A.b1), after which cell death soon followed (Figure 5-9. A.b2). Malonate treated embryos encountered a cell-cycle arrest at 8 or 16-cell stage (Figure 5-9. A.c1) and underwent cell death thereafter (Figure 5-9. A.c2). A similar phenomenon was also seen in sodium azide treated embryos, when treated at 2/4-cell stage, embryos failed to progress to the 16-cell stage (Figure 5-9. A.e1). Although antimycin was not found to affect the cell cycle immediately (Figure 5-9. A.d1), embryos displayed development defects at the blastula stage (Figure 5-9. A.d2), after which they displayed cell death several hours later. Oligomycin showed no overt defects in cleavage stage embryos (Figure 5-9. A.f1-2). An analogous experiment was performed by adding the inhibitor slightly later, at the 16-cell stage embryos to confirm the above phenotype, and as expected, cell division defects were exhibited at the 32 or 64-cell stage embryos (Figure 5-9. B). The number of normally developed embryos versus total number of embryos are listed under each condition, from which we can see, except for oligomycin, embryos treated with mitochondrial inhibitors experienced cell cycle arrest and death after several hours.

Figure 5-9. Mitochondrial inhibitors impair cell division in X. laevis embryo.

(A) Embryos were treated with mitochondrial inhibitors at 2/4-cell stage and images were captured at St. 6.5 and St. 10. (B) Embryos were treated with mitochondrial inhibitors at 16-cell stage and photoed at St. 6.5 and St. 8. Same amount of DMSO was used as control of rotenone, antimycin and oligomycin, while H_2O was used as control of malonate and sodium azide. Number of embryos exhibited displayed phenotype in contrast with the total number of treated embryos are listed under each condition and followed by a calculated percentage. Scale bar is 1 millimeter.

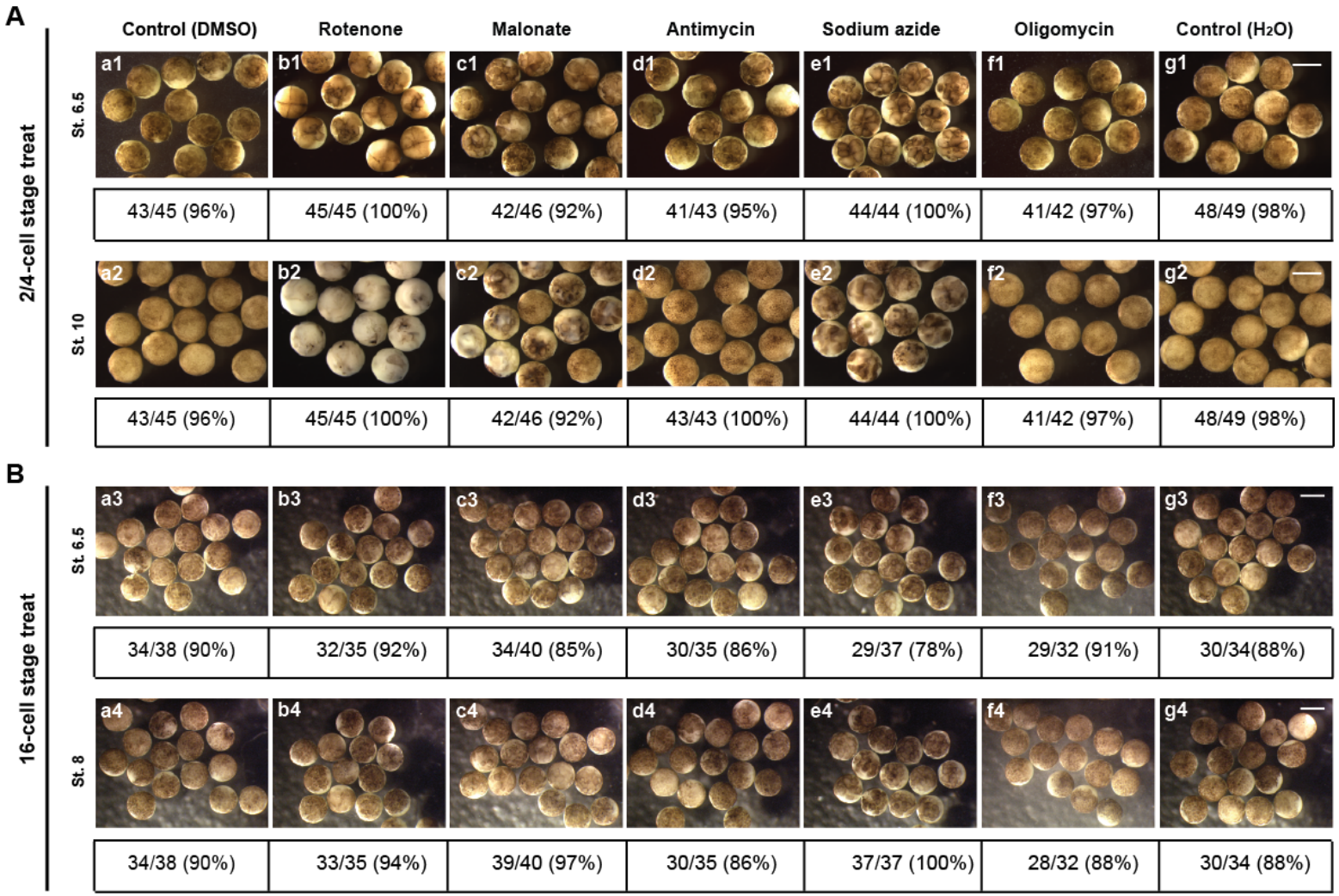

Figure 5-9: Mitochondrial inhibitors impair cell division in *X. laevis* embryo.

We next sought to examine whether these phenotypes were correlated with reductions of ROS levels. 2-cell stage embryos obtained from transgenic females expressing HyPerYFP were treated with mitochondrial inhibitors and monitored for ROS level at the 4/8-cell, 32-cell and mid-blastula (St. 8) stages. An elevated ROS level evidenced by HyPer ratio was observed in control group (DMSO or H_2O treated embryos) (Figure 5-10). Similar to control group, oligomycin treated embryos did not display any reduction of ROS levels (Figure 5-10. I, J) or cell cycle arrest in cleavage stage embryos (Figure 5-9. f1-4). While embryos incubated with malonate (Figure 5-10. C, D) or sodium azide (Figure 5-10. G, H), showed a significant diminution of ROS levels at the 4/8-cell stage, at the time when cell division defects were also apparent (Figure 5-9. c1-4, e1-4). Antimycin, which caused cell-cycle arrest only at the blastula stage (Figure 5-9. d1-4), presented a moderate decline of ROS levels (Figure 5-10. E, F). For rotenone, although it induced cell cycle arrest after treatment (Figure 5-9. A.b1), similar as in oocytes, no decrease in ROS levels was detected in cleavage stage embryos (Figure 5-10. A, B). This cell division defect caused by rotenone has been reported earlier. In 1974, Barham SS and Brinkley BR reported that rotenone could inhibit mitosis by binding directly to tubulin to prevent spindle microtubule assembly [195]. In 2001, Jeffrey S. Armstrong etc. found that rotenone could induce a dose-dependent cell cycle arrest predominantly at the G2/M stage of the cycle and consequently apoptosis in a human B lymphoma cell line PW [196]. These data could explain the phenotype we observed in rotenone treated embryos (cell cycle arrest and cell death), even though the embryos showed no effect on ROS levels, demonstrating that rotenone might have effects that are not mediated through its mitochondrial inhibitor role.

Considering that ROS reduction and cell cycle arrest may come from an interruption in ATP synthesis, we also assessed ATP levels in mitochondrial inhibitor treated embryos at 4/8-cell stage and 32-cell stage. Nevertheless, no recorded recession of ATP level was found (Figure 5-11). Therefore, we suspect that the cell cycle arrest observed in Xenopus embryos might have been caused by decline of intracellular ROS levels. Intriguingly, we saw an increase in ATP levels once again in the oligomycin treated embryos (Figure 5-11. E), suggesting that the ATP synthase might still be functioning in reverse during early embryogenesis.

Figure 5-10. Mitochondrial inhibitors decrease ROS level in cleavage stage embryos of *X. laevis*.

Embryos were treated with mitochondrial inhibitors at 2-cell stage and detected for HyPer signal at 4-cell stage, 32-cell stage and stage 8. Representative HyPerYFP (500/430 nm) images of rotenone (A) (n=13), malonate (C) (n=12), antimycin (E) (n=13), sodium azide (G) (n=12), oligomycin (I) (n=13) treated embryos and their quantifications at different stages. Mann-Whitney test has been used for statistical analysis. Error bar indicates S.E.M, *** represents $P<0.001$. Scale bar is 200 micron. Results have been repeated twice.

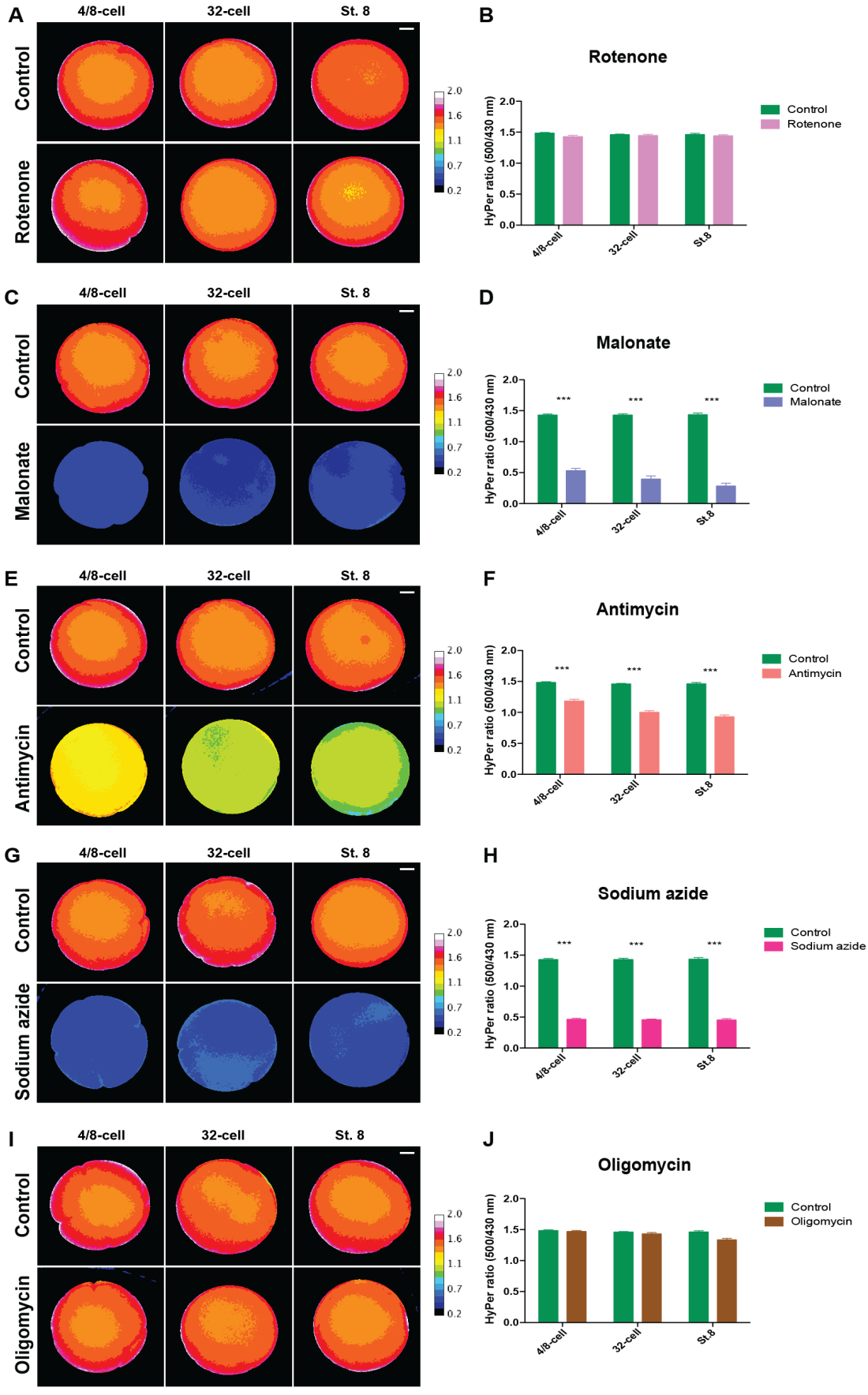

Figure 5-10: Mitochondrial inhibitors decrease ROS level in cleavage stage embryos of *X. laevis*.

Figure 5-11. ATP levels in cleavage stage embryos of *X. laevis*.

Embryos were treated with mitochondrial inhibitors at 2-cell stage and homogenised for ATP measurement at 4/8-cell stage and 32-cell stage. 1 unit/ml Apyrase has been used as a negative control. Data came from 6 replicates, n=6. Mann-Whitney test was used for statistical analysis. Error bar indicates S.E.M, * represents $P<0.05$ and ** represents $P<0.01$.

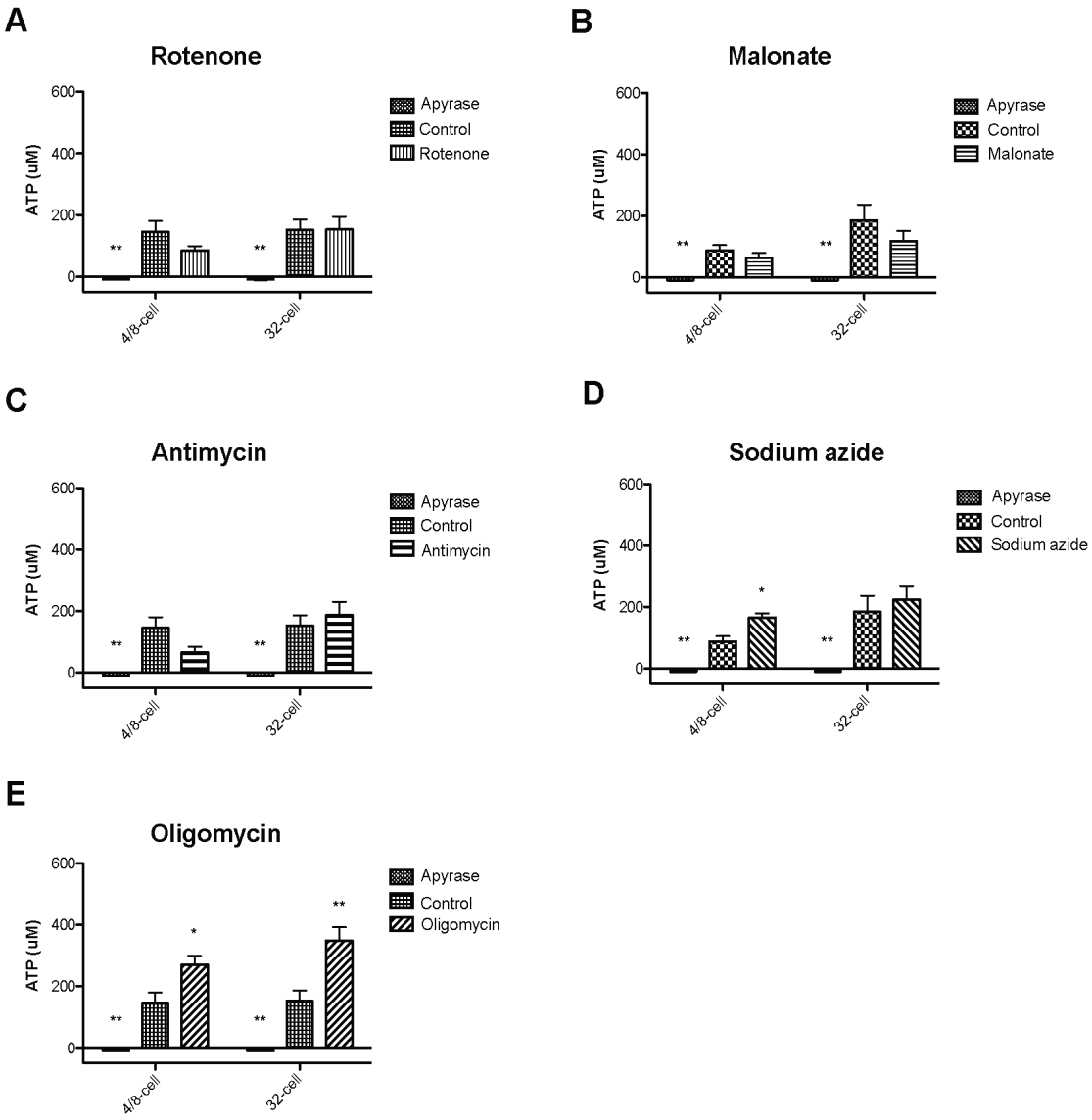

Figure 5-11: ATP levels in cleavage stage embryos of *X. laevis*.

5.2.5. Lowering ROS levels using mitochondrial respiratory chain inhibitors impair gastrulation

As shown in chapter 3, lowering ROS with NAC (an antioxidant) resulted in gastrulation defects in Xenpus embryos, we wonder whether lowering ROS levels using mitochondrial inhibitors also leading to a similar phenotype. We next suppressed ROS production in mid-blastula stage embryos with various mitochondrial inhibitors. Figure 5-12 shows phenotypes observed at St. 11 (mid-gastrula), St. 14 (neurula) and St. 23 (early tailbud) stages, after adding the inhibitors at the mid-blastula stage (St. 8.5). Embryos treated with malonate, sodium azide and antimycin displayed a strong gastrulation defect, where embryogenesis stopped thereafter (Figure 5-12. c1-4, d1-4, e1-4). Oligomycin treated embryos exhibited normal development until St. 15, but then development ceased (Figure 5-12. f1-4). Although rotenone induced cell cycle arrest at cleavage stage, no defect was detected when inhibitor was added from the mid-blastula stage, as assessed at the gastrula, neurula and early tailbud stages (Figure 5-12. b1-4).

To figure out whether these phenotypes correlated with a decrease in ROS levels, mid-blastula stage (St. 8.5) embryos from transgenic females expressing HyPerYFP were incubated with various mitochondrial inhibitors and tested for ROS levels at St. 11 (mid-gastrula stage) and St.14 (neurula stage). Similar to cleavage stage, embryos treated with malonate, sodium azide and antimycin exhibited a reduction of ROS at St. 11 and St. 14 (Figure 5-13. C-H), which correlated with a gastrulation defect. While embryos treated with Rotenone did not show any detectable reduction of ROS levels (Figure 5-13. A, B) and developed normally until died at St. 27. But surprisingly, oligomycin treated embryos also displayed a decrease in ROS levels at St. 11 and St. 14. It is noticed that although no obvious defects were observed in oligomycin treated embryos at gastrula stage, a delay of development was seen at neurula stage, since when embryonic development ceased. Considering the gastrulation defects and ROS level decrease may due to an disruption in ATP synthesis, we tested ATP levels in mitochondrial inhibitor treated embryos at mid-gastrula (St. 11) and neurula (St. 14) stage. Similar to the situation in oocytes or in cleavage stage embryos, we were unable to detect any reduction of ATP levels in embryos treated with mitochondrial inhibitors (Figure 5-14). These results suggest an important role of ROS in the early embryonic development of *X. laevis* embryos.

Figure 5-12. Mitochondrial inhibitors impair gastrulation in *X. laevis* embryos.

Embryos were treated with mitochondrial inhibitors from the mid-blastula stage (St. 8.5) and imaged at St. 11 (mid-gastrula), St.14 (neurula) and St.22-23 (early tailbud). DMSO was used as control for rotenone, antimycin and oligomycin treated embryos; H_2O was used as control for malonate and sodium azide treated embryos. Number of embryos exhibited displayed phenotype in contrast with the total number of treated embryos are listed under each condition and followed by a calculated percentage. Scale bar is 1 millimetre.

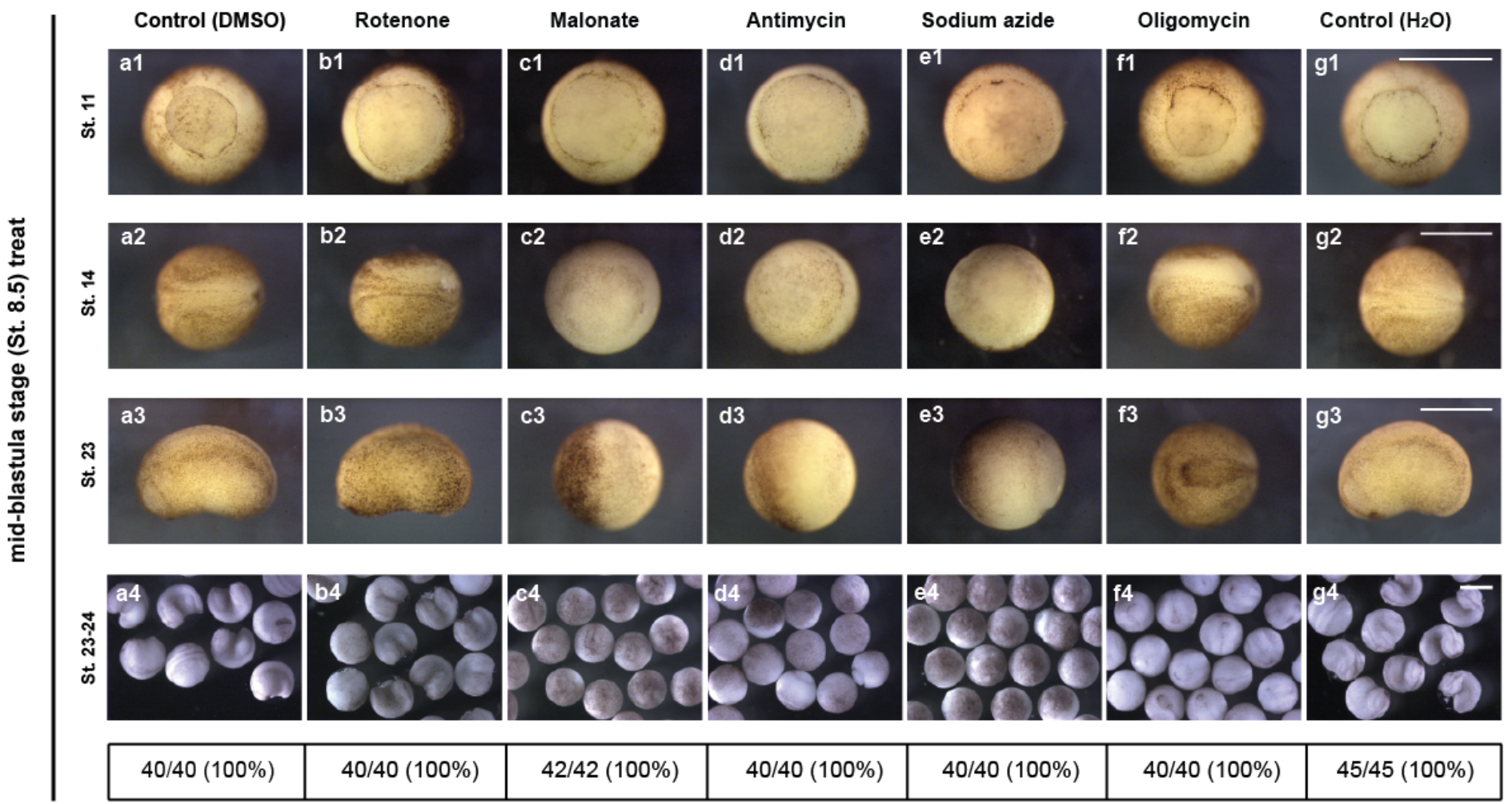

Figure 5-12: Mitochondrial inhibitors impair gastrulation in *X. laevis* embryos.

Figure 5-13. Mitochondrial inhibitors lower ROS level in gastrula stage embryos of *X. laevis*.

Transgenic HyPerYFP embryos were treated with mitochondrial inhibitors at the mid-blastula stage and assayed for ROS levels at St. 11 (mid-gastrula) and St. 14 (neurula). Representative HyPer ratiometric images showing embryos treated with mitochondrial inhibitors and their quantifications at different stages. (A) HyPerYFP ratio of rotenone treated embryos and its quantification (B) (control, n=14, rotenone, n=14). (C) Malonate treated embryos and its quantification (D) (control, n=17, malonate, n=15). (E) Antimycin treated embryos and its quantification (F) (control, n=15, antimycin, n=13). (G) Sodium azide treated embryos and its quantification (H) (control, n=17, sodium azide, n=14). (I) oligomycin treated embryos and its quantification (J) (control, n=14, oligomycin, n=14). Mann-Whitney test has been used for statistical analysis. Error bar indicates S.E.M, **** represents $P<0.0001$. Scale bar is 200 micron. Results have been repeated three times.

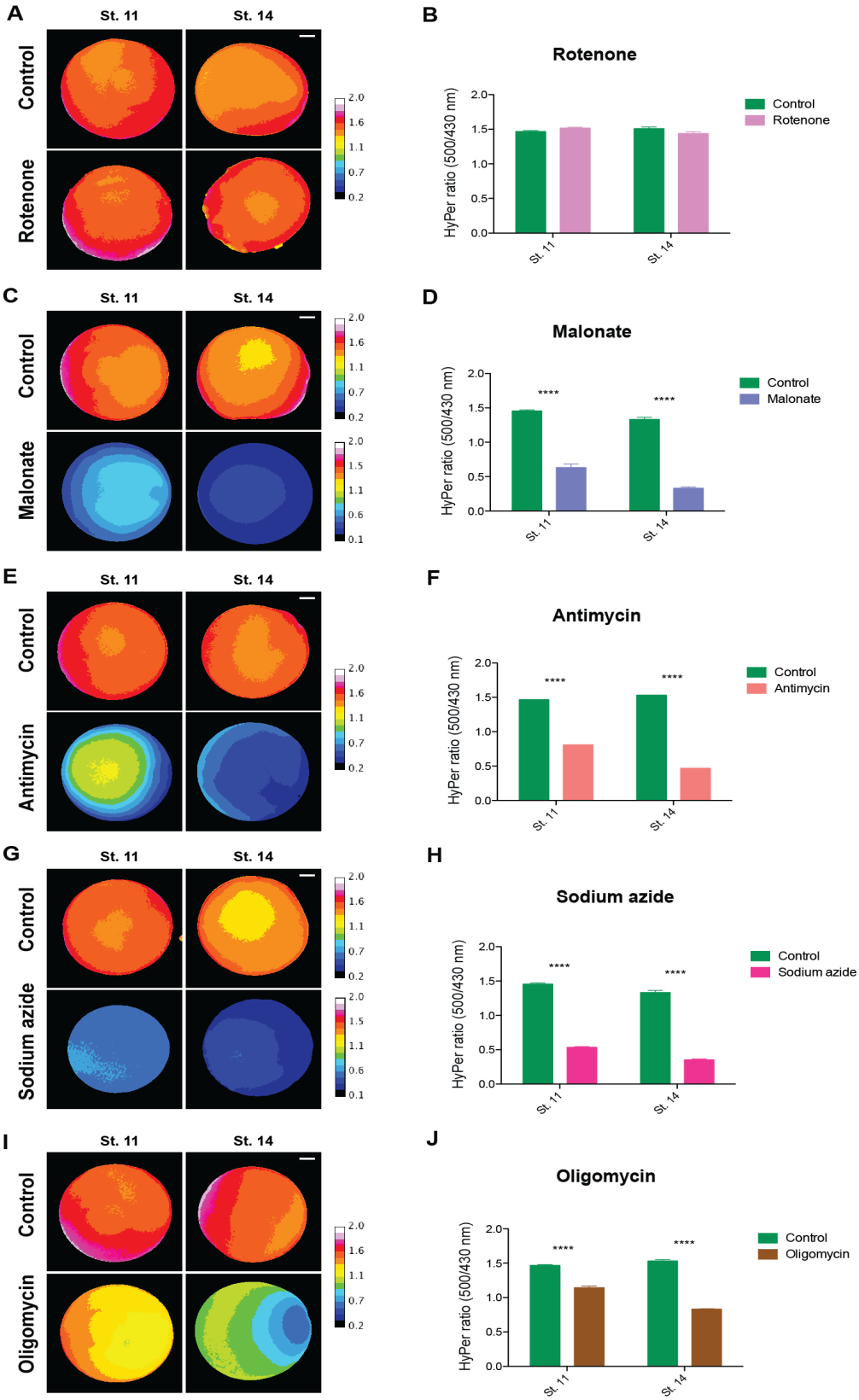

Figure 5-13: Mitochondrial inhibitors lower ROS level in gastrula stage embryos of *X. laevis*.

Figure 5-14. ATP levels in gastrula stage embryos of *X. laevis*.

Embryos were treated with mitochondrial inhibitors at mid-blastula stage and homogenised for ATP measurement at St. 11 and St. 14. 1 unit/ml Apyrase has been used as a negative control. Data came from 6 replicates, n=6. Mann-Whitney test was used for statistical analysis. Error bar indicates S.E.M, * represents $P<0.05$ and ** represents $P<0.01$.

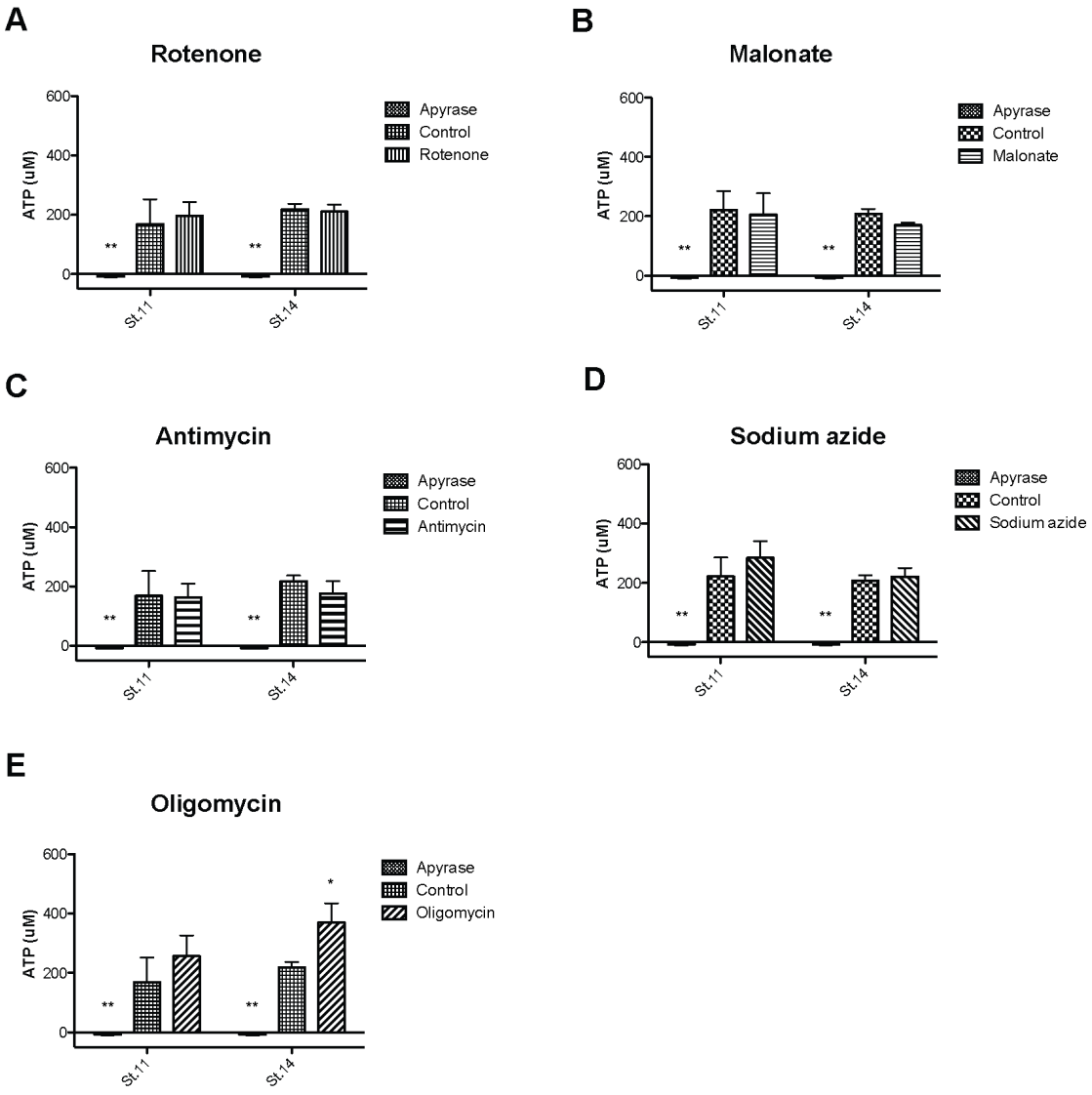

Figure 5-14: ATP levels in gastrula stage embryos of *X. laevis*.

5.3. Summary

This chapter mainly described the initial burst of ROS generated by mitochondria in Xenopus oocytes and early embryos. Through pharmacological gain and loss of function analysis, it was identified that the activation / fertilisation induced calcium wave is necessary for the sudden rise in ROS levels that have seen in early embryos. We then showed that the sudden ROS production, following egg activation, is not mediated by the activity of Nox family genes. Then we tested whether mitochondria might be responsible for generating the ROS that we see following activation / fertilisation. Interestingly, we found that mitochondrial complex II inhibitor, malonate, could greatly suppress ROS production, while the mitochondrial complex I inhibitor, rotenone, had no effect at all. Mitochondrial complex III inhibitor antimycin A, and complex IV inhibitor sodium azide, also greatly inhibited the production of ROS. Furthermore, the ATP synthase inhibitor, oligomycin, did not affect ROS generation, but intriguingly, we saw an increase in ATP levels in oligomycin treated eggs and embryos, suggesting that the ATP synthase might work in reverse mode both in oocytes and the early embryos. Further analysis eliminated the possibilities of mitochondrial inhibitors might block the calcium release or prohibit ATP synthesis, suggesting mitochondria act downstream of calcium rather than upstream. Direct inhibition of mitochondrial derived ROS production after fertilisation caused cell cycle arrest and failure of gastrulation in early embryos. These data suggested an important role of ROS in modulating mitosis and maintaining normal development in early embryogenesis of *X. laevis*.

However, due to time limitation, we did not carry out studies on uncovering the underlying mechanisms of the mitochondrial derived ROS regulation on Xenopus embryonic development. In particular, the mechanisms of mitochondrial ROS modulation on cell cycle progression and the role of mitochondrial derived ROS in germ layer formation need further investigation. Besides, it should be noted that for the gastrulation defects caused by mitochondrial inhibitors, it might involve several aspects. First, although embryos are incubated with mitochondrial inhibitors from mid-blastula stage (St. 8.5), they still undergo several round of cell division slowly during this time. Therefore, given that mitochondrial inhibitors could arrest cell cycles in cleavage stage embryos, the mitochondrial inhibitors induced gastrulation defects may come from a cell division defects. Second, due to the data obtained from NAC treatments, some signalling pathways involved in mesoderm formation are dysregulated, therefore it is possible that mitochondrial inhibitors also affect the signalling events activation. Third, except for lowering ROS levels, these mitochondrial inhibitors probably will induce cell death after the cell cycles arrest, in which process

cells trigger or shut down a series of signalling cascades that required for germ layer formation, thus impairing gastrulation in Xenopus embryos.

Chapter 6: Discussion

ROS have garnered more and more attention in recent years, especially in relation to their potential roles in mediating signal transduction and other cellular activities. In this thesis, I showed that egg fertilisation / activation induces a rapid increase in ROS levels and I further showed that this increase in ROS is dependent on the generation of an IP_3-dependent calcium wave, following egg fertilisation / activation. I also show that this increase in ROS levels is sustained throughout early embryogenesis, and they do not fall to pre-fertilisation levels until the tailbud stages, at which point the rapid phases of early development and growth has subsided. Furthermore, I showed that this sustained increase in ROS during blastula and gastrula stages is required for proper Akt, TGF-β, and Wnt signalling. As such, treating embryos with antioxidants resulted in embryos exhibiting severe developmental defects. Further investigations through loss and gain of function analyses, identified that mitochondria function as the main source for ROS generation, following egg fertilisation / activation. Inhibition of mitochondrial ROS production using mitochondrial respiratory chain inhibitors results in cell cycle arrest and gastrulation defects in Xenopus embryos, suggesting a critical role for mitochondrially derived ROS production in cell cycle progression and early embryonic development. My findings show interesting overlaps with those found previously in the lab, in respect to the role for sustained ROS levels during appendage regeneration [63]. Both early development and regeneration are associated with a sustained increase in ROS levels, and in both circumstances, the increase in ROS levels modulates growth factor signalling, which are required for both development and regeneration. Intriguingly, however, the source of ROS is different in the two scenarios. While NADPH oxidase activity is responsible for ROS production during tail regeneration, my findings suggest that following fertilisation, mitochondria are the primary source of ROS.

6.1. Mitochondria generated ROS

In this thesis I showed that fertilisation / activation induced ROS production is primarily produced by mitochondria in Xenopus eggs and early embryos, in particular through the mitochondrial complexes II, III and IV. As introduced in Chapter 1, using isolated mitochondria and mitochondrial enzymes, complex I and complex III have been highlighted as the main sources for ROS production within mitochondria [9, 10, 12, 13, 197-200]. However, using mitochondrial complex II inhibitor malonate, together with the ROS sensors, HyPerYFP and mito-HyPer, I showed that complex II is a primary source for ROS production after egg fertilisation / activation in Xenopus. This result is consistent with research of complex II ROS generation in female Wistar rats skeletal

muscle cells, in which the authors found that, after inhibiting complex I and complex III, complex II can generate superoxide or H_2O_2 at the flavin site in both forward and reverse reactions [17]. In my study, I saw a dramatic decrease in ROS levels when complex II was inhibited via malonate (a flavin site inhibitor). Interestingly, I also found that, malonate not only reduced ROS levels after fertilisation, but also led to a significant diminution in ROS levels in unfertilised eggs, suggesting a role for mitochondrial complex II in generating ROS levels in pre-fertilisation eggs. Given that complex I inhibitor rotenone did not affect ROS levels in fertilised / activated eggs or embryos, we are able to eliminate a role for complex I generating ROS [9, 11]. Therefore, we conclude that mitochondrial complex II functions fundamentally for ROS production in Xenopus oocytes and early embryos. In addition, we found that complex III also has a role to play in the burst of ROS following fertilisation / activation, as antimycin A is also able to diminish ROS levels post fertilisation / activation. Finally inhibition of complex IV, via sodium azide, also resulted in a similar diminution in ROS levels after fertilisation / activation. However, given that sodium azide may also alter mitochondrial membrane potential [201], this latter effect may be due to a loss in mitochondrial membrane potential effect. Indeed, when I used the uncoupler FCCP on activated eggs, I also observed a sharp decrease in ROS levels, suggesting that mitochondrial membrane potential is required for ROS generation from mitochondria following fertilisation / activation.

It is also important to note that ROS levels change during Xenopus embryonic development (Figure 3-4), from a relative low level in unfertilised eggs to a relative high level after fertilisation, then ROS level decreases gradually, reaching a low level at the tadpole stage, where it is less than half of that in unfertilised eggs. During these early stages of development, ROS play critical roles in regulating embryogenesis. Once ROS levels reach their relatively low levels at the tadpole stages, tail amputation leads to a sustained increase in ROS levels [63]. Given my findings on the role of ROS during early development, we reinterpret Nick R. Love and colleagues' results as suggesting that tail amputation leads to a return of the regenerating tail to an embryonic-like state of oxidation, which is conducive for both signalling and growth. In Nick R. Love and colleagues' findings, Nox enzymes are responsible for ROS production post wounding, as inhibition of Nox derived ROS by DPI (Nox inhibitor) or knocking down *cyba*, (the encoding gene of a common component required for Nox1-4 activation) resulted in reduction of cell proliferation and impaired tail regeneration in Xenopus. Evidence from the process of tail regeneration in Xenopus tadpoles suggests a relative high level of ROS is essential for promoting cell proliferation in tail regeneration. This is consistent with our cleavage stage data, that lowering ROS levels

leadis to the cell cycle arrest in cleavage stage embryos. Together, these data suggest a high ROS level is required for cell proliferation in both embryonic development and regeneration in vertebrate embryos.

When I asked what was acting upstream of ROS production following fertilisation, I was able to show that the fertilisation / activation induced calcium wave was essential for ROS generation. Furthermore, my data showed that calcium acts upstream, rather than downstream of mitochondrial ROS generation. I found that incubation of eggs with mitochondrial inhibitors did not affect the calcium wave, as revealed by the calcium sensor R-GECO. However, the mechanisms by which calcium enters the mitochondria and activated ROS production are still unknown. One possibility is that calcium released from the ER enters into the mitochondria via the mitochondrial calcium uniporter (MCU) [202]. This can be tested using MCU inhibitors, such as ruthenium red or ru360. However, these inhibitors are fluorescent and they interfere with HyPerYFP imaging. We hypothesise that after entering into mitochondria, calcium stimulates electron transport in the mitochondrial, thereby generating ROS [203]. Generally, it is considered that calcium can activate the TCA cycle, ATP synthase and other enzymes within mitochondrial, resulting in faster respiratory chain activity [203].

6.2. Calcium, ROS and cell cycle control

In this study, I showed that ROS production post egg activation / fertilisation is calcium dependent, and this ROS is important for early embryonic development, especially the cell cycle control and mesoderm formation. It has been know for a long time that calcium has been considered as an important messenger, participates in a variety of cellular processes. The transient rises in intracellular calcium induced by fertilisation, initiates the early embryonic development in Xenopus and other species. Calcium and its binding protein calmodulin have been reported to be required for cell proliferation [204]. However, the downstream target of calcium / calmodulin is still elusive. What we found here is that ROS also involved in cell cycle regulation.

In chapter 5, we know that, except oligomycin, mitochondrial inhibitors treated embryos presented a cell division defects to different extend. Malonate and sodium azide strongly affected embryos' cell division with large reductions in ROS levels. Antimycin also arrest cells at early blastula stage (St. 7) with moderate decrease in intracellular ROS levels. These results suggest a role of ROS in controlling cell division. Together with the findings in calcium regulation of cell cycle, it is possible that calcium acts as

upstream of ROS to modulate cell division. However, whether calcium works with ROS or independent of ROS to control cell division need further investigation. One possibility is that this calcium signal might be transmitted into mitochondria, and then triggers mitochondrial ROS generation to regulate cell cycle. To test this hypothesis, dividing embryos can be treated with calcium inhibitor, then observe for cell cycle arrest and test ROS levels change. One of calcium inhibitor called Ruthenium Red, functioning in blocking calcium entry into mitochondria via mitochondrial calcium uniporter (MCU). Through analyse of this inhibitor, my colleague found that Ruthenium Red injected embryos displayed a cell division defect with reductions in ROS levels (not shown). This result suggests that calcium may enter into mitochondria and activates ROS generation for control of cell cycle and other early embryonic events.

6.3. Metabolic reprogramming during vertebrate embryonic development

All cells need a source of energy to maintain homeostasis, during which they break down nutrients to produce the main form of energy ATP. This process is called catabolism. However, cells also need to synthesise new proteins, nucleic acids, lipids, etc. to grow, reproduce, maintain structures and respond to environment, through a process called anabolism. One of the major energy sources in cells is glucose. Glucose can firstly be metabolised through glycolysis to pyruvate thus generating two ATP molecules per glucose. At this point, pyruvate may enter into the mitochondria, where it participates in the TCA cycle thereby producing a large amount of ATP as a result of oxidative phosphorylation [205]. It has been reported that in the embryonic Xenopus retina, dividing progenitor cells use aerobic glycolysis to generate ATP rather than oxidative phosphorylation [192]. In addition, this group found the transition from glycolysis to oxidative phosphorylation is connected to the initiation of cell differentiation within the retina. The authors concluded from their data that the developing retina cells exhibit the Warburg effect (another term for aerobic glycolysis) under physiological cell proliferation *in vivo* until the cells begin differentiation, demonstrating the respective roles of glycolysis pathway and oxidative phosphorylation, as well as their connection and cooperation in producing energy and maintaining homeostasis in Xenopus embryos.

In this dissertation, I have also shown that early embryos do not rely on oxidative phosphorylation for ATP production. During my assessments of ROS production and fluctuation during early Xenopus embryos, using various mitochondrial inhibitors, I

found that none of them caused a decrease in ATP levels in either Xenopus eggs or early embryos. According to the work of Michalis Agathocleous et al. in Xenopus embryonic retinal cells, it is possible that early retinal tissue exhibits the Warburg effect and this appears to be the case also for early embryos as well. Perhaps the reason for this is that early embryos depend more on anabolic pathways, rather than catabolic pathways. In this respect, what is more limiting for cell proliferation and growth are the availability of metabolites for anabolic pathways and not ATP levels, per se. To address whether glycolysis acts as the major source of ATP in eggs or early embryos, we could block glycolysis using glycolytic inhibitors, as 2-deoxy-D-glucose (2DG), which inhibits glycolysis via its actions on hexokinase [192]. If a reduction of ATP is observed after addition of 2DG, this would suggest that glycolysis is the primary pathway maintaining ATP levels in Xenopus eggs and early embryos. If addition of 2DG does not induce a decrease of ATP levels, it may suggest a connection between glycolysis and oxidative phosphorylation, in which situation, double inhibition of both pathways might be needed.

Another intriguing finding of my results is that when I incubated activated eggs and early embryos with oligomycin A, which is a potent inhibitor of ATP synthase, I observed an increase in ATP levels rather than a decrease in ATP levels. Given the possibility that glycolysis might be the main source of ATP in early embryos, we may not have expected an effect on ATP levels after adding oligomycin, but given that I detected a significant increase in ATP levels, suggests that the ATP synthase is functioning in reverse in the mitochondria of Xenopus oocytes and early embryos, such that they are burning ATP rather than generating ATP. The mitochondrial complex V (ATP synthase) is highly conserved throughout evolution, consisting of two functional subunits, namely the F_1 and F_0 subunits. F_1 is capable of catalysing either ATP synthesis or hydrolysis, whereas F_0 is capable of driving the transmembrane proton gradient [193, 206, 207]. Oligomycin A is an F_0 domain inhibitor that prohibits proton ion channel. When ATP synthase functions in catalysing ATP formation, oligomycin A would disrupt H^+ transporting into mitochondrial matrix, thus disrupting ATP formation. In contrast, if ATP synthase functions in catalysing hydrolysis of ATP in order to drive protons across the membrane, addition of oligomycin A would block ATP hydrolysis and lead to an increase in ATP level. Here we observed an increase in ATP levels in oligomycin A treated eggs and embryos, which suggest a possibility that the ATP synthase may function to hydrolyse ATP to maintain the proton gradient in Xenopus eggs and early embryos. The reason why this might be happening is because mitochondria depend on the proton gradient for the transport of metabolites into and out of the mitochondria.

In order to address whether mitochondria are using ATP to maintain the mitochondrial proton gradient, there are several experiments that could be done in future. One could carry out loss of function analyses using ATP synthase inhibitors together with glycolysis inhibitors, to find out which is the major source of ATP during the early embryonic development. In addition, we could perform a series of experiments to test the function of ATP synthase (synthesis or hydrolysis?). To address, we could overexpress an endogenous ATP synthase inhibitor, named $ATPIF_1$ (ATPase inhibitory factor 1) in Xenopus eggs and embryos. The $ATPIF_1$ inhibitor functions as a selective inhibitor of ATP hydrolysis in mitochondria [208]. If overexpression of this endogenous inhibitor causes an increase in ATP levels, which mimics the effect induced by oligomycin A, we can conclude that in Xenopus eggs and early embryos, ATP synthase works in a reverse way to hydrolyse ATPs in order to maintain the proton gradient across the innermembrane. Such a finding would be contrary to the expected role that one might expect for mitochondria in early embryos, but would be consistent with the increased appreciation of how metabolism in the early embryos is more similar to that seen in cancer (i.e. thus, exhibiting the Warburg effect). In addition, it would be of great interest to determine whether the change in intracellular ROS levels contributes to this fascinating metabolic programming that we are uncovering during early embryonic development and during tissue regeneration.

6.4. Potential targets of ROS in regulation of Xenopus embryonic development

In this dissertation, I showed that an increase in ROS levels is important and required for early embryonic development in *X. laevis*. In chapter 3, I showed that lowering ROS levels with the antioxidant, NAC, impairs mesoderm formation and dysregulated several signalling pathways. I investigated several signalling pathways relevant to mesoderm formation, and found that PI3K/Akt, TGF-β/Nodal and Wnt/β-catenin signalling were significantly impaired when the embryos were treated with antioxidants. I also found that, addition of either the oxidant H_2O_2 or ROS inducer menadione to the NAC treated embryos could partially restore the activity of these signalling pathways, and thus provided compelling evidence of the important role of ROS in regulating these signalling pathways and promoting normal embryogenesis. My study provides direct evidence of ROS modulation on signalling cascades during vertebrate embryogenesis. However, the underlying mechanisms of how ROS mediate these signalling effects, hence regulating embryonic development require further study.

Previously, it was reported that a Trx related protein Nrx could negatively regulate canonical Wnt signalling by directly interacting with a Wnt signalling component, Dishevelled (Dvl). This inhibition can be blocked by H_2O_2, which can catalyse the oxidation of Nrx and release Dishevelled (Dvl) thereby promoting canonical Wnt/β-catenin signalling [171]. In addition, through loss and gain of function analyses in Xenopus embryos, the authors confirmed the *in vivo* role of Nrx, which functions as a negative regulator of Wnt/β-catenin signalling, bridging the redox regulation on Wnt/β-catenin signalling [171]. In our experiments, we also observed a down-regulation of Wnt/β-catenin pathway when lowering ROS by NAC. It is possibly that this is due to the reduction of endogenous Nrx, allowing it to bind Dvl, resulting in the degradation of β-catenin, and inactivation of Wnt/β-catenin signalling.

It is known that ROS can modify various proteins by catalysing oxidation reactions at their catalytic cysteine residues (Cys). Amongst the enzymes that have cysteines in their catalytic site are several phosphatases [209-212]. PTEN is a lipid phosphatase that specially catalyses the dephosphorylation of PIP_3, resulting in the inhibition of PI3K/Akt pathway [210]. H_2O_2 can catalyse the oxidation of PTEN at Cys^{124}, leading to up-regulation of PI3K/Akt signalling, whereas Trx can reactivate PTEN and down-regulate the PI3K/Akt pathway [210]. My data showed a drastic loss of phosphorylated Akt in NAC injected embryos at gastrula stage. It is possible that NAC decreases intracellular ROS levels and promotes the reduction of PTEN, which would be expected to retain PTEN in an active state, thus leading to the rapid dephosphorylation of Akt and inhibition of PI3K/Akt signalling. Furthermore, we might expect that PI3K/Akt could also play a regulatory role in canonical Wnt signalling via inhibition of Gsk3β in Xenopus embryos [148].

However, given the large number of signalling proteins that are modified by oxidation, there presumably exist many more developmental mechanisms that rely on embryonic ROS, for instance, the redox-sensitive FoxO transcription factors, which are maternally expressed and present in the early Xenopus embryo [213]. This connection is particularly relevant here, due to the previously identified interaction between FoxO and β-catenin signalling [214].

In chapter 5, I demonstrated that ROS production following fertilisation / activation is generated primarily by mitochondria. In addition, I also described how mitochondrial ROS are important for cell cycle progression in *X. laevis* embryos. In particular, lowering ROS with mitochondrial complex II and complex IV inhibitors caused cell cycle

arrest immediately in cleavage stage embryos, suggesting an important role for ROS in controlling cell proliferation in vertebrate embryonic development. Nevertheless, the mechanisms of ROS regulation on embryonic mitosis cell cycle are still unclear. Therefore, it is necessary to test whether there are cell cycle regulators that might be being affected by the decrease in ROS levels. Since H_2O_2 has been reported to inhibit protein tyrosine phosphatases via cysteine residue oxidation [210, 215]. Cdc25C is a phosphorylated regulated cell cycle modulators and has been reported to be expressed in Xenopus early embryos [216]. Therefore it is possible that mitochondrial generated ROS regulate cell division via modulating the activation of Cdc25C during Xenopus early embryonic development. Further investigation needs to be carried out to confirm whether this might be the case.

6.5. Key conclusions and hypothesis

In conclusion, I found that fertilisation / activation induces a calcium dependent ROS production from mitochondrial, which is sustained throughout the early embryogenesis in Xenopus. I also found that this sustained increase in ROS is important for cell cycle progression and mesoderm formation in Xenopus early embryonic development. Using an antioxidant NAC, I found that ROS play a role in modulation the activity of PI3K/Akt, TGF-β/Nodal and Wnt/β-catenin signalling in early embryonic development of *X. laevis*. Based on these data, I proposed the following model. In Xenopus, egg fertilisation induces a calcium wave, which is released from the ER via IP_3R. The calcium then enters into the mitochondria, possibly via MCU, to activate ROS production from mitochondrial complex II, III and IV, leading to an increase in intracellular ROS levels, which is of great importance for promoting cell cycle progression and mesoderm formation in vertebrate early embryonic development.

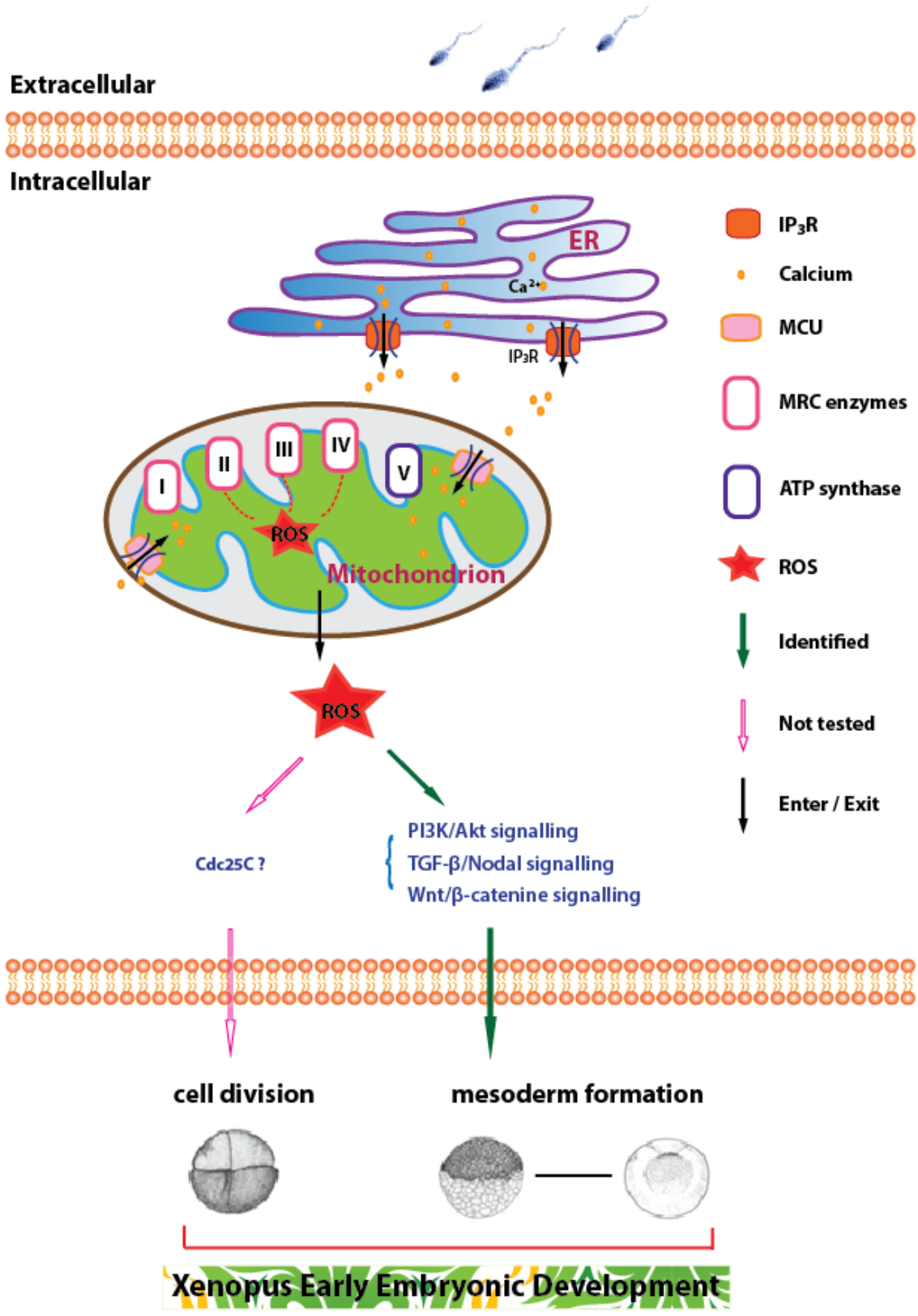

Figure 6-1: Fertilisation-induced ROS and its role during Xenopus early embryogenesis.

This figure shows the sperm entry induced ROS production is important for early embryonic development of *X. laevis*. MCU represents mitochondrial calcium uniporter and MRC stands for mitochondrial respiratory chain.

Reference

1. Ray, P.D., B.W. Huang, and Y. Tsuji, *Reactive oxygen species (ROS) homeostasis and redox regulation in cellular signaling.* Cell Signal, 2012. **24**(5): p. 981-90.
2. Alfadda, A.A. and R.M. Sallam, *Reactive oxygen species in health and disease.* J Biomed Biotechnol, 2012. **2012**: p. 936486.
3. Datta, K., S. Sinha, and P. Chattopadhyay, *Reactive oxygen species in health and disease.* Natl Med J India, 2000. **13**(6): p. 304-10.
4. Castro, L. and B.A. Freeman, *Reactive oxygen species in human health and disease.* Nutrition, 2001. **17**(2): p. 161, 163-5.
5. Brieger, K., et al., *Reactive oxygen species: from health to disease.* Swiss Med Wkly, 2012. **142**: p. w13659.
6. Covarrubias, L., et al., *Function of reactive oxygen species during animal development: Passive or active?* Developmental Biology, 2008. **320**(1): p. 1-11.
7. Holmstrom, K.M. and T. Finkel, *Cellular mechanisms and physiological consequences of redox-dependent signalling.* Nat Rev Mol Cell Biol, 2014. **15**(6): p. 411-21.
8. Turrens, J.F., *Mitochondrial formation of reactive oxygen species.* J Physiol, 2003. **552**(Pt 2): p. 335-44.
9. Murphy, Michael P., *How mitochondria produce reactive oxygen species.* Biochemical Journal, 2009. **417**(Pt 1): p. 1-13.
10. St-Pierre, J., et al., *Topology of superoxide production from different sites in the mitochondrial electron transport chain.* J Biol Chem, 2002. **277**(47): p. 44784-90.
11. Brand, M.D., *The sites and topology of mitochondrial superoxide production.* Exp Gerontol, 2010. **45**(7-8): p. 466-72.
12. Lambert, A.J. and M.D. Brand, *Inhibitors of the quinone-binding site allow rapid superoxide production from mitochondrial NADH:ubiquinone oxidoreductase (complex I).* J Biol Chem, 2004. **279**(38): p. 39414-20.
13. Hirst, J., M.S. King, and K.R. Pryde, *The production of reactive oxygen species by complex I.* Biochem Soc Trans, 2008. **36**(Pt 5): p. 976-80.
14. Iwata, S., et al., *Complete structure of the 11-subunit bovine mitochondrial cytochrome bc1 complex.* Science, 1998. **281**(5373): p. 64-71.
15. Cecchini, G., *Function and structure of complex II of the respiratory chain.* Annu Rev Biochem, 2003. **72**: p. 77-109.
16. Dröse, S., *Differential effects of complex II on mitochondrial ROS production and their relation to cardioprotective pre- and postconditioning.* Biochimica et Biophysica Acta (BBA) - Bioenergetics, 2013. **1827**(5): p. 578-587.
17. Quinlan, C.L., et al., *Mitochondrial complex II can generate reactive oxygen species at high rates in both the forward and reverse reactions.* 2012(1083-351X (Electronic)).
18. Miwa, S., et al., *Superoxide and hydrogen peroxide production by Drosophila mitochondria.* Free Radic Biol Med, 2003. **35**(8): p. 938-48.
19. Chen, Y.R. and J.L. Zweier, *Cardiac mitochondria and reactive oxygen species generation.* Circ Res, 2014. **114**(3): p. 524-37.
20. Wojtczak, L., et al., *Effect of glucose and deoxyglucose on the redistribution of calcium in ehrlich ascites tumour and Zajdela hepatoma cells and its*

consequences for mitochondrial energetics. Further arguments for the role of Ca(2+) in the mechanism of the crabtree effect. 1999(0014-2956 (Print)).
21. Geromel, V., et al., *Superoxide-induced massive apoptosis in cultured skin fibroblasts harboring the neurogenic ataxia retinitis pigmentosa (NARP) mutation in the ATPase-6 gene of the mitochondrial DNA.* Hum Mol Genet, 2001. **10**(11): p. 1221-8.
22. Bedard, K. and K.H. Krause, *The NOX family of ROS-generating NADPH oxidases: physiology and pathophysiology.* Physiol Rev, 2007. **87**(1): p. 245-313.
23. Segal, A.W., *The function of the NADPH oxidase of phagocytes and its relationship to other NOXs in plants, invertebrates, and mammals.* Int J Biochem Cell Biol, 2008. **40**(4): p. 604-18.
24. Lambeth, J.D., *NOX enzymes and the biology of reactive oxygen.* Nat Rev Immunol, 2004. **4**(3): p. 181-9.
25. Brandes, R.P., N. Weissmann, and K. Schroder, *Nox family NADPH oxidases: Molecular mechanisms of activation.* Free Radic Biol Med, 2014. **76**: p. 208-26.
26. Martyn, K.D., et al., *Functional analysis of Nox4 reveals unique characteristics compared to other NADPH oxidases.* Cell Signal, 2006. **18**(1): p. 69-82.
27. Banfi, B., et al., *Mechanism of Ca2+ activation of the NADPH oxidase 5 (NOX5).* (0021-9258 (Print)).
28. Banfi, B., et al., *A Ca(2+)-activated NADPH oxidase in testis, spleen, and lymph nodes.* (0021-9258 (Print)).
29. Pandey, D., et al., *Expression and functional significance of NADPH oxidase 5 (Nox5) and its splice variants in human blood vessels.* Am J Physiol Heart Circ Physiol, 2012. **302**(10): p. H1919-28.
30. Kawahara, T., et al., *Nox5 forms a functional oligomer mediated by self-association of its dehydrogenase domain.* Biochemistry, 2011. **50**(12): p. 2013-25.
31. Ameziane-El-Hassani, R., et al., *Dual oxidase-2 has an intrinsic Ca2+-dependent H2O2-generating activity.* (0021-9258 (Print)).
32. O'Donnell, B.V., et al., *Studies on the inhibitory mechanism of iodonium compounds with special reference to neutrophil NADPH oxidase.* Biochem J, 1993. **290 (Pt 1)**: p. 41-9.
33. Li, Y. and M.A. Trush, *Diphenyleneiodonium, an NAD(P)H oxidase inhibitor, also potently inhibits mitochondrial reactive oxygen species production.* (0006-291X (Print)).
34. McGuire, J.J., et al., *Inhibition of NADPH-cytochrome P450 reductase and glyceryl trinitrate biotransformation by diphenyleneiodonium sulfate.* Biochem Pharmacol, 1998. **56**(7): p. 881-93.
35. Doussiere, J. and P.V. Vignais, *Diphenylene iodonium as an inhibitor of the NADPH oxidase complex of bovine neutrophils. Factors controlling the inhibitory potency of diphenylene iodonium in a cell-free system of oxidase activation.* (0014-2956 (Print)).
36. Stuehr, D.J., et al., *Inhibition of macrophage and endothelial cell nitric oxide synthase by diphenyleneiodonium and its analogs.* (0892-6638 (Print)).
37. Stolk, J., et al., *Characteristics of the inhibition of NADPH oxidase activation in neutrophils by apocynin, a methoxy-substituted catechol.* Am J Respir Cell Mol Biol, 1994. **11**(1): p. 95-102.
38. Ellmark, S.H., et al., *The contribution of Nox4 to NADPH oxidase activity in mouse vascular smooth muscle.* Cardiovasc Res, 2005. **65**(2): p. 495-504.

39. Fu, X., et al., *cAMP-response element-binding protein mediates acid-induced NADPH oxidase NOX5-S expression in Barrett esophageal adenocarcinoma cells.* J Biol Chem, 2006. **281**(29): p. 20368-82.
40. Heumuller, S., et al., *Apocynin is not an inhibitor of vascular NADPH oxidases but an antioxidant.* 2008(1524-4563 (Electronic)).
41. Christen, Y., *Oxidative stress and Alzheimer disease.* American Journal of Clinical Nutrition, 2000. **71**(2): p. 621S-629S.
42. Adams, J.D., Jr., M.L. Chang, and L. Klaidman, *Parkinson's disease--redox mechanisms.* Current medicinal chemistry, 2001. **8**(7): p. 809-14.
43. Chinta, S.J. and J.K. Andersen, *Redox imbalance in Parkinson's disease.* Biochimica et biophysica acta, 2008. **1780**(11): p. 1362-7.
44. Waris, G. and H. Ahsan, *Reactive oxygen species: role in the development of cancer and various chronic conditions.* Journal of carcinogenesis, 2006. **5**: p. 14.
45. Covarrubias, L., et al., *Function of reactive oxygen species during animal development: passive or active?* Developmental Biology, 2008. **320**(1): p. 1-11.
46. Yu, B.P., *Cellular defenses against damage from reactive oxygen species.* Physiological reviews, 1994. **74**(1): p. 139-62.
47. Zafarullah, M., et al., *Molecular mechanisms of N-acetylcysteine actions.* Cellular and molecular life sciences : CMLS, 2003. **60**(1): p. 6-20.
48. Hansen, J.M., *Oxidative stress as a mechanism of teratogenesis.* Birth defects research. Part C, Embryo today : reviews, 2006. **78**(4): p. 293-307.
49. Dennery, P.A., *Effects of oxidative stress on embryonic development.* Birth defects research. Part C, Embryo today : reviews, 2007. **81**(3): p. 155-62.
50. Das, K.C., *Thioredoxin system in premature and newborn biology.* Antioxidants & Redox Signaling, 2004. **6**(1): p. 177-84.
51. Das, K.C. and C.W. White, *Redox systems of the cell: possible links and implications.* Proceedings of the National Academy of Sciences of the United States of America, 2002. **99**(15): p. 9617-8.
52. Masella, R., et al., *Novel mechanisms of natural antioxidant compounds in biological systems: involvement of glutathione and glutathione-related enzymes.* J Nutr Biochem, 2005. **16**(10): p. 577-86.
53. Dickinson, D.A. and H.J. Forman, *Glutathione in defense and signaling: lessons from a small thiol.* Annals of the New York Academy of Sciences, 2002. **973**: p. 488-504.
54. Rahman, K., *Studies on free radicals, antioxidants, and co-factors.* Clin Interv Aging, 2007. **2**(2): p. 219-36.
55. Pryor, W.A. and S.S. Godber, *Noninvasive measures of oxidative stress status in humans.* Free radical biology & medicine, 1991. **10**(3-4): p. 177-84.
56. Harvey, A.J., K.L. Kind, and J.G. Thompson, *REDOX regulation of early embryo development.* Reproduction, 2002. **123**(4): p. 479-86.
57. Dikalov, S.I. and D.G. Harrison, *Methods for detection of mitochondrial and cellular reactive oxygen species.* Antioxid Redox Signal, 2014. **20**(2): p. 372-82.
58. Hernandez-Garcia, D., et al., *Reactive oxygen species: A radical role in development?* Free Radic Biol Med, 2010. **49**(2): p. 130-43.
59. Belousov, V.V., et al., *Genetically encoded fluorescent indicator for intracellular hydrogen peroxide.* Nat Methods, 2006. **3**(4): p. 281-6.
60. Niethammer, P., et al., *A tissue-scale gradient of hydrogen peroxide mediates rapid wound detection in zebrafish.* Nature, 2009. **459**(7249): p. 996-9.

61. Roma, L.P., et al., *Dynamic measurements of mitochondrial hydrogen peroxide concentration and glutathione redox state in rat pancreatic beta-cells using ratiometric fluorescent proteins: confounding effects of pH with HyPer but not roGFP1.* 2012(1470-8728 (Electronic)).
62. Cocheme, H.M., et al., *Using the mitochondria-targeted ratiometric mass spectrometry probe MitoB to measure H2O2 in living Drosophila.* 2012(1750-2799 (Electronic)).
63. Love, N.R., et al., *Amputation-induced reactive oxygen species are required for successful Xenopus tadpole tail regeneration.* Nat Cell Biol, 2013. **15**(2): p. 222-8.
64. Ishibashi, S., K.L. Kroll, and E. Amaya, *Generating transgenic frog embryos by restriction enzyme mediated integration (REMI).* Methods Mol Biol, 2012. **917**: p. 185-203.
65. Davies, K.J., *The broad spectrum of responses to oxidants in proliferating cells: a new paradigm for oxidative stress.* IUBMB Life, 1999. **48**(1): p. 41-7.
66. Thannickal, V.J., et al., *Ras-dependent and -independent regulation of oxygen species by mitogenic growth factors and TGF-beta 1.* Faseb Journal, 2000. **14**(12): p. 1741-1748.
67. Ushio-Fukai, M., et al., *Novel role of gp91phox-containing NAD(P)H oxidase in vascular endothelial growth factor-induced angiogenesis.* Circulation, 2002. **106**(19): p. 240-240.
68. Kreuzer, J., et al., *Platelet-derived growth factor activates production of reactive oxygen species by NAD(P)H oxidase in smooth muscle cells through Gi1,2.* FASEB journal : official publication of the Federation of American Societies for Experimental Biology, 2003. **17**(1): p. 38-40.
69. Kim, B.Y., M.J. Han, and A.S. Chung, *Effects of reactive oxygen species on proliferation of Chinese hamster lung fibroblast (V79) cells.* Free radical biology & medicine, 2001. **30**(6): p. 686-98.
70. Kamata, H., et al., *Reactive oxygen species promote TNFalpha-induced death and sustained JNK activation by inhibiting MAP kinase phosphatases.* Cell, 2005. **120**(5): p. 649-61.
71. Stclair, D.K., et al., *Expression of Manganese Superoxide-Dismutase Promotes Cellular-Differentiation.* Free Radical Biology and Medicine, 1994. **16**(2): p. 275-282.
72. Sauer, H., et al., *Role of reactive oxygen species and phosphatidylinositol 3-kinase in cardiomyocyte differentiation of embryonic stem cells.* FEBS letters, 2000. **476**(3): p. 218-223.
73. Buggisch, M., et al., *Stimulation of ES-cell-derived cardiomyogenesis and neonatal cardiac cell proliferation by reactive oxygen species and NADPH oxidase.* Journal of Cell Science, 2007. **120**(5): p. 885-894.
74. Li, J., et al., *The NADPH oxidase NOX4 drives cardiac differentiation: Role in regulating cardiac transcription factors and MAP kinase activation.* Molecular biology of the cell, 2006. **17**(9): p. 3978-3988.
75. Sardina, J.L., et al., *p22phox-dependent NADPH oxidase activity is required for megakaryocytic differentiation.* (1476-5403 (Electronic)).
76. Ji, A.R., et al., *Reactive oxygen species enhance differentiation of human embryonic stem cells into mesendodermal lineage.* Experimental and Molecular Medicine, 2010. **42**(3): p. 175-186.
77. Tada, S., et al., *Characterization of mesendoderm: a diverging point of the definitive endoderm and mesoderm in embryonic stem cell differentiation culture.* Development, 2005. **132**(19): p. 4363-74.

78. Harman, D., *Aging: a theory based on free radical and radiation chemistry.* Journal of gerontology, 1956. **11**(3): p. 298-300.
79. Sohal, R.S. and R. Weindruch, *Oxidative stress, caloric restriction, and aging.* Science, 1996. **273**(5271): p. 59-63.
80. Sastre, J., et al., *Mitochondrial damage in aging and apoptosis.* Annals of the New York Academy of Sciences, 2002. **959**: p. 448-51.
81. Melov, S., et al., *Extension of life-span with superoxide dismutase/catalase mimetics.* Science, 2000. **289**(5484): p. 1567-1569.
82. Phillips, J.P., et al., *Null Mutation of Copper-Zinc Superoxide-Dismutase in Drosophila Confers Hypersensitivity to Paraquat and Reduced Longevity.* Proceedings of the National Academy of Sciences of the United States of America, 1989. **86**(8): p. 2761-2765.
83. Finkel, T. and N.J. Holbrook, *Oxidants, oxidative stress and the biology of ageing.* Nature, 2000. **408**(6809): p. 239-247.
84. Clutton, S., *The importance of oxidative stress in apoptosis.* British Medical Bulletin, 1997. **53**(3): p. 662-668.
85. Pierce, G.B., R.E. Parchment, and A.L. Lewellyn, *Hydrogen-Peroxide as a Mediator of Programmed Cell-Death in the Blastocyst.* Differentiation, 1991. **46**(3): p. 181-186.
86. Kasahara, Y., et al., *Involvement of reactive oxygen intermediates in spontaneous and CD95 (Fas/APO-1)-mediated apoptosis of neutrophils.* Blood, 1997. **89**(5): p. 1748-53.
87. Watson, R.W., et al., *Augmented intracellular glutathione inhibits Fas-triggered apoptosis of activated human neutrophils.* Blood, 1997. **89**(11): p. 4175-81.
88. Pelicci, P.G., *Electron transfer between cytochrome C and P66SHC generates reactive oxygen species that trigger mitochondrial apoptosis.* Febs Journal, 2005. **272**: p. 319-320.
89. Fleury, C., B. Mignotte, and J.L. Vayssiere, *Mitochondrial reactive oxygen species in cell death signaling.* Biochimie, 2002. **84**(2-3): p. 131-141.
90. Witte, M.B. and A. Barbul, *General principles of wound healing.* Surgical Clinics of North America, 1997. **77**(3): p. 509-+.
91. Singer, A.J. and R.A.F. Clark, *Mechanisms of disease - Cutaneous wound healing.* New England Journal of Medicine, 1999. **341**(10): p. 738-746.
92. Rodriguez, P.G., et al., *The role of oxygen in wound healing: A review of the literature.* Dermatologic Surgery, 2008. **34**(9): p. 1159-1169.
93. Knighton, D.R., et al., *Oxygen-Tension Regulates the Expression of Angiogenesis Factor by Macrophages.* Science, 1983. **221**(4617): p. 1283-1285.
94. Gordillo, G.M. and C.K. Sen, *Revisiting the essential role of oxygen in wound healing.* American Journal of Surgery, 2003. **186**(3): p. 259-263.
95. Li, W.D., et al., *Hydrogen peroxide-mediated, lysyl oxidase-dependent chemotaxis of vascular smooth muscle cells.* Journal of Cellular Biochemistry, 2000. **78**(4): p. 550-557.
96. Morales, H., et al., *Pyruvate prevents peroxide-induced injury of in vitro preimplantation bovine embryos.* Mol Reprod Dev, 1999. **52**(2): p. 149-57.
97. Warburg, O., *Beobachtungen über die Oxydationsprozesse im Seeigelei*, in *Hoppe-Seyler´s Zeitschrift für physiologische Chemie*. 1908. p. 1.
98. Kadomura, K., et al., *Production of reactive oxygen species (ROS) by devil stinger (Inimicus japonicus) during embryogenesis.* Fish Shellfish Immunol, 2006. **21**(2): p. 209-14.

99. Wong, J.L. and G.M. Wessel, *Reactive oxygen species and Udx1 during early sea urchin development.* Dev Biol, 2005. **288**(2): p. 317-33.
100. Vander Heiden, M.G., L.C. Cantley, and C.B. Thompson, *Understanding the Warburg effect: the metabolic requirements of cell proliferation.* Science, 2009. **324**(5930): p. 1029-33.
101. Aykin-Burns, N., et al., *Increased levels of superoxide and H2O2 mediate the differential susceptibility of cancer cells versus normal cells to glucose deprivation.* Biochem J, 2009. **418**(1): p. 29-37.
102. Costa, R.M.B., et al., *spib is required for primitive myeloid development in Xenopus.* Blood, 2008. **112**(6): p. 2287-2296.
103. Chen, Y.Y., et al., *C/EBP alpha initiates primitive myelopoiesis in pluripotent embryonic cells.* Mechanisms of development, 2009. **126**: p. S163-S164.
104. Sive, H.L., R.M. Grainger, and R.M. Harland, *Early development of Xenopus laevis : a laboratory manual*. 2000, New York: Cold Springer Harbor Laboratory Press. ix, 337 p.
105. Hellsten, U., et al., *The genome of the Western clawed frog Xenopus tropicalis.* Science, 2010. **328**(5978): p. 633-6.
106. Amaya, E., *Xenomics.* Genome research, 2005. **15**(12): p. 1683-91.
107. Nieuwkoop, P.D. and J. Faber, *Normal table of Xenopus laevis (Daudin) : a systematical and chronological survey of the development from the fertilized egg till the end of metamorphosis*. 1994, New York: Garland Pub. 252 p., 10 leaves of plates.
108. Dumont, J.N., *Oogenesis in Xenopus laevis (Daudin). I. Stages of oocyte development in laboratory maintained animals.* J Morphol, 1972. **136**(2): p. 153-79.
109. Ferrell, J.E., Jr., *Xenopus oocyte maturation: new lessons from a good egg.* Bioessays, 1999. **21**(10): p. 833-42.
110. Nader, N., et al., *How to make a good egg!: The need for remodeling of oocyte Ca(2+) signaling to mediate the egg-to-embryo transition.* Cell Calcium, 2013. **53**(1): p. 41-54.
111. Bayaa, M., et al., *The classical progesterone receptor mediates Xenopus oocyte maturation through a nongenomic mechanism.* (0027-8424 (Print)).
112. Runft, L.L., L.M. Jaffe La Fau - Mehlmann, and L.M. Mehlmann, *Egg activation at fertilization: where it all begins.* 2002(0012-1606 (Print)).
113. Tokmakov, A.A., et al., *Calcium Signaling and Meiotic Exit at Fertilization in Xenopus Egg.* International Journal of Molecular Sciences, 2014. **15**(10): p. 18659-18676.
114. Elinson, R.P., *Cleavage and Gastrulation in Xenopus laevis Embryos*, in *eLS*. 2001, John Wiley & Sons, Ltd.
115. Schohl, A. and F. Fagotto, *Beta-catenin, MAPK and Smad signaling during early Xenopus development.* Development, 2002. **129**(1): p. 37-52.
116. Fagotto, A.S.a.F., *beta-catenin, MAPK and Smad signaling during early Xenopus development.* Development, 2007. **134**(7): p. 1454-1454.
117. De Robertis, E.M., et al., *The establishment of Spemann's organizer and patterning of the vertebrate embryo.* Nat Rev Genet, 2000. **1**(3): p. 171-81.
118. Dale, L. and F.C. Wardle, *Xenopus Embryo: Mesoderm Induction*, in *eLS*. 2001, John Wiley & Sons, Ltd.
119. Keller, R., *Early embryonic development of Xenopus laevis.* Methods in cell biology, 1991. **36**: p. 61-113.
120. Smith, J.L. and G.C. Schoenwolf, *Neurulation: coming to closure.* Trends in neurosciences, 1997. **20**(11): p. 510-7.

121. Grumolato, L., et al., *Canonical and noncanonical Wnts use a common mechanism to activate completely unrelated coreceptors.* Genes & development, 2010. **24**(22): p. 2517-2530.
122. Miller, J.R., et al., *Mechanism and function of signal transduction by the Wnt/beta-catenin and Wnt/Ca2+ pathways.* Oncogene, 1999. **18**(55): p. 7860-72.
123. Komiya, Y. and R. Habas, *Wnt signal transduction pathways.* Organogenesis, 2008. **4**(2): p. 68-75.
124. White, J.A. and J. Heasman, *Maternal control of pattern formation in Xenopus laevis.* Journal of experimental zoology. Part B, Molecular and developmental evolution, 2008. **310**(1): p. 73-84.
125. Lagna, G., et al., *Negative regulation of axis formation and Wnt signaling in Xenopus embryos by the F-box/WD40 protein beta TrCP.* Mechanisms of development, 1999. **80**(1): p. 101-106.
126. Tao, Q.H., et al., *Maternal Wnt11 activates the canonical wnt signaling pathway required for axis formation in Xenopus embryos.* Cell, 2005. **120**(6): p. 857-871.
127. Funato, Y., et al., *The thioredoxin-related redox-regulating protein nucleoredoxin inhibits Wnt-beta-catenin signalling through dishevelled.* Nature cell biology, 2006. **8**(5): p. 501-8.
128. Kajla, S., et al., *A crucial role for Nox 1 in redox-dependent regulation of Wnt-beta-catenin signaling.* The FASEB journal : official publication of the Federation of American Societies for Experimental Biology, 2012.
129. Shin, S.Y., et al., *Hydrogen peroxide negatively modulates Wnt signaling through downregulation of beta-catenin.* Cancer letters, 2004. **212**(2): p. 225-231.
130. Logan, C.Y. and R. Nusse, *The Wnt signaling pathway in development and disease.* Annual review of cell and developmental biology, 2004. **20**: p. 781-810.
131. Zhang, X., et al., *Receptor specificity of the fibroblast growth factor family. The complete mammalian FGF family.* J Biol Chem, 2006. **281**(23): p. 15694-700.
132. Bottcher, R.T. and C. Niehrs, *Fibroblast growth factor signaling during early vertebrate development.* Endocrine reviews, 2005. **26**(1): p. 63-77.
133. Dorey, K. and E. Amaya, *FGF signalling: diverse roles during early vertebrate embryogenesis.* Development, 2010. **137**(22): p. 3731-42.
134. Amaya, E., T.J. Musci, and M.W. Kirschner, *Expression of a dominant negative mutant of the FGF receptor disrupts mesoderm formation in Xenopus embryos.* Cell, 1991. **66**(2): p. 257-70.
135. Fletcher, R.B. and R.M. Harland, *The role of FGF signaling in the establishment and maintenance of mesodermal gene expression in Xenopus.* Developmental dynamics : an official publication of the American Association of Anatomists, 2008. **237**(5): p. 1243-54.
136. Nutt, S.L., et al., *Xenopus Sprouty2 inhibits FGF-mediated gastrulation movements but does not affect mesoderm induction and patterning.* Genes & development, 2001. **15**(9): p. 1152-66.
137. Pownall, M.E. and H.V. Isaacs, in *FGF Signalling in Vertebrate Development*. 2010: San Rafael (CA).
138. Wu, M.Y. and C.S. Hill, *Tgf-beta superfamily signaling in embryonic development and homeostasis.* 2009(1878-1551 (Electronic)).

139. Faure, S., et al., *Endogenous patterns of TGFbeta superfamily signaling during early Xenopus development.* Development, 2000. **127**(13): p. 2917-31.
140. Henry, G.L., et al., *TGF-beta signals and a pattern in Xenopus laevis endodermal development.* (0950-1991 (Print)).
141. Hill, C.S., *TGF-beta signalling pathways in early Xenopus development.* Curr Opin Genet Dev, 2001. **11**(5): p. 533-40.
142. Shen, M.M., *Nodal signaling: developmental roles and regulation.* Development, 2007. **134**(6): p. 1023-34.
143. Kishigami, S. and Y. Mishina, *BMP signaling and early embryonic patterning.* 2005(1359-6101 (Print)).
144. Jain, M., et al., *Mitochondrial reactive oxygen species regulate transforming growth factor-beta signaling.* J Biol Chem, 2013. **288**(2): p. 770-7.
145. Hu, T., et al., *Reactive oxygen species production via NADPH oxidase mediates TGF-beta-induced cytoskeletal alterations in endothelial cells.* Am J Physiol Renal Physiol, 2005. **289**(4): p. F816-25.
146. Carballada, R., H. Yasuo, and P. Lemaire, *Phosphatidylinositol-3 kinase acts in parallel to the ERK MAP kinase in the FGF pathway during Xenopus mesoderm induction.* Development, 2001. **128**(1): p. 35-44.
147. Nie, S. and C. Chang, *PI3K and Erk MAPK mediate ErbB signaling in Xenopus gastrulation.* 2007(0925-4773 (Print)).
148. Peng, Y., et al., *Phosphatidylinositol 3-kinase signaling is involved in neurogenesis during Xenopus embryonic development.* 2004(0021-9258 (Print)).
149. Cho, S.H., et al., *Redox regulation of PTEN and protein tyrosine phosphatases in H(2)O(2) mediated cell signaling.* FEBS letters, 2004. **560**(1-3): p. 7-13.
150. Maehama, T., G.S. Taylor, and J.E. Dixon, *PTEN and myotubularin: novel phosphoinositide phosphatases.* Annual review of biochemistry, 2001. **70**: p. 247-79.
151. Love, N.R., et al., *pTransgenesis: a cross-species, modular transgenesis resource.* Development, 2011. **138**(24): p. 5451-8.
152. Sive Hl Fau - Grainger, R.M., R.M. Grainger Rm Fau - Harland, and R.M. Harland, *Defolliculation of Xenopus oocytes.* (1559-6095 (Electronic)).
153. Kerksick, C. and D. Willoughby, *The antioxidant role of glutathione and N-acetyl-cysteine supplements and exercise-induced oxidative stress.* J Int Soc Sports Nutr, 2005. **2**: p. 38-44.
154. Shimamoto, K., et al., *Antioxidant N-acetyl-L-cysteine (NAC) supplementation reduces reactive oxygen species (ROS)-mediated hepatocellular tumor promotion of indole-3-carbinol (I3C) in rats.* J Toxicol Sci, 2011. **36**(6): p. 775-86.
155. Gatherer, D. and H.R. Woodland, *N-acetyl-cysteine causes a late re-specification of the anteroposterior axis in the Xenopus embryo.* Dev Dyn, 1996. **205**(4): p. 395-409.
156. Drysdale, T.A. and R.P. Elinson, *Cell Migration and Induction in the Development of the Surface Ectodermal Pattern of the Xenopus laevis Tadpole.* Development, Growth & Differentiation, 1992. **34**(1): p. 51-59.
157. Wallingford, J.B., S.E. Fraser, and R.M. Harland, *Convergent extension: the molecular control of polarized cell movement during embryonic development.* Dev Cell, 2002. **2**(6): p. 695-706.
158. Le Belle, J.E., et al., *Proliferative neural stem cells have high endogenous ROS levels that regulate self-renewal and neurogenesis in a PI3K/Akt-dependant manner.* (1875-9777 (Electronic)).

159. Criddle, D.N., et al., *Menadione-induced reactive oxygen species generation via redox cycling promotes apoptosis of murine pancreatic acinar cells.* J Biol Chem, 2006. **281**(52): p. 40485-92.
160. Ji, A.R., et al., *Reactive oxygen species enhance differentiation of human embryonic stem cells into mesendodermal lineage.* (2092-6413 (Electronic)).
161. Kimelman, D. and M. Kirschner, *Synergistic induction of mesoderm by FGF and TGF-beta and the identification of an mRNA coding for FGF in the early Xenopus embryo.* Cell, 1987. **51**(5): p. 869-77.
162. Nishimatsu, S. and G.H. Thomsen, *Ventral mesoderm induction and patterning by bone morphogenetic protein heterodimers in Xenopus embryos.* Mech Dev, 1998. **74**(1-2): p. 75-88.
163. Hikasa, H. and S.Y. Sokol, *Wnt signaling in vertebrate axis specification.* Cold Spring Harb Perspect Biol, 2013. **5**(1): p. a007955.
164. Huelsken, J., et al., *Requirement for beta-catenin in anterior-posterior axis formation in mice.* J Cell Biol, 2000. **148**(3): p. 567-78.
165. Larabell, C.A., et al., *Establishment of the dorso-ventral axis in Xenopus embryos is presaged by early asymmetries in beta-catenin that are modulated by the Wnt signaling pathway.* (0021-9525 (Print)).
166. Chamorro, M.N., et al., *FGF-20 and DKK1 are transcriptional targets of β-catenin and FGF-20 is implicated in cancer and development.* The EMBO Journal, 2005. **24**(1): p. 73-84.
167. Foerder, C.A., S.J. Klebanoff, and B.M. Shapiro, *Hydrogen peroxide production, chemiluminescence, and the respiratory burst of fertilization: interrelated events in early sea urchin development.* Proc Natl Acad Sci U S A, 1978. **75**(7): p. 3183-7.
168. Brown, G.C. and V. Borutaite, *There is no evidence that mitochondria are the main source of reactive oxygen species in mammalian cells.* Mitochondrion, 2012. **12**(1): p. 1-4.
169. Orient, A., et al., *Novel sources of reactive oxygen species in the human body.* Nephrol Dial Transplant, 2007. **22**(5): p. 1281-8.
170. Sandalio, L.M., et al., *Role of peroxisomes as a source of reactive oxygen species (ROS) signaling molecules.* (0306-0225 (Print)).
171. Funato, Y., et al., *The thioredoxin-related redox-regulating protein nucleoredoxin inhibits Wnt-beta-catenin signalling through dishevelled.* 2006(1465-7392 (Print)).
172. Steinhardt, R., R. Zucker, and G. Schatten, *Intracellular calcium release at fertilization in the sea urchin egg.* Dev Biol, 1977. **58**(1): p. 185-96.
173. Santella, L., D. Lim, and F. Moccia, *Calcium and fertilization: the beginning of life.* Trends Biochem Sci, 2004. **29**(8): p. 400-8.
174. Zhao, Y., et al., *An expanded palette of genetically encoded Ca(2)(+) indicators.* Science, 2011. **333**(6051): p. 1888-91.
175. El-Jouni, W., et al., *Calcium signaling differentiation during Xenopus oocyte maturation.* Dev Biol, 2005. **288**(2): p. 514-25.
176. Boton, R., et al., *Two calcium-activated chloride conductances in Xenopus laevis oocytes permeabilized with the ionophore A23187.* J Physiol, 1989. **408**: p. 511-34.
177. Albrieux, M., C. Sardet, and M. Villaz, *The two intracellular Ca2+ release channels, ryanodine receptor and inositol 1,4,5-trisphosphate receptor, play different roles during fertilization in ascidians.* Dev Biol, 1997. **189**(2): p. 174-85.

178. Runft, L.L., J. Watras, and L.A. Jaffe, *Calcium Release at Fertilization of Xenopus Eggs Requires Type I IP3 Receptors, but Not SH2 Domain-Mediated Activation of PLCγ or Gq-Mediated Activation of PLCβ.* Developmental Biology, 1999. **214**(2): p. 399-411.
179. Sims, C.E. and N.L. Allbritton, *Metabolism of inositol 1,4,5-trisphosphate and inositol 1,3,4,5-tetrakisphosphate by the oocytes of Xenopus laevis.* J Biol Chem, 1998. **273**(7): p. 4052-8.
180. Ayabe, T., G.S. Kopf, and R.M. Schultz, *Regulation of mouse egg activation: presence of ryanodine receptors and effects of microinjected ryanodine and cyclic ADP ribose on uninseminated and inseminated eggs.* Development, 1995. **121**(7): p. 2233-44.
181. Yue, C., et al., *Localization and regulation of ryanodine receptor in bovine oocytes.* Biol Reprod, 1998. **58**(2): p. 608-14.
182. Fill, M. and J.A. Copello, *Ryanodine receptor calcium release channels.* Physiol Rev, 2002. **82**(4): p. 893-922.
183. Soto, X., et al., *Inositol kinase and its product accelerate wound healing by modulating calcium levels, Rho GTPases, and F-actin assembly.* Proc Natl Acad Sci U S A, 2013. **110**(27): p. 11029-34.
184. Whitaker, M., *Calcium at Fertilization and in Early Development.* Physiological Reviews, 2005. **86**(1): p. 25-88.
185. Wong, J.L., R. Créton, and G.M. Wessel, *The Oxidative Burst at Fertilization Is Dependent upon Activation of the Dual Oxidase Udx1.* Developmental Cell, 2004. **7**(6): p. 801-814.
186. Musset, B., et al., *NOX5 in human spermatozoa: expression, function, and regulation.* J Biol Chem, 2012. **287**(12): p. 9376-88.
187. Serrander, L., et al., *NOX5 is expressed at the plasma membrane and generates superoxide in response to protein kinase C activation.* 2007(0300-9084 (Print)).
188. Kirichok, Y., G. Krapivinsky, and D.E. Clapham, *The mitochondrial calcium uniporter is a highly selective ion channel.* Nature, 2004. **427**(6972): p. 360-364.
189. Murphy, M.P. and R.A. Smith, *Targeting antioxidants to mitochondria by conjugation to lipophilic cations.* Annu Rev Pharmacol Toxicol, 2007. **47**: p. 629-56.
190. Dikalova, A.E., et al., *Therapeutic targeting of mitochondrial superoxide in hypertension.* Circ Res, 2010. **107**(1): p. 106-16.
191. Liu, M., H. Liu, and S.C. Dudley, Jr., *Reactive oxygen species originating from mitochondria regulate the cardiac sodium channel.* Circ Res, 2010. **107**(8): p. 967-74.
192. Agathocleous, M., et al., *Metabolic differentiation in the embryonic retina.* Nat Cell Biol, 2012. **14**(8): p. 859-64.
193. Senior Ae Fau - Wise, J.G. and J.G. Wise, *The proton-ATPase of bacteria and mitochondria.* 1983(0022-2631 (Print)).
194. Andreyev, A.Y., Y.E. Kushnareva, and A.A. Starkov, *Mitochondrial metabolism of reactive oxygen species.* Biochemistry (Mosc), 2005. **70**(2): p. 200-14.
195. Brinkley, B.R., et al., *Rotenone inhibition of spindle microtubule assembly in mammalian cells.* Exp Cell Res, 1974. **85**(1): p. 41-6.
196. Armstrong, J.S., et al., *Rotenone-induced G2/M cell cycle arrest and apoptosis in a human B lymphoma cell line PW.* Biochem Biophys Res Commun, 2001. **289**(5): p. 973-8.

197. Fato, R., et al., *Mitochondrial production of reactive oxygen species: role of complex I and quinone analogues.* Biofactors, 2008. **32**(1-4): p. 31-9.
198. Maranzana, E., et al., *Mitochondrial respiratory supercomplex association limits production of reactive oxygen species from complex I.* Antioxid Redox Signal, 2013. **19**(13): p. 1469-80.
199. Batandier, C., X. Leverve, and E. Fontaine, *Opening of the mitochondrial permeability transition pore induces reactive oxygen species production at the level of the respiratory chain complex I.* J Biol Chem, 2004. **279**(17): p. 17197-204.
200. Chen, Q., et al., *Production of reactive oxygen species by mitochondria: central role of complex III.* J Biol Chem, 2003. **278**(38): p. 36027-31.
201. Zhang, L., et al., *[Effect of sodium azide on mitochondrial membrane potential in SH-SY5Y human neuroblastoma cells].* Zhongguo Yi Xue Ke Xue Yuan Xue Bao, 2000. **22**(5): p. 436-9.
202. Santo-Domingo, J. and N. Demaurex, *Calcium uptake mechanisms of mitochondria.* Biochim Biophys Acta, 2010. **1797**(6-7): p. 907-12.
203. Brookes, P.S., et al., *Calcium, ATP, and ROS: a mitochondrial love-hate triangle.* Am J Physiol Cell Physiol, 2004. **287**(4): p. C817-33.
204. Kahl, C.R. and A.R. Means, *Regulation of cell cycle progression by calcium/calmodulin-dependent pathways.* Endocr Rev, 2003. **24**(6): p. 719-36.
205. Lunt, S.Y. and M.G. Vander Heiden, *Aerobic glycolysis: meeting the metabolic requirements of cell proliferation.* Annu Rev Cell Dev Biol, 2011. **27**: p. 441-64.
206. Jonckheere, A.I., J.A. Smeitink, and R.J. Rodenburg, *Mitochondrial ATP synthase: architecture, function and pathology.* J Inherit Metab Dis, 2012. **35**(2): p. 211-25.
207. Dittrich, M., S. Hayashi, and K. Schulten, *On the mechanism of ATP hydrolysis in F1-ATPase.* Biophys J, 2003. **85**(4): p. 2253-66.
208. Sanchez-Cenizo, L., et al., *Up-regulation of the ATPase inhibitory factor 1 (IF1) of the mitochondrial H+-ATP synthase in human tumors mediates the metabolic shift of cancer cells to a Warburg phenotype.* J Biol Chem, 2010. **285**(33): p. 25308-13.
209. Wright, V.P., P.J. Reiser, and T.L. Clanton, *Redox modulation of global phosphatase activity and protein phosphorylation in intact skeletal muscle.* J Physiol, 2009. **587**(Pt 23): p. 5767-81.
210. Lee, S.R., et al., *Reversible inactivation of the tumor suppressor PTEN by H2O2.* J Biol Chem, 2002. **277**(23): p. 20336-42.
211. Meng, T.C., T. Fukada, and N.K. Tonks, *Reversible oxidation and inactivation of protein tyrosine phosphatases in vivo.* Mol Cell, 2002. **9**(2): p. 387-99.
212. Finkel, T., *Signal transduction by reactive oxygen species.* J Cell Biol, 2011. **194**(1): p. 7-15.
213. Pohl, B.S., et al., *The FoxO-subclass in Xenopus laevis development.* Gene Expr Patterns, 2004. **5**(2): p. 187-92.
214. Essers, M.A., et al., *Functional interaction between beta-catenin and FOXO in oxidative stress signaling.* 2005(1095-9203 (Electronic)).
215. Salmeen, A., et al., *Redox regulation of protein tyrosine phosphatase 1B involves a sulphenyl-amide intermediate.* Nature, 2003. **423**(6941): p. 769-73.
216. Kumagai, A. and W.G. Dunphy, Regulation of the cdc25 protein during the cell cycle in Xenopus extracts. Cell, 1992. **70**(1): p. 139-51.